



<https://theses.gla.ac.uk/>

Theses Digitisation:

<https://www.gla.ac.uk/myglasgow/research/enlighten/theses/digitisation/>

This is a digitised version of the original print thesis.

Copyright and moral rights for this work are retained by the author

A copy can be downloaded for personal non-commercial research or study, without prior permission or charge

This work cannot be reproduced or quoted extensively from without first obtaining permission in writing from the author

The content must not be changed in any way or sold commercially in any format or medium without the formal permission of the author

When referring to this work, full bibliographic details including the author, title, awarding institution and date of the thesis must be given

Enlighten: Theses

<https://theses.gla.ac.uk/>
research-enlighten@glasgow.ac.uk

Novel Flexible Multielectrode Arrays for Neuronal Stimulation and Recording

Christopher Adams



UNIVERSITY
of
GLASGOW

Department of Physics and Astronomy

*Thesis submitted for the degree of Doctor of Philosophy in the
subject of physics*

February 27, 2007

© C. Adams February 27, 2007

ProQuest Number: 10391426

All rights reserved

INFORMATION TO ALL USERS

The quality of this reproduction is dependent upon the quality of the copy submitted.

In the unlikely event that the author did not send a complete manuscript and there are missing pages, these will be noted. Also, if material had to be removed, a note will indicate the deletion.



ProQuest 10391426

Published by ProQuest LLC (2017). Copyright of the Dissertation is held by the Author.

All rights reserved.

This work is protected against unauthorized copying under Title 17, United States Code
Microform Edition © ProQuest LLC.

ProQuest LLC.
789 East Eisenhower Parkway
P.O. Box 1346
Ann Arbor, MI 48106 – 1346

GLASGOW
UNIVERSITY
LIBRARY:

To My Family

Abstract

This thesis will focus on developments in coupling the multidisciplinary research interests of Physics, Microengineering and neurobiology towards the development of a proof of concept retinal prosthetic device.

With recent developments in low-power electronics and semiconductor fabrication techniques many applications in the life sciences have emerged. One such application is in the development of a retinal prosthetic device which relies on the ability to record information from and feed information directly to small retinal neuronal cells which are approximately $5\mu\text{m}$ diameter. Where successful, we achieve the possibility of restoring sight to people affected by degenerative visual diseases such as Age Related Macular Degeneration and Retinitis Pigmentosa. Both these conditions affect the photosensitive elements of the eye yet leave the remaining pathways to the visual cortex, the area of the brain responsible for our visual precept, intact.

High-density electrode arrays are becoming well established as tools for the measurement of neuronal signals. The fabrication of arrays on flexible materials allows for 2D position sensitive recording of cellular activity *in vivo* and for the possibility of direct *in vivo* stimulus. Using flexible polymer materials (Pryalin PI2545), compliant with semiconductor fabrication techniques, a process allowing the fabrication of flexible multi-site microelectrode neuronal recording and stimulating arrays is presented.

The development of both 8 and 7- μ m electrode arrays on polyimide substrates with 50 μ m and 5 μ m minimum linewidths respectively is described. Implementing low noise amplification, 8 μ V rms (bandpass typically 80-2000 Hz), the polyimide 8-electrode arrays have been used to stimulate and record electroretinogram and ganglion cell action potentials *in vivo* from the frog retina (*Rana temporaria*).

Such arrays coupled to our application specific pixellated CMOS sensors, the IPIX, incorporating an ability to apply neural network algorithms should allow for the recovery of basic functionality in the human retina. The IPIX detector is an Active Pixel Sensor which responds to incident light in the visible region. It responds to the varying intensity of light over 3 log units and outputs varying frequency voltage pulses of similar form to that of a healthy retina.

Stimulation studies for electro-deposited platinum electrodes of 4 nA/ μ m² indicate upper breakdown limits for charge density approaching 100 μ Cm⁻². Investigations of lifetime stimulation of a 50 μ m diameter electrode, of typical impedance less than 20 k Ω at 1 kHz, suggest operational limits over lifetime in the order of 10 μ Cm⁻². These charge densities are adequate for neuronal cell stimulation.

It is believed that the system described in this thesis can form the basis on which to deploy a retinal prosthetic device. Moreover, in the short term, the information provided by this system will allow for investigations into

deciphering the 'wiring diagram' of the retina.

Contents

| | | |
|----------|--|-----------|
| 1 | Introduction | 21 |
| 1.0.1 | Applications of microelectrode arrays | 23 |
| 1.1 | Retinal Disease | 25 |
| 1.1.1 | Age Related Macula Degeneration | 26 |
| 1.1.2 | Retinitis Pigmentosa | 27 |
| 1.2 | Prosthetic developments to restore vision | 28 |
| 1.2.1 | Retinal Implants | 32 |
| 1.2.2 | Optic nerve implants | 33 |
| 1.2.3 | Deep brain stimulation | 33 |
| 1.3 | A flexible microelectrode array for in-vivo retinal prostheses | 34 |
| 1.3.1 | Overview of thesis objectives | 39 |
| 2 | Theory | 41 |
| 2.1 | The Eye. | 43 |
| 2.1.1 | Structure of The Eye. | 44 |
| 2.1.2 | The Retina | 46 |
| 2.1.3 | Physiology | 47 |
| 2.1.4 | The Fovea | 50 |
| 2.1.5 | Rod Function | 51 |

| | | |
|----------|--|-----------|
| 2.1.6 | The cellular resting potential | 53 |
| 2.1.7 | Neuronal Functionality and the Action Potential | 56 |
| 2.2 | Diseases | 61 |
| 2.3 | Prosthesis | 61 |
| 2.3.1 | Implanting | 62 |
| 2.3.2 | Biocompatibility | 64 |
| 2.3.3 | Heating | 64 |
| 2.3.4 | Cellular Coupling to the Electrode Arrays | 65 |
| 2.4 | Neural Computation | 68 |
| 2.4.1 | Overview of the proposed technological model | 69 |
| 3 | Fabrication | 71 |
| 3.1 | Introduction | 71 |
| 3.2 | Material biocompatibility | 74 |
| 3.2.1 | Electrode Biocompatibility | 76 |
| 3.3 | Lithography | 79 |
| 3.3.1 | Photolithography | 79 |
| 3.3.2 | Electrode Array Layout | 81 |
| 3.3.3 | Photolithographic Mask Design | 82 |
| 3.4 | Device fabrication procedure | 83 |
| 3.4.1 | PI2545 Polyimide preparation | 83 |
| 3.4.2 | Method for evaluating film thickness and surface roughness | 86 |
| 3.4.3 | Metal Deposition | 87 |
| 3.5 | Etching techniques | 89 |
| 3.5.1 | Dry Etching | 90 |

| | | |
|----------|--|------------|
| 3.5.2 | Wet Etching | 91 |
| 3.5.3 | Patterning the metal layers | 92 |
| 3.5.4 | Surface encapsulation and vias opening | 94 |
| 3.5.5 | Platinisation of electrodes | 96 |
| 3.5.6 | Model of cell-electrode interface | 106 |
| 4 | IPIX | 111 |
| 4.1 | The IPIX imaging device | 115 |
| 4.1.1 | IPIX Design | 115 |
| 4.1.2 | Design Parameters | 117 |
| 4.1.3 | Photodiode | 118 |
| 4.1.4 | Voltage Buffer | 119 |
| 4.1.5 | Voltage Controlled Oscillator | 120 |
| 4.1.6 | VCO Characterisation | 123 |
| 4.1.7 | Light Response | 128 |
| 4.1.8 | Stimulation Pulse Amplitude | 130 |
| 4.1.9 | Pixel Cross Talk | 131 |
| 5 | Biological results from in-vivo testing | 139 |
| 5.1 | Introduction | 139 |
| 5.2 | Sample Preparation | 141 |
| 5.2.1 | Biological Tissue preparation | 142 |
| 5.2.2 | Initial preparation studies. | 143 |
| 5.2.3 | Signal Amplification | 145 |
| 5.2.4 | Data Acquisition Software | 147 |
| 5.3 | Recorded Signals | 148 |

| | | |
|----------|---|------------|
| 5.3.1 | Light Evoked Response | 154 |
| 5.3.2 | Cellular Classification | 156 |
| 5.4 | Stimulation Studies | 157 |
| 5.4.1 | Single electrode stimulation studies | 158 |
| 5.4.2 | Stimulation Artefact | 159 |
| 5.4.3 | Voltage threshold for cellular stimulation | 162 |
| 5.4.4 | Action Potential recording from an applied voltage stimulus | 163 |
| 5.4.5 | Stimulus Range | 166 |
| 6 | Conclusions | 171 |
| 6.0.6 | Future Work | 175 |
| A | appendix1 | 205 |

List of Figures

| | | |
|-----|---|----|
| 1.1 | Left, A schematic of the eye with the position of the retina indicated. Right, an expanded image showing in more detail the cellular layers which make up the basic structure of the retina. | 23 |
| 1.2 | An image of the Optobionics silicon device implanted sub-retinally in the eye, upper left grey circle. | 29 |
| 1.3 | A schematic representation of the approach employed by second sight at restoring vision. The user wears a pair of eye glasses which record and process the image before passing the details through an RF link to the device which is coupled to the eye. | 29 |
| 2.1 | Diagram of Visual pathway showing the eye, optic nerve and visual cortex on right hand diagram. Exploded view of the retina is shown on left. | 42 |
| 2.2 | Schematic cross-section of the eye, highlighting the key functional components. | 45 |

| | | |
|-----|---|----|
| 2.3 | Schematic of the retina showing five classified neuronal species found in the retina and the layered structured of the cellular tissue. | 47 |
| 2.4 | An example of the connections between a sensory neurone, the cell body and the synaptic endings. The axonal connection is a fast acting link that conveys the information between the cells. (Image from www.biologymad.com) | 48 |
| 2.5 | A image of the human retina showing the fovea, photoreceptors and the displacement of cellular tissue around the foveal pit. | 50 |
| 2.6 | A schematic image of a human rod cell indicating the outer segment, inner segment and the synaptic terminal. The outer segment connects to the pigment epithelium. | 52 |
| 2.7 | A schematic of an action potential (referenced intracellular). The resting potential is commonly -70mV and peaks at +40mV when an action potential occurs(modified from http://z.about.com). | 59 |
| 2.8 | Schematic of the surgical locations of a sub-retinal and epi-retinal implant. (Note the lack of external connections). | 63 |
| 2.9 | Schematic of the surgical locations of the Epi-retinal IPIX (monolithic active pixels sensor) chip implant on the flexible microelectrode array. Although the exact position of the IPIX chip is variable it does indicate a likely position for future in-vivo implantation (Note the lack of external connections). | 67 |

| | | |
|-----|--|----|
| 3.1 | Measured charge limit for electrodes of varying size. The applied pulse was 500 μ s per phase and of varying amplitude until degradation was seen. The Red, blue and green lines correspond to a simulated electrode. | 77 |
| 3.2 | Photolithographic mask transfer using projection masking. The lens allows for the reduction in size of the image while the wafer below is stepped to pattern the whole area. In contact masking, the lens is absent and the mask is in contact with the substrate material with light incident normal to the surface. | 80 |
| 3.3 | Polyimide spin speeds vs. layer thickness | 84 |
| 3.4 | An image of microfabricated titanium on polyimide substrate material. | 93 |
| 3.5 | An image of the 74-electrode array post surface encapsulation and vias opening. The small image, top right, gives a high magnification view (x50) of a single electrode. This electrode has been electrodeposited with platinum. | 95 |
| 3.6 | An image of the full 74-electrode array post surface encapsulation, vias opening and removal from the silicon carry wafer. . | 96 |
| 3.7 | A schematic showing the measurement technique for the determination of the impedance values for the 8 electrode arrays. The switching unit for the 8 electrode array activates a single channel at a time and allows for the measurement of the 1kHz, 100mV impedance value. The bath is filled with buffered saline solution. | 98 |

| | | |
|------|---|-----|
| 3.8 | A schematic showing the measurement technique for the determination of the impedance values for the 74 electrode arrays. The micromanipulator probes activate a single channel at a time and is stepped across all the bond pads allowing for the measurement of the 1kHz, 100mV impedance value. The bath is filled with buffered saline solution. | 99 |
| 3.9 | A schematic showing the technique for the deposition of platinum black from a platinum chloride solution. The Keithly 427 supplies a constant current and the micromanipulator is stepped across all electrode bond pads till platinisation is complete. | 100 |
| 3.10 | Scanning Electron Microscope image of Electrode Showing surface growth on polyimide under voltage controlled limits . . | 101 |
| 3.11 | 50 μ m feature 8-Electrode Array - The electrodes have been electroplated with platinum under a current limit of 4nA / μ m | 102 |
| 3.12 | An example of the average electrode impedance measured for a 50 μ m electrode from an 8-electrode array as a function of frequency as measured in buffered saline solution. | 103 |
| 3.13 | An example of the average electrode impedance measured for a 5 μ m electrode from an 74-electrode array as a function of frequency as measured in buffered saline solution. | 105 |
| 3.14 | Electrical representation of the cell-electrode interface for a single working electrode. | 108 |
| 3.15 | Electrical representation of the cell-electrode interface for a single working electrode. | 109 |

| | | |
|-----|--|-----|
| 4.1 | The 10x10 array of pixels is shown with the bond pads seen at the outer edges of the chip. A magnified image of a single pixel can be seen at the top right of the figure. | 112 |
| 4.2 | Schematic of a mono-phasic pulse (top) and a bi-phasic pulse (bottom). The time t corresponds to 1ms for a monophasic pulse or 500 μ s for the bi-phasic pulse. The bi-phasic pulse can be seen to represent a charge balanced system. | 114 |
| 4.3 | Schematic of a Pixel onboard the IPIX chip | 116 |
| 4.4 | A schematic of a photodiode showing the 3 transistor readout scheme | 118 |
| 4.5 | 100x100 μ m 3D scan of a single pixel. surface profiled at x100 Magnification | 120 |
| 4.6 | VCO controlled oscillator block diagram. The non-overlapping clock $\phi 1$ and $\phi 2$ which control the comparator switching rate are shown. The capacitors C1 and C2 which affect the voltage step from V_{amp} are also evident. | 122 |
| 4.7 | Frequency of the output stimulation pulses as a function of the voltage supplied to the voltage controlled oscillator | 125 |
| 4.8 | Variation in the frequency output of the stimulation pulses as a function of the voltage supplied to the voltage controlled oscillator. | 127 |
| 4.9 | The standard deviation averaged across all pixels for the frequency output of the stimulation pulses as a function of the voltage supplied to the voltage controlled oscillator. | 127 |

| | | |
|------|--|-----|
| 4.10 | Neutral Density filter Light variation vs. frequency output Hz. The red line is a least square fit to the experimentally realised values. | 129 |
| 4.11 | Stimulation pulse amplitude with associated RMS Noise out- put from a single channel | 130 |
| 4.12 | Pixel layout showing the 10x10 array and then zoomed into the central region. Bottom right is a schematic showing the numbering of the pixels as referenced in this work. | 132 |
| 4.13 | Pixel cross talk measured on neighbouring pixels as the voltage increased on pixel 1 | 133 |
| 4.14 | Percentage of an increasing stimulation pulse, as applied to pixel 1, detected on neighbouring pixels. | 134 |
| 4.15 | PCB layout showing the 9 stimulating tracks close to each other and the IPIX chip in the central region of the figure. The crosstalk measurements are likely to be a result of having the output channels running parallel. | 135 |
| 5.1 | Overview of engineering representation of biological system . . | 141 |
| 5.2 | Overview of preparation of the frog retina and the array im- planted into the eyecup. The electrode array is inserted with the electrodes face down and in contact with the ganglion cells of the retina. | 144 |
| 5.3 | 8-electrode array connected to low noise 16 channel LIMO connector | 146 |
| 5.4 | Electroretinogram with superimposed spiking activity | 149 |

| | | |
|------|--|-----|
| 5.5 | The breakdown of a typical measured ERG response into its 3 main components, the a,b and c-waves. | 151 |
| 5.6 | Recorded retinal activity upon light activation with the electroretinogram removed using a 80Hz high pass FFT filter. . . | 152 |
| 5.7 | Recordings from a electrode of $5\mu\text{m}$ diameter. The recording was made on an ITO array of electrode size $5\mu\text{m}$ | 153 |
| 5.8 | Electroretinogram showing faster response from the retina to increasing intensity for the human. (From Webvision.med.utah.edu) | 154 |
| 5.9 | Recordings from an 8-electrode array of the ON cell response in relation to the initiation of light at the retinal surface. Recordings were made at 10kHz sampling rate and the recording starts at the onset of light at the retinal surface, $t=0$ | 157 |
| 5.10 | Recordings from an 8-electrode array of the off cell response in relation to the termination of light at the retinal surface. Recordings were made at 10kHz sampling rate and the recording starts at the termination of light on the retinal surface. time = 0. | 158 |
| 5.11 | Recordings from 4 electrodes of $50\mu\text{m}$ diameter. The 4 electrodes are showing the OFF response at independent points on the retinal surface. The light termination started at time 0 and recording continues for 100 ms. The amplitudes of the responses are all of the order $-200\ \mu\text{V}$ to $100\ \mu\text{V}$ | 159 |

| | | |
|------|--|-----|
| 5.12 | The stimulation artefact as recorded on a $50\mu\text{m}$ electrode $50\mu\text{m}$ away from the stimulation site. The amplitude of the artefact was measured for 5 voltage increments for a 1ms pulse applied to, and measured from the same electrodes. | 160 |
| 5.13 | Measured waveform of a single action potential recorded from a 400mV applied electrical pulse. | 162 |
| 5.14 | Temporal occurrence of APs over 18 trials in response to an applied voltage pulse of 1ms. | 164 |
| 5.15 | Temporal spike occurrence in response to applied voltages of 400mV and 1200mV | 165 |
| 5.16 | Image of a microelectrode array post test. As can be seen the electrodes are still well coated with platinum black (except for electrode 6 which was not working pre test) and there is no delamination of the polyimide layers. | 166 |
| 5.17 | Graph showing the time of detection of AP's on electrodes with varying distance from the stimulation electrode. | 168 |
| 5.18 | Graph showing an increased time resolution of fig 5.15 indicating more specifically the detection of AP's on electrodes with varying distance from the stimulation electrode. | 169 |
| A.1 | Revinial Readout electronic circuit for a single channel amplification module. | 206 |

Acknowledgements

I think it is only just that the work undertaken, and the outcomes achieved in this thesis be considered a culmination of hard work and opportunity. I am blessed with having being offered the opportunity to undertake this research in the first instance by Dr. Mahfuzur Rahman and later through the continual guidance and supervision offered by Dr. Keith Mathieson. If it was not for Keith's leadership, patience, and hard work, this thesis would never have made it to it's current form. Dr. Jim Morrison as my second supervisor and the lead neurophysiologist deserves a medal for his belief in the possibilities of the project. His desire to enable the neurological studies and his technical capacity to bridge the gaps between his research and the microengineering field is a desire that will never cease, nor cease to impress those who work with him. I will be forever grateful to Keith and Jim for their input and guidance and hope I will be forever privileged with their company.

The undertaking of a PhD is a 3 (or 4 year :P) commitment to research. A lot can change in that time. And it did. There was however one unfaltering

commitment, and that was from my family. I have the best parents in the world, they have supported me throughout the years taken to complete this thesis. Without that support I doubt this thesis would ever have made it to print, thank you. And to my brother Jason, you have lightened the load of the thesis. You gave me the opportunity to travel to New Zealand (twice!!) and experience some of the most magical moments of my life to date, Te-Ani, need I say more!!. Incidentally, you probably are also partially to blame for the time it took to write this thesis, if you had not got married, I would not have spent a month writing your best mans speech!!. Cheers, bro for all your input and help.

This thesis has covered several scientific disciplines and as such I am in debt to the kindness and patience of an enormous amount of people. My office mates over the last few years have suffered me well. Debbie, you are a star!, you put up with my poor jokes, poor music and complaints more than any one person ever should, it is a saint hood you should get not a PhD!!. Francesco, Tats, Derck and Alison, you were the best of office mates and some of the most entertaining people I have ever had the privilege to know. thanks!.

I would also be doing a great in-service if I did not recognise the effort that Val O'Shea, Andrew Long and Ken Smith put into my project. You offered support in a time when the project needed it most, thank you.

The support offered by the technical staff in the physics department, en-

gineering department and institute for biological and life sciences has enabled this project to reach its potential. I am grateful for all the support I have received and through your own capacities allowed this project to reach completeness. I will never underestimate the "bribing" power of doughnuts!! Cheers.

And to all the people at university who made the social aspect of my time during my thesis such an enjoyable and memorable (well if we neglect the loss of memory on the times whereby I was led astray on copious quantities of alcohol!) experience. Andy, Liam, Hero, John, Stan, Chris, John, Ian, Julian, David and Alan, Cheers for the fond memories!

And to the buddies, Lindsey, Fiona, Neil, Big Guy, Alistair, Julie, Gillian, Martin, Beard, Nicole and Jo thanks for all your support and friendship... and for the numerous times I have had the luxury of sleeping on your floors!!

Lastly, but not least I would like to thank Hannah. It has been said that only through the mysterious equations of love can any logical reasons be found. I think if we solved the theory of everything, substituted these mysterious equations of love somewhere into them, we would discover only a fraction of what you have done and meant to me over these last two years. With you, I am blessed.

Chapter 1

Introduction

Perhaps one of the most significant interests of the last decade [74] has been the convergence of multidisciplinary research activities within the fields of physics, engineering and neurobiology. Detector developments within the physics community have benefited from increased sensitivity and miniaturisation, this in conjunction with the microfabrication techniques found in the engineering community, can be combined to provide a means of selective high precision neuronal monitoring [69]. The ability to monitor multiple cellular response in-vivo opens many exciting avenues in the field of neurobiology [2].

One such avenue is in deciphering “wiring diagrams” of neuronal circuitry. Under situations where the neurones are active, detectors positioned close enough will be able to detect the response. If we have multiple detectors in place then we can detect the interactions between these neurons under activation. It follows additionally, if we supply a response from a man made

system that mimics this multiple response then subsequent neuronal layers will respond in a natural manner. This characteristic opens opportunities to restore function to areas where the natural ability of the neurones to respond has been compromised [21]. This thesis presents the ability to use a CMOS imaging chip to respond to light, in a coded form, with the output comparable with activity recorded from a healthy retina. These streams of pulses are passed to a microfabricated array of electrodes which can be coupled to retinal tissue. The electrode arrays have been tested on the frog retina and have successfully recorded and stimulated retinal activity. This is seen as the basis on which to develop a retinal prosthesis in the long term.

An accessible region in which to study neuronal activity can be found in the eye, more specifically the retina, see Fig 1.1. There are certain conditions in which the retina can lose its light sensitivity. When this occurs, in extreme cases, the host will be rendered blind. It is believed that if the activity of a fully functional retina is recorded under natural light conditions, and this neuronal response understood, then by electrically stimulating a damaged retina in the regions that still function normally, we can induce the perception of a visual scene [6]. It is also believed that through stimulation of the retinal cells, recovery of cellular functionality can be achieved and in effect allow for visual rehabilitation [11, 12].

It is therefore of great scientific interest to understand retinal processing and how this can be used to reconstruct vision in blind patients. Given the success of cochlear implants in restoring hearing to previously deaf subjects

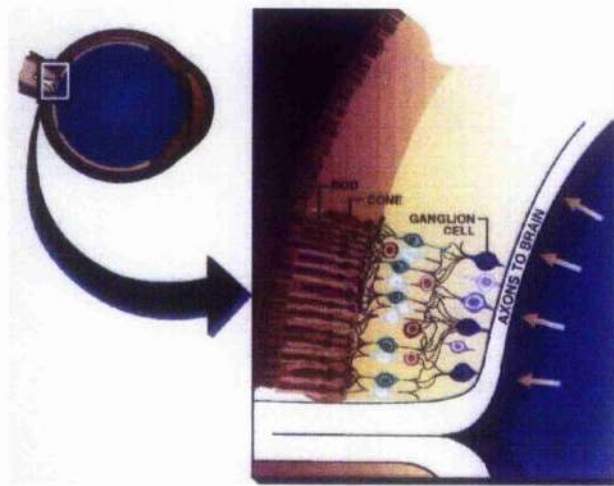


Figure 1.1: Left, A schematic of the eye with the position of the retina indicated. Right, an expanded image showing in more detail the cellular layers which make up the basic structure of the retina.

and, that the technology behind the auditory implant is similar to that employed to the visual domain, it is with keen interest that the infancy period of the retinal implant is monitored.

1.0.1 Applications of microelectrode arrays

The development of microfabricated microelectrode arrays for neurobiological studies became established in the mid 90's [136, 141, 144, 142, 149] and they have found applications in many neurobiological studies. The ability of microelectrode arrays to electrically couple to neuronal cells and provide a useful means of electrically activating the cells has been well documented

[138, 150, 163, 104].

The successful application of microelectrode arrays as tools to record long term information from neurones of the retina and their pathways including the optic nerve and optic tectum [137, 157, 158, 159, 162, 140, 153] is well established. In addition to the pursuit of devices for visual rehabilitation, the application of electrode arrays to record information in-vitro from the central nervous system is another area of enormous scientific interest [151, 152, 155, 146, 148]. The application of microelectrode arrays have been useful in monitoring Parkinsons disease and more recently, microelectrode arrays have found an excellent application in the pursuit of controlling and monitoring epileptic activity [143, 147].

A further application of microelectrode arrays has been for studying and directly influencing cell cultures and their growth factors [139, 145, 154] with results suggesting that electrical stimulation and control of the surface pattern of the electrode arrays can affect the patterning of neuronal networks. Given the opportunity to monitor and affect the growth patterns of neurones through multiples electrode sites, an understanding of neural networking is becoming available as is the ability to model such systems [156, 164, 165]. More recently studies into the effects of drug evaluation using cultured neurones utilising the high sensitivity of electrode arrays has developed [160].

The specific interest for this project is the application of microelectrodes as a means to restore some form of visual sensation. Several groups are using

microelectrode technology to aid in the restoration of sight [35, 14, 130, 129, 16] with encouraging results. Each research group is addressing the problem of restoring sight lost through visual degeneration by different approaches, be it stimulating the outer retinal cells, stimulating the optic nerve or brain stimulation. The common feature is the use of microfabricated microelectrode arrays. These microelectrode arrays must be able to couple electrically to the neurones and provide focussed stimulation from the electrode sites, whilst at the same time maintaining biocompatibility.

Given the success of microelectrode arrays at helping to understand neuronal signalling I believe that the fabrication of such devices on flexible substrates will provide an alternative approach to successfully providing a visual sensation for some forms of blindness. Through the ability of the flexible substrates arrays to conform to the contours of the retinal surface, more efficient coupling to retinal cells is likely with less trauma at the cellular interface.

1.1 Retinal Disease

The function of a retina can be compromised through damage, disease, trauma and physiological dysfunction. Each of these degenerative occurrences affect the functionality of the retina in differing ways [100]. As such, it is unlikely that any one attempt to manufacture a means to restore function will be applicable to all.

In order to restore functionality to the retina we must understand the way

in which the functionality has been reduced. For damage, this will be obvious through lesions or detachment. Trauma however, is much more psychological in effect. In this instance the retina is likely to remain functional with the processing in the visual cortex becoming compromised [25]. Disease of the visual system can impact various components of the visual pathway and will require specific tailoring of engineered systems to have maximum benefit. Physiological dysfunction is a complex area, however, there are two known forms of degenerative effects that are well understood Age Related Macula Degeneration (AMD) and retinitis Pigmentosa (RP). In these cases, the understanding of the cause and its long term impact to visual conformance are well documented. We therefore benefit from histological knowledge of the disease from onset to complete blindness. In this instance engineered systems may offer an ability to recover functionality [59, 124].

1.1.1 Age Related Macula Degeneration

Within the western world, age related macula degeneration is the most common cause of blindness in persons over the age of 65, ranking second after diabetic retinopathy in patients aged between 45-64. Several factors have been linked to AMD including, hypertension, cardiovascular disease, sex (women are more likely than men to develop the disease), light ocular pigmentation and smoking [127]. The degenerative effects of AMD affect the pigment in the epithelium layer of the retina and later kill off the cone photoreceptors (See Fig 1.1). Approximately 1 person per hundred over 65 have either AMD or RP and this number increases to 1 in 8 of people over 85.

There are two forms of AMD, wet and dry (atrophic and choroidal neovascularization). Generally, the occurrence of abnormal new blood vessel growth below the sensory retina or epithelium leads to haemorrhaging and is responsible for visual desensitvity. The new vessel growth is complimentary to new fibrous growth which become the dominant change to the sensory retina.

1.1.2 Retinitis Pigmentosa

Retinitis pigmentosa is characterised by visual dysfunction of the photoreceptors and thereafter subsequent cellular layers. It affects approximately 30,000 families in the UK [127] and roughly 1.5 million people globally. Although RP is a group of disorders, the common form of degenerative effect is through the reduction of rhodopsin in the retina, responsible for the adsorption of light. The characteristic onset of RP is through loss of rods, see Fig 1.1, (which are responsible for night vision) and progressive loss of the visual field. Subjects with advanced RP will have no retinally detectable response to light stimulus (no electroretinogram response).

There have been many approaches to treat the disease with little or no benefit reported. These treatments are similar to that used for AMD and have included minerals, ozone, muscle transplants, cortisone and more recently high doses of vitamin A to slow the progressive rate of the disease [110]. There is also research into gene therapy which is very much in its infancy although shows promise. In principal gene therapy is a preferred

treatment strategy as it allows for targeted regeneration of the neuronal tissue. By the use of gene guns to inject material directly into the cells or via implantation of slow release capsules regenerative material can be localised at the retinal surface [129]. In this way adverse effects can be avoided and dose levels monitored in a highly controllable way.

1.2 Prosthetic developments to restore vision

There are over 40 groups around the world looking to develop prosthetic devices to restore vision. Several are already looking at commercialisation of such devices including, Optobionics (www.optobionics.com) who have implanted their silicon pixel detector into 6 patients for biocompatibility studies over a period of 18 months, seen in fig 1.2, Second Sight(www.2-sight.com) who have reported the perception of visual phosphenes upon stimulation of human retina with their device in the short term ,fig 1.3. and the Dobbie institute(www.dobbie.com) who have used a 3D bed of nails array implanted in the visual cortex to restore some form of vision in 1 patient since 1998. Each of these groups are reporting success in clinical trials of their devices [13, 14, 23, 129] however, what is still not clear is which approach at restoring vision represents the better opportunity long term.

The approach undertaken in this thesis is to couple the optical detector directly to a microfabricated array which is placed directly onto the surface of the retina. In this way we use the natural optics of the eye to focus the image onto the optical sensor. By the use of an active pixel sensor as the detector, the opportunity to program a neural network on chip exists and as such it

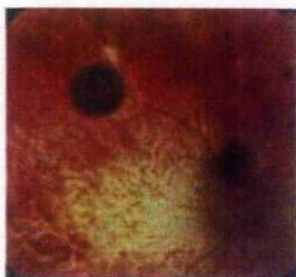


Figure 1.2: An image of the Optobionics silicon device implanted sub-retinally in the eye, upper left grey circle.

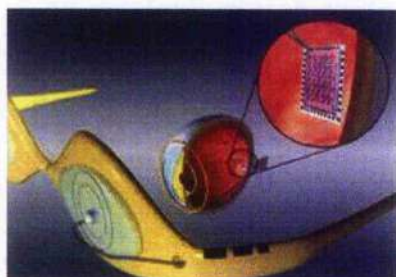


Figure 1.3: A schematic representation of the approach employed by second sight at restoring vision. The user wears a pair of eye glasses which record and process the image before passing the details through an RF link to the device which is coupled to the eye.

can accommodate the processing undertaken by the retina and be modified as our understanding of the retinal encoding develops. The flexible polymeric material used for the microelectrode array (which couples to the retinal cells) is able to effectively communicate information to and from the cells without damage due to the low tensile stress. In this way a unique system has been developed to realise in the long term a viable retinal prostheses.

In determining the success of retinal prostheses outwith clinical trials we must be satisfied with detecting responses from cells that have been stimulated. This is achieved by measuring the response of retinal cells under natural light conditions in the first instance, to show coupling between biological tissue and the engineered devices. We then look to apply an electrical signal to the cells via our microengineered devices and detect a similar response. This type of testing allows the determination of stimulation thresholds and the effect of local stimulation upon neighbouring cell activation [35]. If our manufactured devices elicit a response similar to the response of retinal tissue under normal light illuminated conditions then it is likely the device will cause a natural response in the visual cortex.

In clinical trials the measure of success is determined directly from the host. When an image is presented to the subject, with a prosthetic device implanted, sensations in the form of phosphenes of light have been reported. It has also been established that stimulating different areas of the retina or visual cortex results in varying localities of the perceived phosphenes (small white circles of light)[55, 67]. From these clinical trials we can be confi-

dent that existing approaches in the developments of a prosthetic device are, although in their infancy, viable.

A key parameter in the development of a prosthesis is determining the number of cells that need to be successfully stimulated in order that the host will perceive an improvement in the visual sensation (the cellular structure of the eye is detailed in chapter 2). Recently it has been suggested that the number of retinal ganglion cells needing to be stimulated by a prosthetic device is of the order of 625 (which is significantly below the 1,000,000 ganglion cells found in the adult retina) with increases above this value offering, as we would expect, increasing visual awareness [49, 50]. The fabrication of micro-electrode arrays to have 625 stimulating sites in an area the size of the retina is currently well within fabrication capabilities. The power consumption of the electrodes and localised heating of the surrounding cellular tissue is likely to limit the maximum number of electrodes at this time [71].

Approaches to develop retinal prostheses can be separated into 3 categories depending on which part of the visual system they couple to. Firstly, there are those which look to reconstruct the retinal function by coupling optical sensors directly to the retina, epi- and sub- retinal implants. This approach requires the greatest remaining functionality of the visual system. Secondly, those which bypass the retina and couple devices to the optic nerve, the communication link between the retina and the brain. Thirdly, those which stimulate visual cortex region of the brain directly [83].

Each approach at developing a prosthetic described previously looks to deliver an electrical signal to biological tissue. The arrangement of the cellular tissue in each of the 3 cases is significantly different. For retinal implant devices, the cells are relatively 2D in arrangement, typically 3 cells deep [1]. For the devices that look to stimulate the optic nerve, they have to be cuff shaped and stimulate cells which are contained in a cylindrical formation. And finally, to stimulate the visual cortex region of the brain, a device which offers full 3D stimulating capabilities is required [61].

1.2.1 Retinal Implants

Of the 3 approaches described, retinal implants benefit greatly from having the easiest access to neurones of the visual pathway. As such, the surgery required to deliver an implant to the desired location is the least difficult. Situated at the rear of the eye, a functional retina has an area of approximately 5cm^2 of optically activate tissue. Once the retina is subject to a visual scene, chemical interactions occur which relay this information as electrical pulses to the brain [27]. The information contained in the visual scene is coded as trains of spikes both spatially and temporally [131, 132, 133]. If the retina is degenerate, the ability to convert the optical scene to an electrical representation is compromised.

However, if the output cells of the retina are still functional (see figures 2.1 and 2.3), there exists a means of passing electrical signals to the brain even if these signals have to be generated outwith the retina. Thus, a digital imaging system coupled to the retina serves to represent the optical scene in

an electrical form. This information is then passed to the optic nerve in a manner which is common for processing by the brain.

The 2D arrangement of cells in the retina has the potential to couple individual cells directly to a microfabricated detector array. This allows the possibility of high resolution detectors with high precision to utilise much of the surviving neuronal cells.

1.2.2 Optic nerve implants

Optic nerve implants utilise cuff electrodes that surround the 10^6 cells found in the optic nerve [64]. This technology is disadvantaged by the difficulty in stimulating spatially isolated cells. Any applied electrical signals will predominantly have an effect on the outer cells of the optic nerve first in addition to cells found further inside. At this time it is unknown if enough cells can be stimulated independently to allow for useful vision. It benefits from being less invasive and of a lower clinical health risk than direct brain stimulation and is less likely to detach than retinally stimulating devices.

1.2.3 Deep brain stimulation

The most direct approach to restoring vision comes from stimulating the visual cortex. This form of visual restoration requires the least amount of pathway function but has the biggest ethical consideration. Fortunately the visual cortex extends inwards from the surface of the brain and is therefore considered an accessible region [61]. The visual cortex is a 3D structure. Although there are currently 5 reported distinct functional layers, this number

could be as high as 15. The area of the visual cortex is subject to change depending upon the degree of visual sensation. A realisable visual prosthesis for brain stimulation must be able to access the discrete layers of the brain and be fixed in position post surgery.

Several groups are looking at stimulating the brain directly and the Doherty institute has had clinical trials in place for almost a decade [16]. There are 2 approaches currently under investigation, the first is surface mounted electrodes that stimulate the visual layers via increased electrical stimulation currents and secondly by the use of 3D probes, “bed of nails” which are implanted deep in the visual cortex. Each of the “nails” has multiple stimulation or recording sites along its length and as such can access the 3D structural layers of the cortex [17, 18]. Results from brain monitoring using the 3D arrays has given rise to the understanding of local cortical field activity and have allowed for the determination of stimulation parameters that have led to the perception of phosphenes of light through direct electrical stimulation [16]. Patient numbers are low, and Doherty has implanted only 1 patient with surface mounted electrodes.

1.3 A flexible microelectrode array for in-vivo retinal prostheses

As has been established, there are many possible approaches for retinal prosthetic implants. The approach I have undertaken is for epi-retinal stimulation

of the retinal ganglion cells. A process has been developed for the manufacture of flexible microelectrode arrays which can accommodate the curvature of the retinal surface and couple electrically with the biological tissue [1]. In addition, through collaboration with the Rutherford Appleton laboratories an Active Pixel Sensor (APS) has been developed as the optical detector. The eventual aim is to bond directly the APS onto the flexible microelectrode array. As this PhD has looked to develop the proof of concept processes and detector for the next generation of implant this has not been the primary focus. It is envisaged that the next generation of the technology will successfully realise this.

Our flexible microelectrode arrays utilise a commercially available polyimide, PI2545 for the substrate and encapsulation layers as it is biocompatible and compliant with microfabrication techniques [128]. The availability of a world-class research cleanroom facility at the University of Glasgow has enabled the development of multielectrode arrays. Collaboration with the Rutherford Appleton Laboratory (RAL) has realised a functional APS photodetector for our studies. Work undertaken at the University of Glasgow's Institute for Biomedical and Life Sciences has successfully shown that we can record and stimulate in-vivo retinal tissue in the *Rana Temporaria* frog [1]. It is likely that the ability to record large volumes of data from experiments with ever increasing stimulation electrodes will be a key issue in the long term development of neuroprosthetic devices. As the number of stimulation sites increases the correlated response from the biological neural network on a larger scale can be recorded and as such the understanding of the complex

processing involved in the biological system can be derived. The successful experimentation using the frog retina for this thesis is significant as the neuronal cells are comparable in size to the cells found in the human retina. In this way it can be expected that thresholds for stimulation of the frog retina will be similar to those for human retinal tissue.

This thesis reports the success of developing flexible arrays which are suitable for stimulating and monitoring retinal neuronal ganglion cells. The characterisation of an optical detector suitable to replace the optical sensitivity of the retina is presented and the results from in-vivo biological testing is also shown.

The manner in which light enters the eye and is converted to electrical pulses suitable for representation of a visual scene in the brain are presented in Chapter 2. The electrical representation of a light evoked response from biological tissue is discussed. The functional layers of the retina and the way the microelectrode arrays couple to the cellular layers are described. The key functional concepts of the eye are explained and the way the engineered devices can best describe them is presented.

The process by which the arrays are fabricated is described in chapter 3. The multistage processing steps required to realise a multi-site flexible recording array is explained. The electrical characteristics of the array electrodes are shown. The scalability of the fabrication process is outlined as we develop the number of active electrodes from 8 to 74.

In chapter 4 the IPIX APS detector is described and characterised. The IPIX chip is mounted on a specifically designed PCB connected to analogue and digital lines through wire bonds. The frequency output response of the detector to varying light intensities is shown and the output under mono-phasic and bi-phasic output settings is verified. The pixel to pixel uniformity and crosstalk levels are measured. The peak to peak pulse height levels are confirmed and we show that the maximum output level of 3.3V is in excess of what is required for successful stimulation of retinal tissue. It is demonstrated that the APS detector can be successfully operated from external applied voltage pulses and from the internal operative master clock.

The success of the microfabricated arrays for in-vivo studies is presented in chapter 5. Results from experimentation indicate the success of the device in coupling to the biological tissue and hence its suitability for recording and stimulating retinal cells. Analysis of the experimental data shows that a SNR in excess of 18 is readily achievable and verify the techniques employed in preparing the biological tissue. The ability to initiate responses from retinal ganglion cells to varying input pulse characteristics and derive a threshold voltage for stimulation of 400mV for pulse durations of 1ms is presented. It is also shown that by increasing the applied voltages the number of cells stimulated increases accordingly.

Finally, in chapter 6 I conclude the results from the studies undertaken for this thesis. The successful development of a flexible substrate microelectrode array of less than $20\mu\text{m}$ has been achieved for 8 and 74 electrode arrays.

The platinum electrodes exhibit impedances of typically $20\text{k}\Omega$ and $50\text{k}\Omega$ at 1kHz as shown. Optimisation of the current densities for electrodeposition of the platinum electrodes was experimentally realised at $4\text{nA}/\mu\text{m}^2$. The inter-channel resistance between the fabricated channels was measured at $90\text{G}\Omega$ with inter-channel capacitance of 0.3pF . This results in discrete recordings from independent electrodes with no observable electrical crosstalk between channels.

The preparation of the retinal (*rana temporaria*) tissue allowed for excellent electrical coupling between the array electrodes and the biological tissue. As a result signal to noise ratios of 25:1 were achieved upon recording activated retinal cells. From the high level of confidence in detecting actual retinal tissue response we then looked to electrically stimulate the tissue to determine threshold responses. For the successful stimulation of retinal cells using arrays developed by the processes stated in this thesis it is concluded that a voltage level of 400mV was the minimum voltage required to stimulate an action potential response from retinal ganglion cells. By applying voltage levels above this we conclude that we are able to activate and record action potential responses from cells distant to the activation site.

The development of an application specific pixel detector, the IPIX, allowed for the reproduction of electrical output waveforms consistent with typical action potential responses upon detection of light across a 10×10 array of $100\mu\text{m}$ pixels sensors. The output frequency of the waveforms in response to the light stimulus incorporated the 1ms bi-phasic nature of typ-

ical action potentials with a period and amplitude which could be varied as required. The amplitude of the output waveform from the chip can be raised to a maximum level of 3.3V, in excess of what has been previously described as necessary. The combination of the variable period and amplitude of the response is seen as an important functional characteristic as we look to incorporate the internal processing undertaken by the retina. In addition, the possibility to utilise the neural networking architecture of the chip will further compliment the application of the chip towards retinal prosthetic development as understanding of retinal processing develops.

1.3.1 Overview of thesis objectives

The first step for any retinal prosthetic device is to develop a procedure for the successful fabrication of the key components. The fabrication of microelectrode arrays, which couple electrical systems to the biological tissue, will be presented for planar flexible substrate materials conforming to the curvature of the retina, these are intended for in-vivo placement.

The development and characterisation of an optical detector specifically tailored to meet the demands of a visual prosthetic device will also be presented. The fabricated device will have an optically sensitive matrix of 10x10 pixels. The design of the device is such that the electrical output from these light activated pixels will be in a form typical of a normal biological system.

Finally, I will use my developed microelectrode arrays to record light activated responses from retina. I will look additionally to stimulate the retina electrically with independent electrodes on the microelectrode array of waveforms typically recorded from the in-vivo light response studies. From this, a optimum or threshold condition for the electrical stimulation parameters can be established.

Chapter 2

Theory

The retina is best described in three discrete layers for our approach to engineer a prosthetic device. The first layer, the optically sensitive biological tissue of the retina, the rods and cones, convert the incident visual scene into electrical waveforms. Once the optical scene is detected, the output from the retina is transferred through three cellular layers to the optic nerve via the retinal output cells, the ganglion cells. We assume the pathways from the ganglion cell outputs of the retina to the visual cortex are intact, see Figure 2.1. The ganglion cells represent the 3rd layer of our retinal model. The remaining consideration is the processing undertaken between the photoreceptive cells and the ganglion output cells. The intermediate processing between the cells in this layer are compounded to be the 2nd layer of our engineered model with the processing represented by a neuronal network.

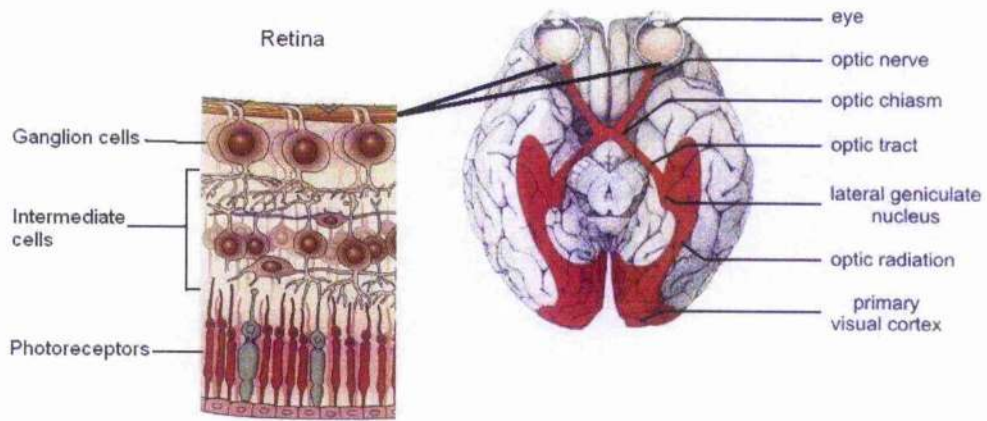


Figure 2.1: Diagram of Visual pathway showing the eye, optic nerve and visual cortex on right hand diagram. Exploded view of the retina is shown on left.

Having described the layers of the retina as a 3-stage system our engineered approach to representing this systems also is described in 3 levels. The optically sensitive rods and cones are represented in our engineering approach by a 10x10 array of active pixels. The output waveform of the pixel sensor is based upon previously recorded data from a light activated retina [1, 5]. The next step was to incorporate functionality associated with the processing undertaken between the photoreceptors and the ganglion cells on the pixel array and this is achieved via a computer controlled neural network. Finally, the detected and processed information must be coupled to the existing pathways of the retinal tissue, the ganglion cells, and this is achieved through microfabricated electrode arrays.

This chapter outlines the functionality of the retina, the physiological steps that govern the detection of an optical image and how this is electrically represented by neurological signalling. The processing undertaken by the retina to achieve this conversion is outlined as is the approach to reconstruct this system via microengineered “intelligent” pixellated optical detecting devices. I highlight the considerable engineering success achieved and the difficulties experienced in implanting and controlling adequate coupling between the array and the retinal tissue surface.

The feasibility of our approach to develop a retinal prosthesis should become apparent. The underlying technologies used in developing our retinal prosthesis are in some instances well known with the others developed specifically for this project. The approach undertaken in this thesis to combine knowledge of existing particle physics pixel detectors with micro-engineered and neurobiological systems as a complementary system is novel. Hopefully the information presented within this chapter will convince the reader that the question of “when” an implant will be available is more appropriate than “if” such a device will ever be useful as an approach to reconstruct vision.

2.1 The Eye.

The human eye is an exceptionally complex pixellated detector detecting both colour and monochromatic vision. It does so at approximately 25 frames per second. It is a direct outgrowth of the brain and is easily accessible through

careful surgery. Owing to the complexity of the functional aspects of the eye, only a brief overview is provided with more detailed sections on areas of specific interest to the project. Several of the concepts presented in this chapter are derived from a lecture course presented by Dr. J. D. Morrison of the Institute of Biomedical and Life Sciences at the University of Glasgow.

2.1.1 Structure of The Eye.

The sclera and cornea provide the outermost protective layers of the eye and consist of layers of collagen, see figure 2.2. The significant difference between the transparent cornea and the opaque sclera results from the orderly arrangement of collagen. The sclera is penetrated by the optic nerve and the ciliary nerves at the rear of the eye, which circle the optic nerve at the junction.

The iris (Godless of the Rainbow) is an extension of the choroid (a tissue layer rich in blood vessels that supplies oxygen and nutrients to the photoreceptor layers of the eye) and forms the pupil (deriving from pupilla meaning little girl), an aperture of variable diameter controlled by the of smooth muscle cells in the iris. The iris is coloured depending on whether the posterior surface only is pigmented (blue eyes) or both the anterior and posterior surfaces are pigmented (brown eyes). Circular smooth muscles form the sphincter pupillae and act to constrict the pupil (miosis) while radial muscle form the dilator pupillae are responsible for the dilation of the pupil (mydriasis).

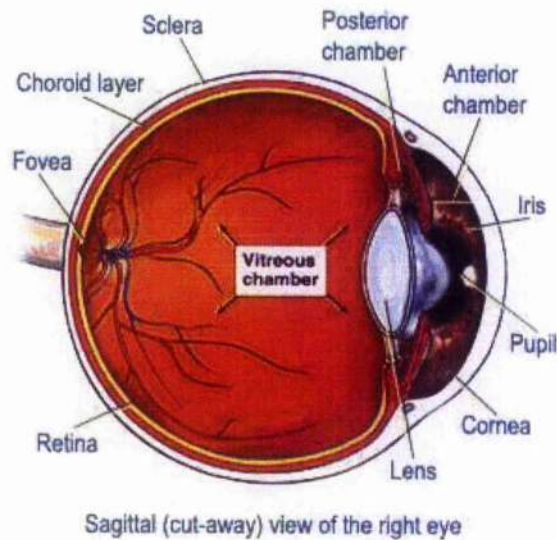


Figure 2.2: Schematic cross-section of the eye, highlighting the key functional components.

The optical elements of the eye, including lens and cornea, attribute an optical power of +55 dioptres (optical power = $1 / (\text{focal length})$) and are responsible for the focussing of light from the outside world onto the retina. The lens fine-tunes the focus and ensures the sharpness in visual acuity. The human retina covers an area of about 5 square cm and is situated approximately 18.2 mm behind the lens of the eye. Visual images incident on the retina are more commonly referred to in terms of the arc that they subtend as opposed to their height and distance. By this notation, 1 degree of arc spans a distance of $290\mu\text{m}$ across the retina on average.

2.1.2 The Retina

The retina consists of ordered layers of tissue that can be found coating the rear inner surface of the eye. Functionally, the retina converts incident light into a series of electrical signals (similar in concept to a digital imaging camera). Once the electrical signals are generated they propagate through the layers of the retina before being passed along the optic nerve to the visual cortex region of the brain. On propagating through the various layers of the retina, there are known to be several processing functions that occur and which act to converge the output from the 10^8 optical sensory elements (rods and cones) to the 10^6 output cells of the retina (ganglion cells). There is a key functional distinction between the rods and cones in that the rods function in dim light, scotopic vision, whereas the cones are responsible for bright light or colour vision, photopic vision.

A point to note at this stage is that only the photoreceptors, the rods and cones, are responsible for representing the visual scene. A very small number of ganglion cells are light responsive however are involved only in maintaining circadian rhythm. Whenever reference is made to the stimulus of other cell types, it is important to note that this has included a response from the photoreceptors (or via our externally generated representation of these electrical signals) and is concerned with the elicited electrical response that follows.

2.1.3 Physiology

The retina (a net) consists of a combination of neural layers that are an outgrowth from the brain (diencephalon innermost). The development of the retina is observable at very early stages of foetal development. The retina can be thought of as consisting of two primary parts (of combined thickness $300\mu\text{m}$): the pigment epithelium (PE) and the neuronal layers, see figure 2.3. (There are five classified neuronal species found in the retina; the photoreceptors, ganglion cells, horizontal cells, bipolar cells and amacrine cells).

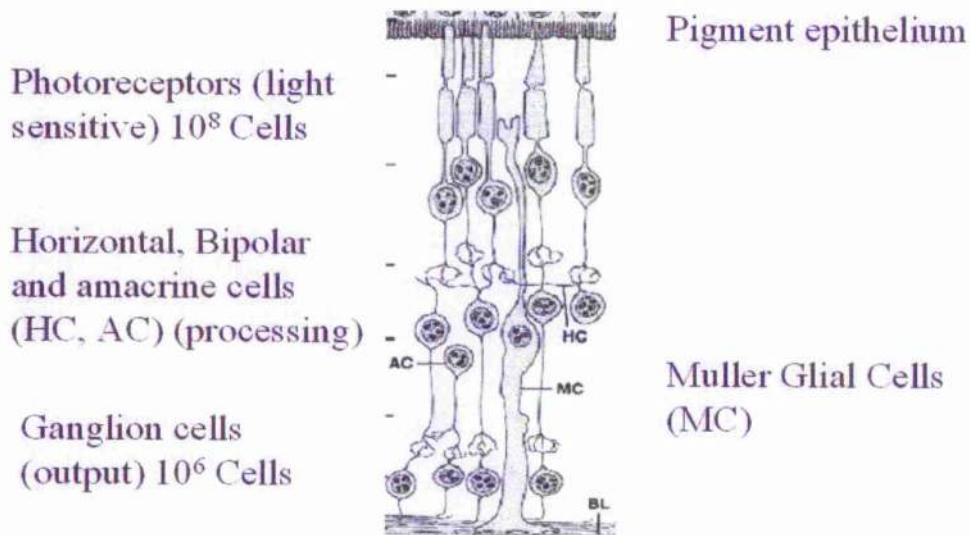


Figure 2.3: Schematic of the retina showing five classified neuronal species found in the retina and the layered structured of the cellular tissue.

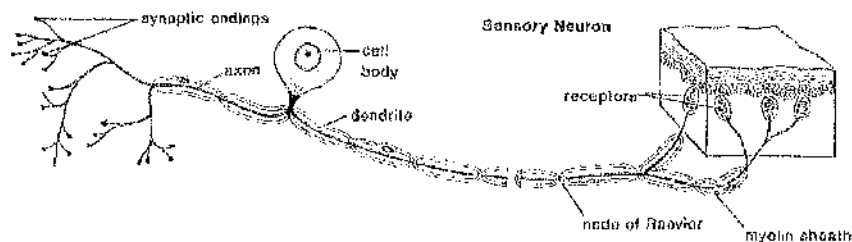


Figure 2.4: An example of the connections between a sensory neuron, the cell body and the synaptic endings. The axonal connection is a fast acting link that conveys the information between the cells. (Image from www.biologymad.com)

Adjacent to the PE exist the photoreceptors which are linked to the ganglion cells via bipolar neurons. Retinal neurones are arranged in discrete layers with the cell bodies of the photoreceptor cells forming the Outer Nuclear Layer (ONL), the cell bodies of the bipolar cells form the Inner Nuclear Layer (INL) and the cell bodies of the ganglion cells form the Ganglion Cell Layer (GCL). Between these layers are the plexiform layers which contain dendrites, narrow branching projections from the neuronal cell bodies. The dendrites receive impulses from the axons of other neurons and feed this to the cell body.

There are many cell types found in the discrete layers of the retina. Most important to this study are; Horizontal cells, laterally orientated in the INL, amacrine cells which connect between bipolar cells and ganglion cells.

There is considerable importance associated with the Muller Glial cells

which envelop all the neurones and their processes acting as a discrete insulating layer. They extend from the photoreceptors to the inner margin of the retina.

The ganglion cell layer forms an important layer for this project. The ganglion cells are the output cells of the retina and feed the information incident on the photoreceptors to the optic nerve via axonal interaction, see figure 2.4. In turn, the optic nerve feeds information to the visual cortex of the brain. Histological sectioning of the human retina reports around 10^6 ganglion cells feeding the optic nerve. In terms of our ambition for a retinal prosthesis we need the connections from the ganglion cells to the visual cortex to be intact. This is why we envisage our prosthesis being best suited to Age Related Macular Degeneration and Retinitis Pigmentosa [108]. Recent investigations have shown that the effect of degeneration on the ganglion cells is greater in subjects with RP than AMD though preservation of ganglion cells still exists. [109]

It seems counter intuitive that the set-up of the retina appears to work as an apparent 'back-propagation' system. The light must travel the depth of the retina to reach the rods and cones. The reason for the retina's seemingly inverted architecture is that the photoreceptors require a continuous supply of oxygen and a means to remove debris from the continually regenerating rods. Thus the retina evolved with the rods and cones positioned close to the blood flow found at the rear of the retina or at the pigment epithelium.

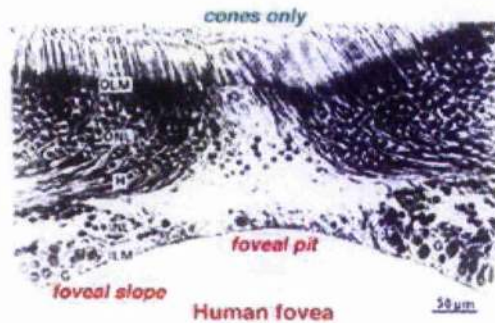


Figure 2.5: A image of the human retina showing the fovea, photoreceptors and the displacement of cellular tissue around the foveal pit.

2.1.4 The Fovea

Within the retina there exists a pit of radii 5 degrees. This pit is a characteristic of all primate retinæ and is an area of increased cell density, an area centralis. Generally the smallest neurones are found in this area centralis with dendritic tree and axonal diameter increasing at increased eccentricity. Primate fovea develop a further dimpling between 18-45 months after birth and the area centralis is exposed via the displacement of neurones in the ganglion cell layer (GCL) and inner nuclear layer (INL). This exposes the foveal photoreceptors directly to incoming light and increases their light sensitivity (as shown in Fig 2.5).

Within the central 2 degrees of the fovea, the only photoreceptors that are present are cones (responsible for colour vision). In the primate fovea, the cones are very slender to increase the packing density and are $1\mu\text{m}$ in

diameter with an inter cone spacing of $0.5\mu\text{m}$. It is this fine mesh that is the essence of our visual resolution. Outwith this area centralis the diameter of the cones increase and rods become involved in the visual sensation.

In general, the photoreceptors of the eye hyperpolarise when subject to light stimulus (the strength of the electric field across the cell is increased). The amount of hyperpolarisation that occurs depends logarithmically on the intensity of the input stimulus and lasts as long as the stimulus remains (negating the effects of retinal adaptation) [81]. Retinal adaptation occurs in the presence of a continued intensity background luminosity. Under such conditions the retina “adapts” to the background and extracts the variation in intensity as a percentage of the background. In this way the retina maintains its visual acuity across several log units of intensity range. For this reason the response of the cells is often called a graded potential.

2.1.5 Rod Function

The process by which light entering the eye is absorbed by rod photoreceptors and mediates an electrical response to the brain is explained only in brief here and in detail in [24, 40, 41, 75, 78] and the following section, section 2.1.6

A rod is has four primary components, an outer segment which connects to the pigment epithelium (PE), an inner segment, a cell body and a fast acting synaptic terminal which connects the rod to the neural pathway leading to the optic nerve and the brain, see figure 2.6. The outer segment contains

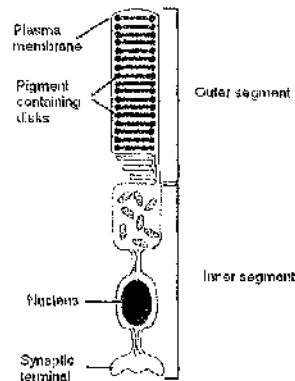


Figure 2.6: A schematic image of a human rod cell indicating the outer segment, inner segment and the synaptic terminal. The outer segment connects to the pigment epithelium.

a stack of disks that are continually replaced and ensures the health of the photoreceptor. The disks and the surrounding membrane contain rhodopsin (also known as visual purple, and is the photo-reactive protein stored in rod cells of the retina) which constitutes 85 per cent of the total amount of protein present in the outer segment. Rhodopsin is a rod specific opsin (a spectrally selective protein which accounts for spectral sensitivity) which is responsible for photosensitivity. Photons entering the eye are absorbed by the cis-retinal with the transduction cascade catalysed by the high concentration of rhodopsin.

Once the light has been detected the information is passed through the layers of the retina, see fig 2.3 for diagram. The first synapse involved is that

between the photoreceptors and the bipolar cells and is activated through the neurotransmitter glutamate. This information is correlated with that passed between the horizontal cells (which pass information laterally across the retina between photoreceptors) found at the connection between the photoreceptor / bipolar interface. This is the first step in processing the image from the high number of photoreceptors to the factor of 100 less ganglion cells. The bipolar cells then make connections with the ganglion cells in the inner plexiform layer. The inner plexiform layer has amacrine cells which connect across multiple ganglion cells and mediate the input from the bipolar cells. After this stage of processing, the ganglion cells become active and a signal is sent along the optic nerve [40].

The key contribution to RP derives from the shedding of the outer disks contained in the outer segment. If the shedding of the disks is either over-active or disrupted then the delicate renewing process of the photoreceptor becomes imbalanced and the onset of RP is likely.

2.1.6 The cellular resting potential

The fundamental relationship between ion concentration and the potential of a cellular membrane is defined by the Nernst equation which was published in 1888 [189]. Nernst derived this equation from statistical mechanics and it was later incorporated into the Goldman-Hodgkin-Katz. The derivation of this equation is outlined in the following text as it helps outline the processes

involved at the cell surface [105]. These processes are fundamental to action potential formation and an understanding of this is crucial to this thesis.

Consider a cell with a high concentration of a positively charged ion S inside and a lower concentration of ion S outside which are separated by a membrane permeable only to ion S. Owing to the large concentration gradient across the membrane ion S will diffuse out of the cell. The diffusion of ions down a concentration gradient is explained by Fick's first law:

$$M_{diffs} = -D_s \frac{dc_s}{dx}$$

Where M_{diffs} is the molar flux density of ion S (due to diffusion), c_s is the local concentration of S and D_s is the diffusion coefficient of S. As the diffusion of ion S from the inside of the cell to the outside occurs, the outside of the cell becomes more positively charged with respect to the inside of the cell. This movement of ions is defined by the electrophoretic (Drift) equation:

$$M_{drifts} = -\mu_s c_s \frac{d\psi}{dx}$$

Where M_{drifts} is the molar flux density of ion S (due to drift), μ_s is the mobility of S in the membrane and ψ is the potential of the membrane. The equations for diffusion and drift combine to give the overall molar flux density:

$$M_s = -D_s \frac{dc_s}{dx} - \mu_s c_s \frac{d\psi}{dx}$$

In order to get the current from molar flux you must multiply by the valence z_s of the ions, and Faradays constant.

$$I_s = -z_s F D_s \frac{dc_s}{dx} - z_s F \mu_s c_s \frac{d\psi}{dx}$$

where F is Faradays constant, R is the gas constant (8.314 J/mol K), and T is the absolute temperature

Using the Nernst-Einstein relationship,

$$D_s = \frac{\mu_s RT}{z_s F}$$

and substituting this into the current represented form we obtain a common form of the Nernst-Planck Equation:

$$I_s = -z_s F D_s \left[\frac{dc_s}{dx} + \frac{z_s F}{RT} c_s \frac{d\psi}{dx} \right]$$

By now setting $t=0$ as we are interested in the steady state condition

and integrating across the width of the membrane we obtain the Nernst Equilibrium Condition:

$$\Psi_i - \Psi_o = -\frac{RT}{z_s F} \ln \frac{[s]_i}{[s]_o}$$

Where Ψ_i is the potential inside the cell, Ψ_o is the potential outside the cell $[s]_i$ is the concentration of ion s inside the cell and $[s]_o$ is the concentration of ion s outside the cell.

The use of the Nernst equation is limited to determining the potential for a single type of ion. There are multiple types of ions at a cell membrane interface and the equilibrium potential depends on the permeability of the membrane and the concentration of ions. The membrane potential in this case is represented by the Goldman-Hodgkin-Katz equation where E is the equilibrium resting potential:

2.1.7 Neuronal Functionality and the Action Potential

Primary neurobiology investigations in the literature were concerned with the movement of ions across the cellular membrane and the resulting change in potential. It is a direct result of this change in potential that all cellular mechanisms are controlled.

Any living cell has a surface membrane called the plasma membrane.

$$E = \frac{RT}{F} \ln \frac{[A]_o P_A + [B]_o P_B + [C]_o P_C}{[A]_i P_A + [B]_i P_B + [C]_i P_C}$$

Where [A], [B] and [C] correspond to the relative concentrations of ions A,B and C and "i" and "o" indicate either inside or outside of the cell respectively. The notation A,B and C represent the ions of interest and P is the permeability of the cell membrane for a specified ion. The highest permeability of a cell membrane at rest is for potassium hence the resting potential approximates to the Nernst approximation for potassium.

This membrane separates the intracellular environment from the extracellular environment. A further membrane is concerned with the nuclear region and so is termed the nuclear membrane. Although each type of membrane tends to act as an impenneable barrier to the flow of ions there exist aqueous pores deriving from the presence of proteins that permit specific transitional ionic species across the membrane. The thickness of the membrane governs the transmembrane potential. Historically the potential is referenced to the outside of the cell and, for a small cell, is temporally uniform across its surface to within 100 pico-seconds [116]. The transmembrane potential for cells found in the retina is typically in the range of -50 to -80mV, see figure 2.7.

Should there be a sudden increase in the charge potential (resulting from a flow of ions) across the membrane the magnitude of the voltage across the membrane is also altered. This gives rise to a more negative transmembrane

potential. In this instance, the cell has become hyperpolarised. Should there exist a sudden decrease in the charge potential then the cell is deemed to depolarise. The change in charge potential results from ionic transfer through an aqueous pore and a corresponding redistribution of charge. It is this electrotonic spread which conveys information across the bulk of the cell.

Aqueous pore channels are not the only way in which ions can traverse the membrane. There exist pumps and exchangers which exhibit other methodologies for variations in membrane potentials. For our studies however, the aqueous pores provide the ionic channels of interest, more specifically, they are responsible for the existence of voltage-gated ionic channelling.

With the electrotonic distribution of charge, parts of the cell contain channels that are adapted to sense this fluctuation in electric field and open or close in response to it. Cells containing channels which respond in this way are called voltage-gated ionic channels. There are two types of voltage gated channels both acting in response to depolarisation of the cell. When the depolarisation is sufficient to open the first of these channels, sodium ions travel from a relatively high concentration outside the cell across the membrane. The flow of positive charge further reduces the charge separation across it causing further depolarisation. In response, the second type of voltage gated channel acts to reduce the magnitude of the depolarisation by the slow opening of the potassium ion channel allowing the flow of the ions out of the cell. Ionic channels are common to all cells, though in neurons they respond to the variations in the transmembrane potential.

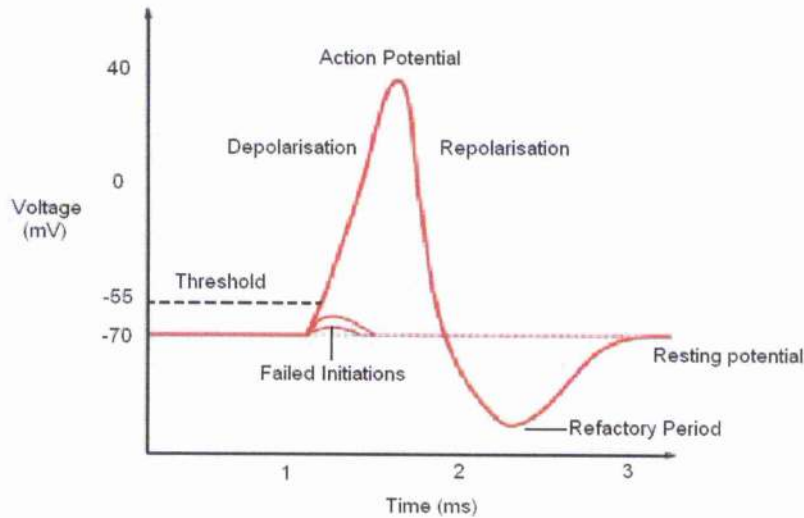


Figure 2.7: A schematic of an action potential (referenced intracellular). The resting potential is commonly -70mV and peaks at $+40\text{mV}$ when an action potential occurs(modified from <http://z.about.com>).

The electrotonic signal is experienced very locally and does not allow the propagation of information over long distances. However, axonal connections allow the neuron to pass information over longer distances. The combined effect of the voltage gated channels and the presence of the axon is what gives rise to a measurable action potential from ganglion cells. Crucially, for the production of action potentials depolarisation of the transmembrane potential must occur.

Once the action potential has been realised, the sodium and potassium levels are restored by the influence of pumps and exchangers. Molecular

pumps contained in the membrane push the sodium ions out of the cell and thus allow the potassium ions to recover in the cell. Exchangers primarily affect the flow of calcium and use the energy gained from the flow of the sodium and potassium ions to provide the energy for the transfer.

Given the physical process of spike train production from the chemical interactions involved above, the significance of how this spike train information relates to a visual scene is pertinent to the development of the image reconstruction. When exposed to a time varied stimulus it is known that the ganglion cells respond with an initial brief cluster followed by a sustained period of inactivity [13]. If the data is analysed historically over many trials then the clusters of spike trains can be seen to occur reliably on occasion to within 1ms. Coincidentally, the spike clusters that are produced are not only reproducible in their timing but also in the number of spiking activity per cluster. It is suggested, though not published, that the key parameters in the spike clusters for the representation of the visual scene are the timing of the initial spike resulting from the optical stimulus and the number of spikes contained therein, but not the timing between spikes for the event. If this result indeed holds true then it simplifies the requirements for spike train deployment into the visual pathways from our fabricated arrays [111].

2.2 Diseases

From section 1.1 we know there are many diseases that affect the functionality of the retina including vascular, inflammatory or infectious. For our approach in developing a retinal prostheses we require the functionality of the pathways, irrespective of the cause, post-photoreceptors, to be maintained.

Both AMD and RP are photoreceptor degenerative diseases that affect the visual system as it ages, more specifically where it ages outwith the normal aging process. Both diseases more prevalent in persons aged over 50 years. AMD and RP are respectively the main forms of blindness in the western world. AMD affects 1 person per 100 over 65 with this number reaching 1 in 8 of those over 85. RP affects approximately 1:3500 persons over 65 with 10 per cent of those becoming registered blind each year [128].

2.3 Prosthesis

The understanding of retinal function is a prerequisite to the possibility of restoring sensory input to the visual pathways. To achieve a retinal prosthesis we are constrained by engineering capabilities and neuronal requirements. The extent the visual system will adapt to an “engineered” input is largely unknown. It is therefore essential that we ensure our approach mimics closely the observed outputs of retinal ganglion cells, even though this may prove to be “over-engineered”.

There are various approaches when attempting to restore the functionality of the retina, each exhibit advantages and disadvantages. At this stage, there is little evidence to suggest which will prevail in the eventual goal of realising a retinal prosthesis. In primitive terms the optical system can be divided into the detector (the retina), higher order processing (visual cortex, brain) and the intermediate connection (optic nerve). Electrical stimulation of any of these elements has been seen to offer some sensation of vision [13, 14, 22]. This is reported as the perception of phosphenes (generally annular areas of increased light intensity for the subject). Stimulation of the optic nerve is unlikely to be able to offer the position sensitivity required for functional vision given the 3D geometry of the cellular layer. Direct brain stimulation has ethical opposition and considerable consequences for surgical complications. Retinal stimulation is hoped to provide the required spatial awareness and a minimal safety risk, though is limited to repairing retinal degeneration only.

2.3.1 Implanting

For the retinal prosthesis to be viable, a means of coupling effectively and consistently with the retinal output cells must be achieved. The process of implanting a device must be compliant with the environment of the surrounding retinal tissue and non-agitating. The device must therefore be self contained and surgically robust. For our manufactured devices this is a future consideration. However, we have been aware of these requirements and the fabrication process has incorporated miniaturisation capabilities (an ability to reduce the feature size yet maintain yield) needed for realisable retinal im-

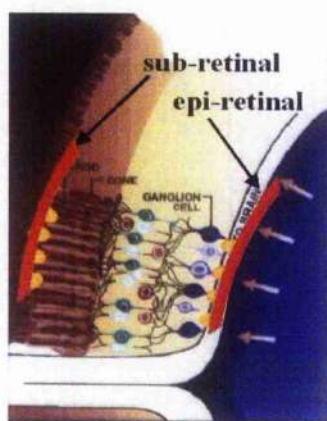


Figure 2.8: Schematic of the surgical locations of a sub-retinal and epi-retinal implant. (Note the lack of external connections).

plantation from the engineering outset. Fig 2.8 shows the locations of retinal implants either sub-retinally or epi-retinally.

A means of ensuring that the implanted device will remain in absolute position irrespective of eye movement or cranial shock is of paramount importance. The possibility of implementing surgical tacks that will fix the implant in position has been adopted by Humayun et al.[29, 35]. Other approaches include placing the array between the retina surface and the inner lining membrane [113]. Either of these approaches could be eventually realised in our final array design and research in this avenue will prove which is likely to offer the most suitable method for future implants.

2.3.2 Biocompatibility

An important consideration for implanting devices in the body is that the host will not reject them. The considerations for biocompatibility are discussed in more detail in chapter 3, sections 3.2.1 and 3.2.8 and in references [7, 9, 89, 91]. Fundamental requirements are that the device must be of a size allowing for adequate positioning on the retinal surface and provide long-term functional benefit post surgery.

The physical process of inserting any form of neuroprosthesis is likely to initiate the bodies natural defence mechanisms (in the short term post surgery). Careful attention must be given to ensure that no excess inflammatory response from the host is likely. In addition, the material of choice for the implant must not initiate an immune response and hence a likely rejection mechanism from the host.

2.3.3 Heating

Given the active pixel sensor is an electrically powered device, there will exist local heating around the implanted array as the device dissipates power. The amount of heat released could be of significant impact in terms of the effect on retinal cells. Alternative approaches are underway (in other research establishments [67]) to accommodate external imaging devices and pass the detected and processed image to an implanted array of electrodes [3, 16, 29].

Typically this is achieved using eye glasses with imaging cameras substituting the lens. This removes problems of electrically powering the optical detector at the retinal surface and therefore benefits from removing any unwanted localised heating of the retina. Detected information could either be hard wired to the electrode array through a small incision at the side of the retina or alternatively, RF coupled through the use of wound wire coils. Both these solutions have their associated problems but provide a suitable solution in the first proof of concept designs.

The aqueous humour of the retina will offer some heat sinking capacity for the active pixel sensor. The amount of heating that can be dissipated in this way may not offer a suitable temperature gradient to accommodate the local heating of the IPIX chip however. It has been reported [71] that a temperature increase of 0.4°C at the retina surface may well degrade its lifetime although more recently [134] that 0.7°C may well be tolerable. It is also likely that if the temperature increase is too great, the rate at which the waveforms are pulsed onto the retina can be reduced which will correspondingly reduce the power requirements and hence localised heating at the retinal surface.

2.3.4 Cellular Coupling to the Electrode Arrays

In order that a suitable electrical signal can be presented locally to the retinal surface, sufficient coupling between the electrode array and the retinal cells must be established. If the array is not coupled directly to the ganglion

cells of the retina then the signal from the stimulation or recording site will be dissipated across a residual fluid layer. If the array is positioned on the retinal surface with too much pressure then it is possible the cells will be damaged.

Achieving the optimal condition for coupling relies heavily upon the flexibility of the electrode array. Primarily the substrate provides the major mechanism for affecting the overall flexibility of the arrays. Previous attempts at fabricating devices by the process outlined in section 3 has seen the use of kapton polyimide substrate materials from $7.5\ \mu\text{m}$ to $125\ \mu\text{m}$ thick. The thinner substrates proved through previous engineering experience to be very difficult to fabricate on due to the need to use vacuum positioning tables at various stages in the processing. The thicker substrates were more susceptible to neural tissue damage when moving into contact (epi-retinally, see figure 2.8 for location) with the retinal tissue, see figure 2.9 for location of the IPIX array on the flexible substrate material and represented schematically in the eye. However, by utilising multilayer methods of spinning polyimide (P12545), we were able to control directly (and in sub $2.5\ \mu\text{m}$ steps) the thickness of the substrate layer and these problems were largely overcome. This is outlined in more detail in Chapter 3 section 3.4.

The quality of the interface between the electrodes and the retinal surface can be determined by utilising the recording capabilities of the arrays. If the retina is stimulated by light and the electrodes detect suitable signal strength action potentials (Signal to Noise Ratio, SNR, greater than 10), the

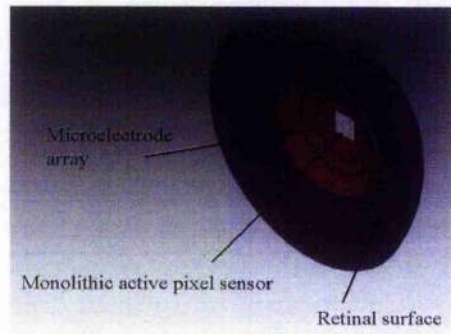


Figure 2.9: Schematic of the surgical locations of the Epi-retinal IPIX (monolithic active pixels sensor) chip implant on the flexible microelectrode array. Although the exact position of the IPIX chip is variable it does indicate a likely position for future in-vivo implantation (Note the lack of external connections).

coupling can be assumed to be good. Detection of an Electroretinogram (ERG) response at this stage also indicates the health of the retina. This method gives confidence in the success of the retinal preparation and the positioning of the array before electrical stimulation studies are undertaken.

Should there be a lack of signalling from the retina then there exists the possibility of repositioning the array on the retinal surface. This may be necessary on occasion due to the possibility of fluid layers being trapped between the retinal surface and the arrays. If this is the case then the fluid layers can be absorbed mechanically from the surface before the experimentation is repeated. In these studies, due to the adsorption of oxygen from

the atmosphere and the cold-blooded nature of the frog, the preparation will remain viable for a few hours increasing the opportunity of successful experimentation.

2.4 Neural Computation

The neural computations performed by the retina are extremely complicated processes. This processing is immediately apparent when comparing the number of output cells, the ganglion cells, to the optically sensitive cells, the photoreceptors. We find there be a factor of 100 less ganglion cells than photoreceptive cells in the retina [188]. The processing is further complicated given that there are many cell types that perform different tasks. There are cells which respond to the onset of light, on cells [77], cells which respond when light stimulus is terminated, off cells, cells that detect motion only in one direction [81], cells that detect only the edges of objects and cells that respond only to either red, green or blue light.

Each of the cell types can be identified by providing a selective visual stimulation. Once the cells have been identified, differing stimulation patterns can characterise their function [86]. The difficulty is in ascertaining what computations are applied by the visual system when multiple stimulation sites are activated. Moreover, determining what cell types are coupled to proximal electrodes is often not obvious [85].

Given the presented difficulties, the ability to incorporate coding algorithms to the detected image, allowing pre-processing of this information before passing to the retinal surface, should allow increased effectiveness. There has been a large volume of research into neural networking algorithms with many forms specifically focussing on the retina [37].

2.4.1 Overview of the proposed technological model

A system has been developed that couples electrically microfabricated micro-electrode arrays to biological tissue. In achieving this it is possible to monitor the output of the biological tissue in response to known light stimuli. The recorded activity recorded in this way can be used to programme the output of a specially developed pixel detector.

In this study a 10x10 monolithic active pixel sensor (IPIX) has been developed to mimic the photoreceptors of the retina for a prosthetic device. The electrical signals generated by the IPIX chip are designed to create output action potential waveforms from ganglion cells (using microelectrode arrays) in response to incident light.

Through successful development of the required microfabrication techniques and success of the IPIX chip when evaluated, it was possible for me to develop a proof-of-concept system using $5\mu\text{m}$ and $50\mu\text{m}$ stimulating and recording electrodes. The electrodes were seen under experimentation to couple extracellularly, with high cellular precision, to ganglion cells of the

retina. It was possible to achieve signal-to-noise ratios that were routinely in excess of 18:1 (see section 5) for the fabricated electrodes whilst recording from retinal cells. As a result of this success, a platform has been realised that will allow for the coupling of microfabricated microelectrode arrays and electronic detector technologies that mimic retinal response.

The design of the hexagonal close packed electrode geometry offers the highest packing density of electrodes onto the retina surface and hence the highest possible realisable visual acuity. Finally, through the effective recording of large volumes of experimental data the ability to decipher the wiring diagrams of the retina becomes a possibility and therein the opportunity to develop more appropriate neural network algorithms becomes a reality.

Chapter 3

Fabrication

3.1 Introduction

In recent decades micro fabrication technologies have been in ever increasing demand by consumer electronics markets. As such, they have been subject to exceptional technological advancements. Realisation of miniaturised devices coupling highly resolved and spatially controlled features has enabled the possibility of applying this technology to the biological sciences (more specifically in the field of neuronal experimentation) and has become a multidisciplinary research interest.

There has been significant research interest in the application of multiple micro-electrodes towards the study of retinal function [3, 4, 5, 129, 134, 1, 123, 102]. Previous to the application of microelectrode arrays, research recorded single unit responses using micro pipette patch clamping (a thin glass tube heated and stretched to form a needle like tip of a few microns

diameter), but until recently there has been not existed the capability of looking at global retinal responses by such means. Fabricated microelectrode arrays offer a key advantage over patch clamping technologies as they require only one surgical step for positioning yet allow for the monitoring of multi-unit responses through a 2-D array of multiple recording sites. This multiple recording capability allows for increased functional understanding as the interconnected pathways of the retina are probed.

An additional benefit of the fabricated microelectrode arrays is the ability to use some of the electrodes to apply a controlled electrical pulse directly to the retinal surface [57]. This allows the opportunity to apply a known waveform directly onto the cellular tissue and measure, in-vivo, the neuronal response. Hence, there is the opportunity to measure both the response of light activated retinal tissue from the array recording electrodes and to electrically activate retinal tissue using the stimulating electrodes. This gives an opportunity to determine correlated stimulation thresholds. The correlation of the optical response of the retina (more specifically the ganglion cell bodies) with an electrical response is central to any future work on retinal prostheses. With the microelectrode arrays we can monitor responses from electrically activated neurons through nearest neighbour recording electrodes and hence evaluate the respective threshold currents. This will further aid neurobiologists to develop an increasingly more detailed understanding of retinal functionality through measuring correlated functionality. Eventually this will enable the possibility of electrically stimulating the retina in a discrete high density manner thus offering the possibility to restore some form

of useful vision.

There is considerable diversity in the fabrication methods and materials chosen for development of microelectrode arrays [5, 167, 168, 169, 170] and each address a different technological challenge. Many devices are fabricated on solid materials such as indium tin oxide or silicon which offer the possibility of high electrode counts due to highly planar substrates and excellent compatibility with existing microfabrication technologies. They are however unable to accommodate any curvature normally found in neuronal clusters for implantation be it the retina or other area of the central nervous system and therefore they would be unable to maintain good cellular coupling in this instance. My choice of flexible polymeric substrate material addresses this issue.

In comparison to other flexible microelectrode arrays that have been developed [171, 172, 173] the careful control to the scalability requirements allows the arrays I have developed to realise high yields of devices with $5\mu\text{m}$ electrodes. This greatly exceeds the work in the field especially at the high electrode counts realised in this project.

This section outlines the procedure for the fabrication of microelectrode arrays as used in neurobiological experimentation. In developing the array fabrication procedure I was keen to satisfy biocompatibility, flexibility and scalability demands. In achieving this it is envisaged that the fabrication process will remain viable for arrays with increased electrode counts and

densities as required for future higher density studies. The photolithographic processes are outlined and the experimentally realised microfabricated arrays presented.

3.2 Material biocompatibility

A key issue in the design and fabrication of our arrays has been to implement biocompatible materials. The scientific community has a great deal of interest in this issue and, as a whole, suffers from the problem that materials technology develops faster than the standards that governs biocompatibility testing can accommodate. The International Standards Organisation (ISO) has produced a series of documents (10993 series) [112] that govern the biological requirements for an implant prior to clinical trials. A generally accepted definition of what we should expect for biocompatibility is the ability of our chosen material to perform with an appropriate in-vivo response for a specific biological application [7]. More specifically, this definition can be sub-divided into key components and an implant can be considered biocompatible if:

- It does not induce a toxic, allergic or immune system response.
- It does not destroy or harm enzymes, cells or tissues.
- There is no evidence of thrombosis (formation of a solid mass of blood) or tumours.
- After extended periods of implantation there exists no evidence of fibrous tissue encapsulation or rejection.

Even under guidance of the above definition, biocompatibility is still disputed and very much depends on the application of interest. Critically, because the immune response and repair functions of the human body are complicated, there are no single set of tests that can offer positive conclusions under all cases. In some cases the surface properties of the materials are crucial to the biological success of the implants and this is especially true if you require tissue to adhere to the device, whereas in other applications it is more the physical properties (size, shape, stiffness) that are the major determinants of biocompatibility especially if located on a peripheral limb and likely to be subject to damage.

One of the many problems in ascertaining biocompatibility is to specify likely reaction mechanisms and define the impact on the functionality of the implant. This, coupled with the challenges in defining tests that can simulate repeatedly the biological reactions, presents serious issues in the availability of suitable qualified materials. For the development of microelectrode arrays it is important to ensure biocompatibility at the design stage such that the maximum achievable biological safety, functionality and stability can be realised.

The most common materials for substrate or surface encapsulation are epoxy resins, polytetrafluoroethylene, silicon rubbers and polyimides. The polymers have proven to be biocompatible, insulating and stable upon long term implantation in the retina of rabbits and dogs [7, 9, 45]. They also experience very little gliosis, or proliferation of tissue which naturally encapsulates

any foreign body prior to rejection. They also benefit from tolerance to sterilisation techniques including autoclaving at 120°C and the use of high power UV sterilisation techniques. A secondary advantage rests with the ease of fabrication of these materials and that they allow for bulk and surface modifications through micro-engineering to increase their biocompatibility and flexibility as implants [52, 54, 88]. Another proven material for biocompatibility is silicon nitride [42] (SiN) which possesses excellent tolerances to the fabrication techniques used for industrial miniaturisation. Silicon nitride, however, is a very rigid material and cracks when flexed. As such it is not a suitable material for a flexible in-vivo implant.

3.2.1 Electrode Biocompatibility

For microelectrode array recording electrodes, Platinum has proven to be the material of choice due to its inert and stable nature [11]. It has been suggested [180] that even after extended periods of implantation the amount of potentially hazardous platinum ions released into the surrounding tissue may be neglected. When stimulating cells using platinum electrodes, it has been seen for our fabricated 5 μ m diameter electrodes that platinum operates close to its charge injection limit (which relates the maximum amount of current that can be injected for a given pulse duration) of 200 μ C per cm² measured using a 1ms (500 μ s / phase) pulse. The charge density measured from experimentation with varying size electrodes is shown in Figure 3.1. The measurements were made by placing the array in a bath of isotonic saline and passing bi-phasic waveforms of 500 μ s per phase with varying amplitude

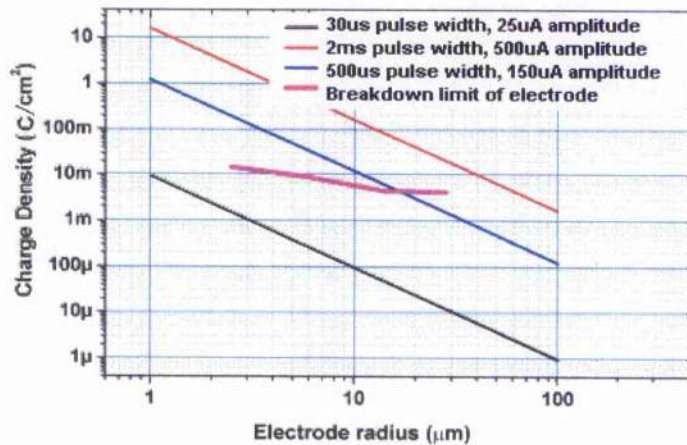


Figure 3.1: Measured charge limit for electrodes of varying size. The applied pulse was $500\mu\text{s}$ per phase and of varying amplitude until degradation was seen. The Red, blue and green lines correspond to a simulated electrode.

through the electrodes. The waveform at which an increase in impedance was measured on the electrode was taken to be the limit for the electrode, or commonly called the breakdown limit. The maximum safe limit was taken as being 1/10th less than this value.

Iridium is also a material of interest as it builds up a stable surface oxide coating. The main benefit reported is an increased charge injection limit which permits larger possible stimulation currents [72, 80, 90, 97]. This minimises the possibility of any surface changes occurring from the electrical activity. Aside from current injection limits it is important to maintain the voltage levels below 0.6V as this has been seen in experimentation to cause the electrolysis of water and the evolution of hydrogen with the evolution of

oxygen occurring where a voltage of 0.8V has been sustained [14].

A further issue of biocompatibility concerns the effects of permanent sustained charge injection into the neuronal cells. It is known that sustained electrical stimulation can damage tissue with gliosis (proliferation of connective tissue or glial cells), calcification (deposition of calcium salts) and astrocytes (one of the main supporting cells of the central nervous system) [9]. Absence of damage to neuronal cells can be expected if the charge density remains below $100\mu\text{C}$ per cm^2 [191]. What is evident from our electrodes is that their charge injection capacity, measured using $500\mu\text{s}$ per phase pulse across various electrode sizes, is well in excess of the limits that neuronal damages is suggested to occur for stimulation. The charge density that was measured is in excess of what is commonly reported in literature and is likely to result from a short testing period. If extended periods for determining the damage threshold were used, it is likely that the value measured would be more in agreement with published results [191, 190].

Part of developing new technologies is to evaluate risk properties generated by implantation in a worst case scenario. If for any reason the body either rejects the implant or infection occurs, the health of the host becomes a concern. From this view the approach to reconstructing vision from a retinal stimulation site provides significant benefits over cortical implants. Should infection or rejection occur in the retina it is localised in an area which should not provide any significant threat to the longevity of the host, the same confidence is difficult to apply to cortical implants.

3.3 Lithography

Lithography is the means by which a predetermined pattern can be transferred selectively by masking material commonly referred to as resists (an intermediate polymer material). A pattern can be transferred onto the resist by altering the photoreactive resist material via light illumination or alternatively by bombardment with focussed electron beams. For many years optical lithography (OL) has been the dominant technology, see fig. 3.2. Advances in the spatial resolution achievable by optical pattern transfer has involved moving into the high Ultraviolet or extreme ultraviolet optical region. This involves specialised and costly optics which have been offset in part by advances in developing materials allowing high contrast at lower wavelengths. The technology of electron beam lithography has allowed feature resolutions in the region of 5nm. The main constraint of electron beam lithography is primarily the pattern transfer time. More recent developments however have seen the application of multiple beams to overcome this limitation. There are five main criteria on which to base the selection of appropriate lithographic techniques; cost, throughput rate, scalability, resolution and overall flexibility. Although these factors are not of paramount importance in a research environment, the limitations of scalability, flexibility and resolution have impacted the project as we endeavoured to accommodate wafer fabrication techniques.

3.3.1 Photolithography

Optical lithography is typically subdivided into either contact and projection. Both have advantages depending on the application. Contact lithography

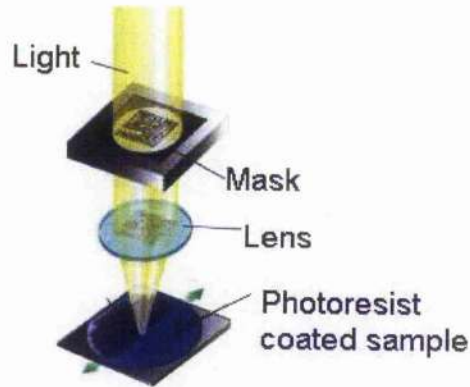


Figure 3.2: Photolithographic mask transfer using projection masking. The lens allows for the reduction in size of the image while the wafer below is stepped to pattern the whole area. In contact masking, the lens is absent and the mask is in contact with the substrate material with light incident normal to the surface.

as the name suggests brings the mask and the resist into contact before illumination by the source. Projection utilises a series of lenses (fig 3.2) to project the mask detail onto the resist material. Contact printing offers a repeatable and cost effective method of resolving features of a few microns although can suffer from defect contamination when multiple samples are being masked.

The mask detail and the volume of samples processed at any time for the purposes of this project favoured contact printing. Fabrication was undertaken on a Karl-Suss contact mask aligner for 8-electrode arrays with

good success. The registration size, the factor governing how close subsequent layers can be aligned is approximately $5\ \mu\text{m}$ with a resolution, using Shipley S1818 photoresist, of approximately $2\ \mu\text{m}$. For 74-electrode arrays and for 3-inch wafer fabrication of the 8-electrode arrays, a Karl Suss MA6 mask aligner was used realising registration of approximately $1\ \mu\text{m}$ with the resolution limited to $2\ \mu\text{m}$ by the Shipley photoresist of choice.

3.3.2 Electrode Array Layout

The initial studies for the project involved the development of an 8-electrode array (2 columns of 4 electrodes) designed with a minimum feature size of $50\ \mu\text{m}$. This was chosen principally to develop a process that could be used for the next generation, higher electrode count designs.

For the final design of the electrode array there was a requirement for stimulating and recording sites on the electrode array. The layout of the electrodes in this instance was for a hexagonal close packed design as this would allow the highest uniform packing density. It also allowed each of the stimulating electrodes to be surrounded by 6 neighbouring recording electrodes. A single large electrode was included in the design to be used as a reference or earth electrode.

3.3.3 Photolithographic Mask Design

Key to the realisation of optimised experimental data is the careful attention to detail at the mask design stage. For the purposes of this project various designs were required. The proof of concept for neuronal signal recording was achieved by an 8-electrode 50 μm minimum feature mask design. Once the recording capabilities were repeatably realised the final design for the reduced feature size, 5 μm , 74-electrode array, which incorporated stimulating electrodes, was written as a photolithographic mask plate.

Design of the photolithographic mask plates was undertaken using L-Edit design software. On completion of the mask design it is written using e-beam lithography to ensure maximum resolution and minimum defect levels. Once the design was written and the mask plate complete, a working copy would be made and the original stored. This allowed further copies to be made quickly should the mask become damaged. It was important to optically examine the mask as defects introduced onto the mask would likely have a severe impact upon the quality of the fabricated array at any later stage.

The final versions of the mask designs looked to improve the volume of samples that could be achieved in any fabrication run by using 3-inch wafer substrates. The large increase in area offered by the wafer allowed 5 8-electrode arrays per run and significantly reduced the fabrication overheads.

3.4 Device fabrication procedure

For the fabrication of the arrays I used Pyralin PI2545 polyimide, an established high temperature polyimide coating used for a variety of microelectronic applications [128]. The factors governing this choice of material are that it is:

- compliant with microfabrication techniques.
- flexible (with this a variable depending on the number of spun layers).
- largely hydrophobic.
- insulating.
- biocompatible.
- of acceptable density (inertial constraints).

The material also has a semi-transparent appearance under optical illumination which proves useful for failure analysis and quality control of the multi stage fabrication procedure.

3.4.1 PI2545 Polyimide preparation

The PI2545 is stored in a freezer at -18°C to increase the shelf life (approx 1 year) and a suitable volume must be allowed to warm to room temperature and decanted from the storage vessel. This increase in temperature aids in the out-gassing of bubbles introduced during the decanting process as well as decreasing the viscosity. The method of spin coating a film of polyimide

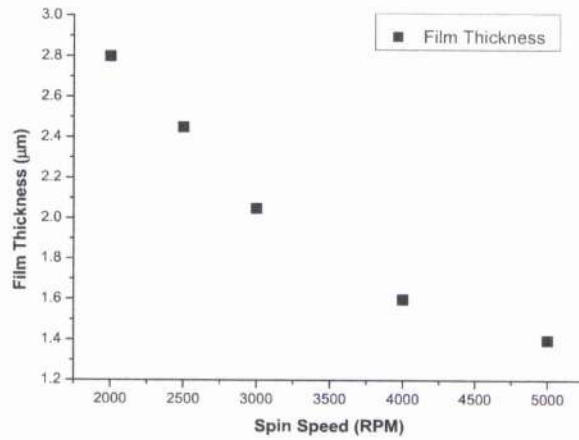


Figure 3.3: Polyimide spin speeds vs. layer thickness

requires the application of liquid polyimide onto the centre of the sample. When the sample is spun, the centripetal force causes an even spread of the liquid polyimide across the sample surface. All bubbles must be removed from the liquid polyimide as during the spin coating process, the bubbles cause 'comet' like streaks in the surface film. Should bubbles continue to be present once a suitable temperature of the bulk polyimide has been achieved, placing in a vacuum chamber (under low vacuum) will complete the outgassing process. When the decanted polyimide has been elevated to room temperature, control of the spin speed will repeatably control the thickness of the spun layers. Multiple layers are achievable in this way allowing for control of the overall polyimide substrate thickness. Once at room temperature the life of the polyimide is reduced to a few days in the uncured state.

To ensure uniformity of the layers a polished 3 inch, 300 µm thick silicon

wafer is used as a substrate. This wafer is used as a platform for the fabrication process as the silicon is robust, flat, conforms with our processing steps and is in good supply. The wafer plays no part in the final array and is removed as the final step in the fabrication process. To begin the process of spinning the polyimide layers, the silicon wafer is cleaned ultrasonically in deionised water and rinsed with acetone and finally Isopropanol. Next, the liquid polyimide is applied to the wafer surface and given a few seconds to settle. Thereafter, controlled stepping of the spin speeds realises a uniform layer to within $0.2 \mu\text{m}$. Figure 3.3 shows the effect of spin speed on the film thickness. All films were spun initially at 500 revolutions per minute (RPM) for 10 seconds before ramping at 200 revolutions per second until the desired spin speed was realised. The initial spin at 500 RPM for 10 seconds allows for a thick and non-uniform polyimide coverage of the wafer surface. The final ramp to 2500 RPM is stepped over 10 seconds before being allowed to spin for 30 seconds. Once the spinning of the polyimide is complete, it is placed on a hot plate for 2 minutes at 140°C to soft bake, or initially cure the polyimide. After this bake cycle, further layers can be applied in the same manner to achieve the desired thickness.

A feature of spinning multiple layers is 'beading', a build up of material on the outer rim of a spun sample as a result of surface tension. It is important that the amount of beading is minimised when multiple layers are required as the progressive build up of beading can compromise the contact between the applied photoresist and mask during the patterning process. One method of reducing this, is to bring a swab lightly doused in acetone into contact with

the rim of the sample while spinning the surface layers. The results of this method prove to be adequate for successful fabrication of the MEAs (Micro Electrode Arrays).

After the polyimide layers have been applied and the initial soft bake of the sample (on the hot plate) is complete it must be oven baked in a nitrogen atmosphere. The oven bake cycle requires the sample to be held at 100°C for 1 hour and slowly ramped at a rate of 4°C / minute until 200°C where it remains for 30 minutes. The final ramp to 350°C, again at 4°C / minute is then the final cure (imidization) stage and is held for 1 hour. Careful control of the cooling rate, which must also be limited to 4°C / min, is required to minimise any possibility of introducing stress into the film and allow for safe handling of the fully cured film. In the fully cured state, the films are tolerant to microfabrication processing.

3.4.2 Method for evaluating film thickness and surface roughness

A key parameter affecting the flexibility of the microelectrode arrays is the thickness of polyimide that is used. The thicker the polyimide the less malleable to the retinal surface it becomes.

In order to address the issue of the thickness of polyimide applied and ensure repeatability, a protocol for spinning the layers was employed, as described in section 3.4.1. The measurements of the surface roughness and the film thickness were undertaken using a DekTak surface profiler. For each

spin speed, a layer of polyimide was spun on a piece of silicon and fully cured. The layer was then cut in half and half removed by mechanical peeling from the surface of the silicon wafer. The step profile could then be measured from the surface profiler (this was repeated 5 times for each layer). This was repeated several times for each sample and is in good agreement with the results published in the material datasheet.

For our chosen thickness, 5 layers were spun on the wafer surface at a speed of 2500 rpm resulting in a total film thickness of $12.5\mu\text{m}$. The film uniformity at this stage was measured to be uniform to within $0.2\mu\text{m}$ for the bulk material with an increase in thickness at the outer rim of the sample due to a small effect from beading. The surface roughness at this stage was not detrimental to the fabrication of the devices and after low power oxygen plasma treatment offered excellent adhesion for metal deposition.

The adhesion of metals, both gold and titanium, were excellent and no problems were observed as long as the correct protocol of $4^\circ\text{C} / \text{minute}$ ramp rate was observed and a vacuum chuck holder similar in size to the silicon wafer was utilised. In instances where this was not the chosen procedure small cracks could often be seen across the sample surface.

3.4.3 Metal Deposition

The choice of metals used in the fabrication of the microelectrode arrays must ensure scalability, flexibility and biocompatibility. With this consideration, the metals of choice are gold (which is inert, highly flexible and can be easily

removed with chemical etchants) and titanium (offering flexibility at thickness of a few 10's of nm and highly definable using dry etching techniques). These metals are standard in most metal evaporators and offer controllable film thickness, to the level of a few 10's of nanometres.

Prior to the deposition of metals, the surface of the cured polyimide film was roughened to promote adhesion [99]. The roughening of the surface (increase in the surface energy) was achieved via a low-pressure oxygen plasma discharge, known as ashing. The sample was placed horizontally in the barrel of the ashing chamber and the chamber evacuated of atmospheric gasses. A nitrogen flush was undertaken before filling the chamber with oxygen. An electrical discharge was initiated to abrade the sample surface for 4 minutes. The ashing time was optimal at 4 minutes with any further increase in time seen to degrade the adhesion of the metal to the surface of the polyimide film.

The deposition of the gold and titanium metal layers were undertaken using a Plassys MEB450 electron beam evaporator. Samples were mounted horizontally with their source-sample distance large compared to the feature sizes. In this way, the evaporator can be considered unidirectional with deposition of metal normal to the surface. The rate and thickness of the deposited metals were controlled by an intellemetrics IL900 quartz crystal monitor to an accuracy of +/- 5 percent.

For arrays of minimum feature size $50\mu\text{m}$ a seed layer of 30nm titanium

preceded a 150nm layer of gold to promote adhesion. For feature sizes less than 50 μ m a single titanium layer between 130 and 150nm was deposited. The reasons for the dual layer metal deposition on the larger feature size devices is that we can remove thick layers of gold quickly (approx. 2.5nm / sec) through wet chemical etching techniques. A thicker layer of gold is preferred to a thick titanium layer due to the availability of liquid chemical removal (wet etching, see section 3.5.2) and given the increased tolerance to flexing over titanium. Also, it is a noble metal and does not form a surface oxide readily unlike titanium.

3.5 Etching techniques

Etching is the means by which we remove unwanted metal regions through the application of lithographic steps. The correct choice of the etching technique is governed by the feature size, metal utilised and to a lesser extent the substrate material. Metal layers are etched selectively by correctly applying chemical species to the surface. This can be in the gaseous form, dry etching, or in the liquid form, wet etching. Both have relative advantages and limitations and for our process steps these are outlined in the following two sections.

3.5.1 Dry Etching

Dry etching utilises ions in a gaseous mixture to remove unwanted metal regions. The physical aspect of the etch is increased by the application of a DC bias between the loaded sample and the gas input vents which accelerates the ions. A second method of increasing the physical nature of the etch is through a controlled increase in the gas pressure within the chamber. It is common that the chamber may contain several gasses at any one time with the ratios of gases in the chamber also affecting the etching rates and the resulting etch profile. Standard processes have been employed for the etching of the titanium [5, 20, 82].

The distinct advantage offered by dry etching metal layers over other etching techniques is the feature sizes that can be resolved. In a perfect situation, the incoming accelerating ions can be assumed to contact the sample perpendicular to its surface. This in theory would result in vertical profiles of the side walls on any remaining metal layers. In essence this negates the possibility of thinning the horizontal features as material is removed in the vertical direction only. In practice there is some slight lateral etching but the effects are negligible for our feature sizes. The under etching in the horizontal direction becomes important where you have an aspect ratio (depth of etch to surface feature width) of approx 10:1. This ratio can be increased through careful process control under optimal conditions to achieve 20:1 or more. This therefore is the preferred method when feature sizes below $10\mu\text{m}$ are required and gases for the etching process are available.

3.5.2 Wet Etching

In the wet etching process the ions are in liquid form. The process of etching in this instance is limited to chemical interactions and does not benefit from the added physical impact of accelerated ions in the perpendicular direction (as in dry etching). Again we have chosen metal layers where the etch chemistry is well known and available in our laboratories.

In terms of the realisable feature sizes that can be achieved, wet etching is limited in comparison to that of dry etching. However, wet etching has several advantages over dry etching:

- Cost.
- Ease of use.
- Wide range of readily etchable metals.

The main limitation of etching in this way is that the chemical removal of metals is not limited to the perpendicular direction but has a significant parallel (or horizontal) aspect to the etch. This is often obvious as a thinning of the remaining features. The amount of thinning is dependant on the thickness of the metal layers and some control can be applied at the metal deposition stage to limit this effect. Where the aspect ratio of the features to be resolved is less than 10:1 the process of wet etching is quick, efficient and proves to be a very valuable and reliable technique.

3.5.3 Patterning the metal layers

Once a suitable choice of metals has been deposited the required microelectrode array pattern must be transferred. This requires the selective removal of unwanted metal regions. Many options are available for this and the most suitable for our needs is to employ a positive photoresist (a material that is photoreactive). The positive resist allows for a direct copy of the mask detail onto the metal surface, whereas a negative resist (if it were used) would give the inverse of the features on the mask.

The metal deposited on the substrate surface is typically spin coated with Shipley S1818 photoresist and the resist is baked in a 90°C oven for 30 minutes. A spin speed of 4000RPM for 30 seconds results in a film of thickness 1.8 μm .

Once the photoresist has been baked and the mask detail transferred by illumination under an intense UV source, the sample is flushed in developer solution (1:1 ratio of concentrated developer with RO water) exposing the unwanted region of the metal layer. The metal layers can be selectively etched to adopt the patterned profile of the remaining photoresist. For the 8-electrode arrays, the gold is wet etched using a potassium iodide solution and the seed layer (adhesion promoter) of titanium etched using a 1:27 diluted solution of Hydrofluoric Acid (HF) and de-ionised water. The etch rate for gold is 2nm per second and titanium of the order 3.5nm per second. To

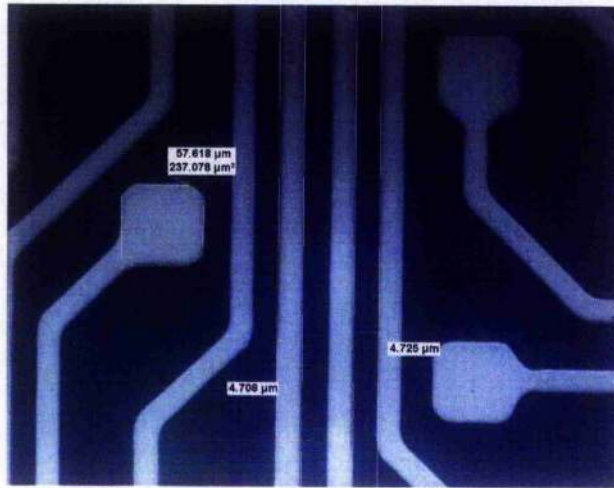


Figure 3.4: An image of microfabricated titanium on polyimide substrate material.

ensure that no unwanted material remains a technique of over etching is employed and typically we add between 10 and 15 percent to the minimum calculated etch time. The 74-electrode array ($5\mu\text{m}$ min feature) has the titanium etched using SiCl_4 in an Oxford Instruments System 100 plasma dry etching machine. The parameters are 18mtorr, 9 sccm and a forward RF power of 250W. An example of the microfabricated titanium as used in the 74-electrode array can be seen in Fig 3.4.

Once the mask detail has been etched from the metal layer, the remaining photoresist must be removed. We remove the photoresist by either;

- Flood exposure in UV light and then developing
- An acetone rinse

-Gentle agitation in n-butyl-acetate solution.

3.5.4 Surface encapsulation and vias opening

Once satisfactorily cleaned, the final two layers of polyimide are applied in the same way as the substrate layers. After oven baking the polyimide, a layer of photoresist, AZ4562 (a thicker resist than S1818) is applied and patterned such that the electrode regions and bond pads are defined for the etching process. For the $5\mu\text{m}$ minimum feature size 74-electrode array the polyimide is etched using a dry etch $\text{C}_2\text{F}_6/\text{O}_2$ plasma in a ratio of 80/20. For the 8-electrode arrays the polyimide is left soft baked at 200°C and rinsed with developer solution, which wet etches the $50\mu\text{m}$ vias in the surface layer [51]. The final process for the fabrication is to remove the photoresist and ensure the layers are baked to 350°C . Figure 3.5 shows an example of a 74-electrode array which has been surface encapsulated and has had the vias etched through the surface passivation layer. The electrode shown in the magnified image, at the top right of Fig 3.5, shows a typical form for electrodeposited platinum.

Once the fabrication has been completed, the arrays are removed from the silicon carry wafer by mechanically peeling the layer or by immersion in deionised water. The arrays are then cut to the desired shape and are ready for connecting to the amplification circuitry. Figure 3.6 shows a photograph of a full 74 electrode array removed from the silicon carry wafer.

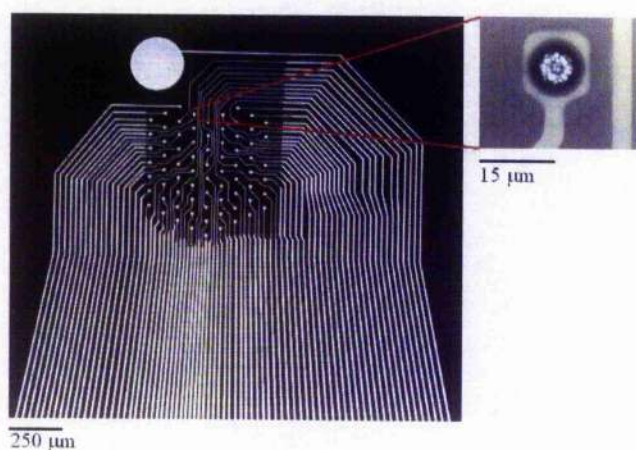


Figure 3.5: An image of the 74-electrode array post surface encapsulation and vias opening. The small image, top right, gives a high magnification view (x50) of a single electrode. This electrode has been electrodeposited with platinum.

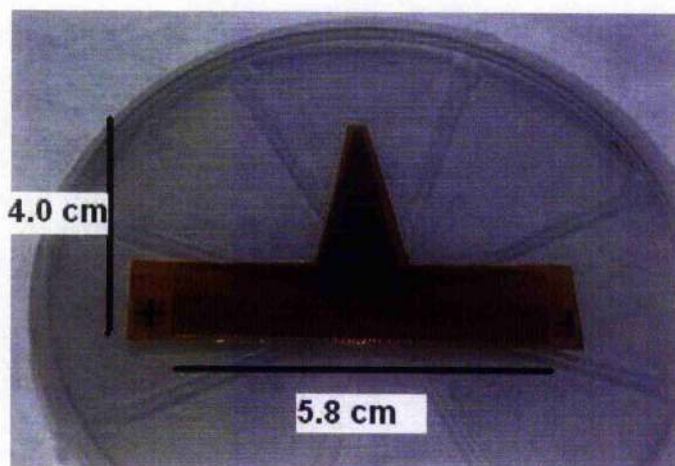


Figure 3.6: An image of the full 74-electrode array post surface encapsulation, vias opening and removal from the silicon carry wafer.

3.5.5 Platinisation of electrodes

After fabrication of the microelectrode arrays, the impedance of the gold electrode sites are measured at 1kHz and 100mV (using a HP4274A LCR meter) and are of the order of a few $M\Omega$, see fig 3.7 and 3.8 for a schematic representation of the measurement technique for 8 and 74 electrode arrays. For neuronal signal detection and stimulation studies this value must be significantly reduced. There are several ways to reduce the impedance and the most common techniques include; the electrodeposition of a higher surface area material, modification of the surface profile through etching and deposition of iridium (which then undergoes cyclic voltametry) [30, 72, 88, 90, 98]. To achieve the reduction in impedance we employed the electrodeposition of

platinum.

The electrochemical deposition of platinum from an aqueous solution, with careful control of the current limits, results in a porous structure. The porous structure achieves an increase in surface area with respect to the geometric area. Commonly the porous structure is referred to as platinum black due to the visibly dark nature of the electrode, fig 3.9 shows the experimental arrangement for the deposition of platinum from an aqueous solution of platanic chloride solution (74 electrode array). The platinum black electrode satisfies biocompatibility requirements although for long term stimulation the electrode may suffer some degradation [93, 95].

For the electrochemical deposition of platinum black, a solution of 1% platinic chloride, 0.08% lead acetate and 98.92% RO water is prepared and a small volume carefully applied over the electrode region. A platinum wire is also immersed in the solution which dissolves (upon current flow) to ensure a constant concentration of Pt ions in solution as they are deposited on the electrode surface. The electrodes are held at a negative potential with respect to the platinum reference wire thus attracting the freely moving positively charged platinum ions from the solution.

Initial attempts at growing the platinum electrodes utilised a voltage

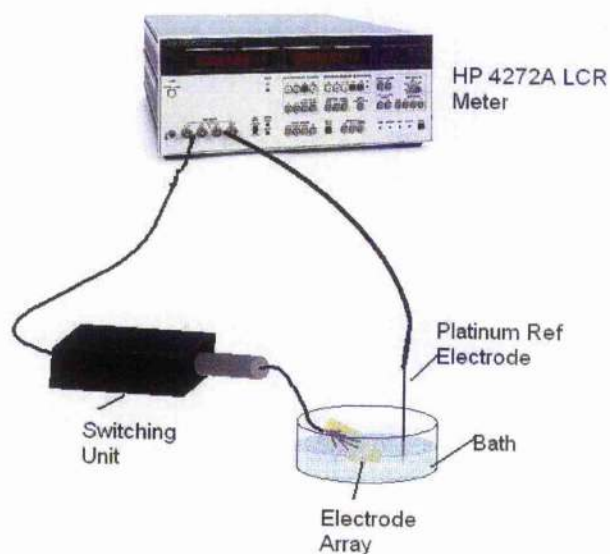


Figure 3.7: A schematic showing the measurement technique for the determination of the impedance values for the 8 electrode arrays. The switching unit for the 8 electrode array activates a single channel at a time and allows for the measurement of the 1kHz, 100mV impedance value. The bath is filled with buffered saline solution.

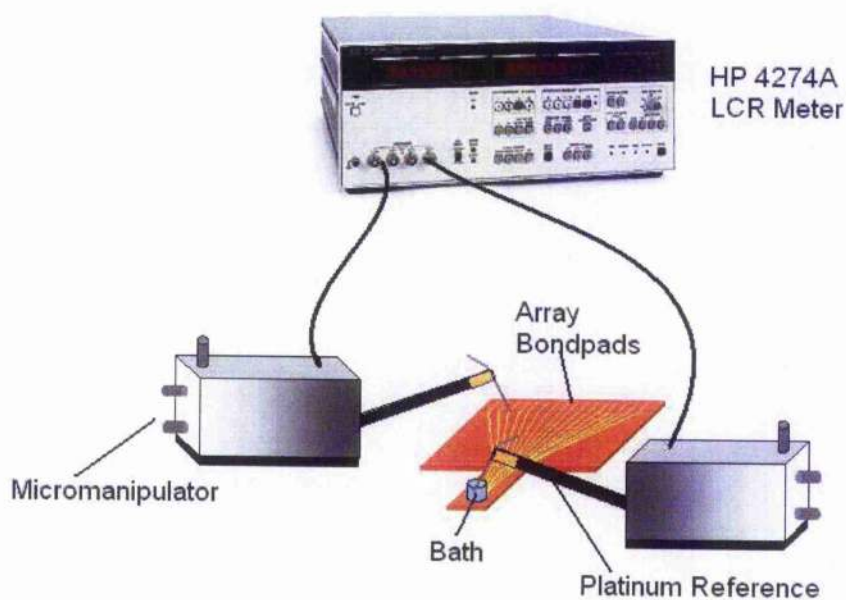


Figure 3.8: A schematic showing the measurement technique for the determination of the impedance values for the 74 electrode arrays. The micromanipulator probes activate a single channel at a time and is stepped across all the bond pads allowing for the measurement of the 1kHz, 100mV impedance value. The bath is filled with buffered saline solution.

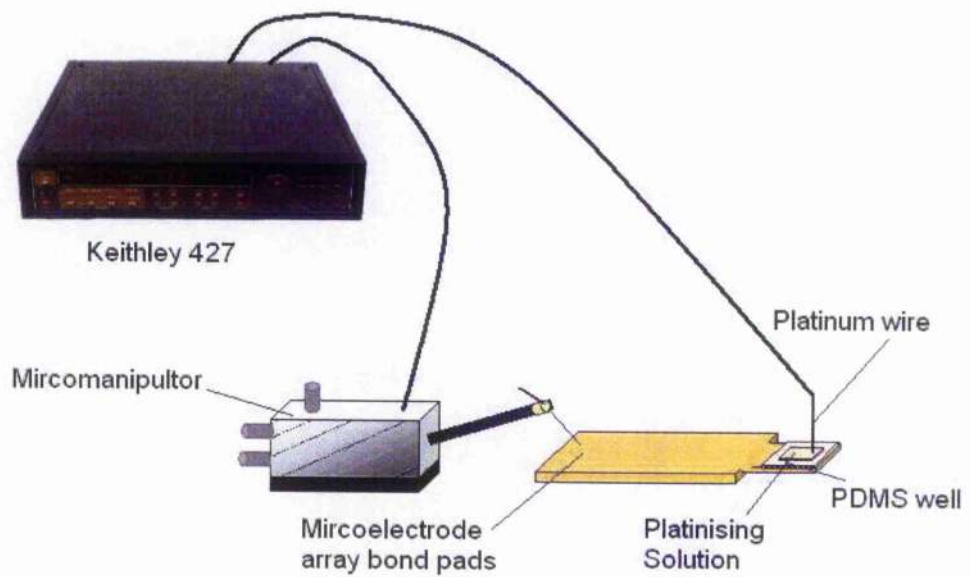


Figure 3.9: A schematic showing the technique for the deposition of platinum black from a platinum chloride solution. The Keithly 427 supplies a constant current and the micromanipulator is stepped across all electrode bond pads till platinisation is complete.

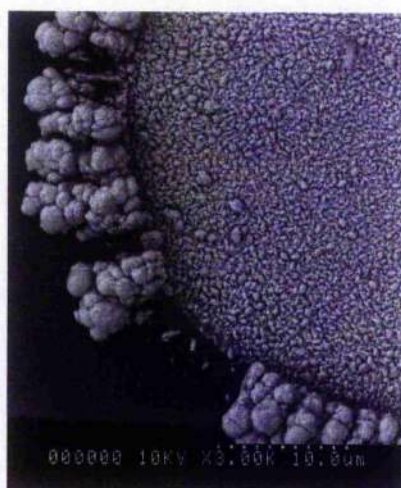


Figure 3.10: Scanning Electron Microscope image of Electrode Showing surface growth on polyimide under voltage controlled limits

controlled method to electrochemically limit the deposition rate. This results in poorly formed electrodes which were frequently seen to prefer growing along the surface of the polyimide layer as opposed to forming a protruding column with a diameter limited by the radii of the via as see under scanning electron microscopy, Fig. 3.10. Although this does result in low impedance electrodes compatible with the requirements of biological experimentation, the lack of confinement to the opening of the passivation and poor adhesion limit the long term viability of such electrodes.

The preferred method for depositing the electrodes relies upon limiting

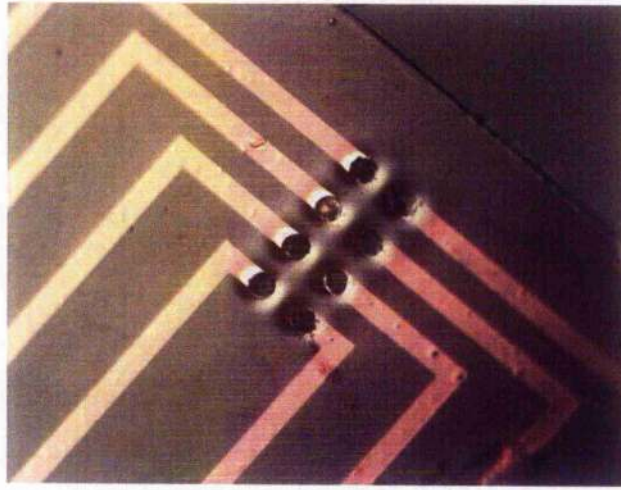


Figure 3.11: $50\mu\text{m}$ feature 8-Electrode Array - The electrodes have been electroplated with platinum under a current limit of $4\text{nA} / \mu\text{m}$

the current flow between the electrode and the platinum reference wire. This controls the electrodeposition rate and hence the electrode growth rate. Investigations in altering the current limits showed that a current limit of $4\text{nA} / \mu\text{m}^2$ is optimal with successful electrode growth achieved, see fig 3.11. Reductions to the current limit could be seen to deposit platinum metal ranging from a smooth film at low current densities, (less than $0.6\text{nA} / \mu\text{m}^2$), through to a growth of platinum ball like structures. The platinum ball structures are of varying (and decreasing size with increasing current) size until at $4\text{nA} / \mu\text{m}^2$ the deposit was the highly porous platinum black structure.

In order to characterize the electrical response of the microelectrode ar-

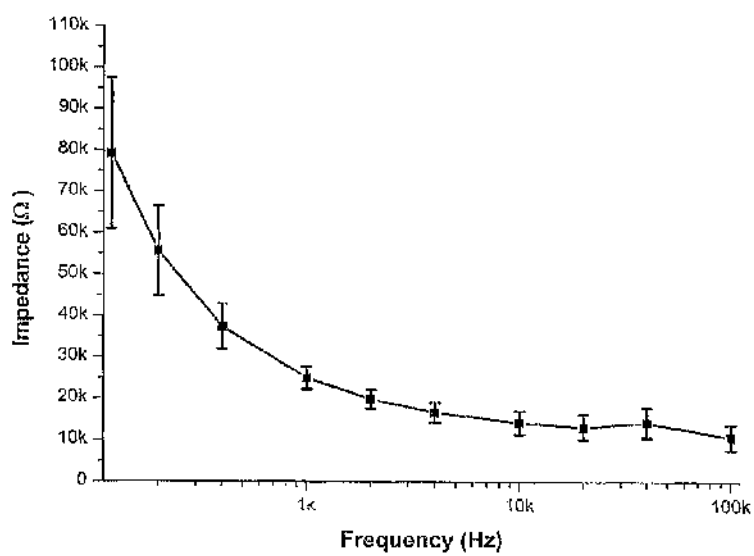


Figure 3.12: An example of the average electrode impedance measured for a $50\mu\text{m}$ electrode from an 8-electrode array as a function of frequency as measured in buffered saline solution.

rays impedance measurements of the 8 and 74-electrode arrays were performed. The experimental results were obtained under the following conditions. The electrode array was covered with a 0.1 molar saline solution and a platinum wire electrode was used to supply a sinusoidal AC voltage of 100mV peak to peak. A needle probe made contact with the bond pad of the electrode under study. A Hewlett Packard 4274A LCR meter was used to vary the frequency of the 100mV AC voltage signal and recorded the impedance of the electrode. All electrodes were measured 5 times and the averaged reading taken. The experimental arrangement used for recording the impedance is shown in (previous) figures 3.7 for the 50 μ m electrode and 3.8 for the 5 μ m.

Impedance values for the 50 μ m electrodes, as used in the 8-electrode array, are typically 25k Ω , see figure 3.12. For the 5 μ m 74-electrode arrays the impedance is typically between 50 to 100k Ω , see fig 3.13, and this relates directly to the decreased surface area in comparison to the 50 μ m electrodes. These impedance values are suitable for neurobiological experimentation. The electrodes are also robust and have been used for multiple experiments without the need to re-deposit or 'top-up' the electrodes. When the array has been tested on several retinal tissues for long term experimentation however it has been seen that the impedance of the electrodes does increase. This is primarily to the detachment of platinum onto the retinal tissue upon removing. When several such tests are undertaken the platinum electrodes benefit from a 'top-up'.

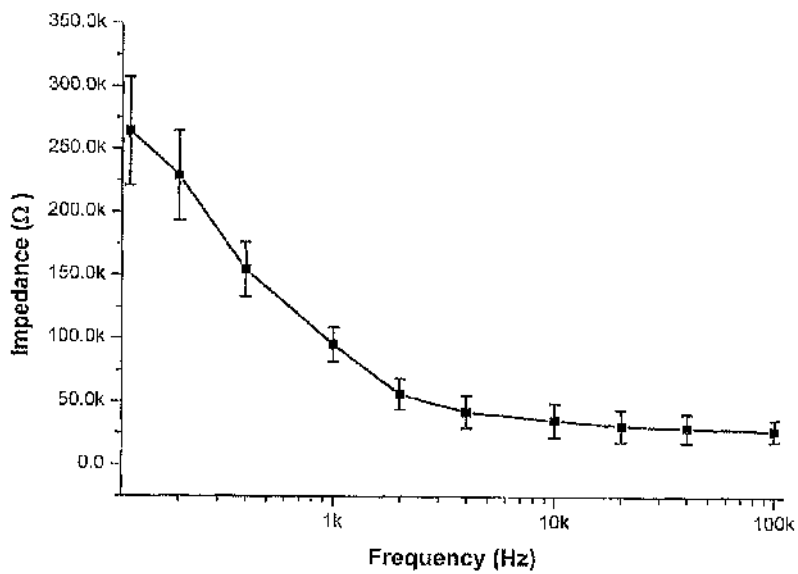


Figure 3.13: An example of the average electrode impedance measured for a $5\mu\text{m}$ electrode from an 74-electrode array as a function of frequency as measured in buffered saline solution.

3.5.6 Model of cell-electrode interface

An important factor in the use of microelectrodes to study cell behaviour or influence it through the application of electrical stimulation is to understand the mechanism of what is happening at the cell-electrode interface. Whenever a metal electrode is placed in an electrolyte (a solution containing moving ions) an electrochemical interface always occurs. The interface can be represented by capacitive and resistive components.

The components of the electrochemical interface are dominated by 3 main terms, the interfacial capacitance C_i , the charge transfer resistance R_t and the spreading resistance R_s . An in-depth review of these components exists [24] and only an overview is presented here.

The interfacial capacitance results from the space charge region formed at the surface of the electrode when a metal is placed in an electrolyte. This model was first devised by Helmholtz in 1879, and the region is known as the Helmholtz plane, and was further revised by Gouy - Chapman and Stern in 1913. It arises from electrons at the surface of the metal orientating the nearby water molecules which act as a dielectric medium. As such the Helmholtz model predicts that the layer would act as a simple capacitor. The revision by Gouy - Chapman and Stern advanced the model proposed by Helmholtz by representing the capacitive region as more widely distributed and allowed the space charge region to extend further into the bulk electrolyte. It also added that the model for the dielectric capacitance was of a time averaged flow of ions as opposed to Helmholtz fixed sheet of

ions approach. A detailed mathematical approach can be found in several books [174, 175].

In addition to the capacitive term above there exists a resistive component acting in parallel at the interface. This resistive component is termed the charge transfer resistance and results from the faradaic transfer of charge across the interface [176].

For our model, the last element that need be considered is the spreading resistance. This term affects how the spread of current from one electrode to a reference occurs. It can be seen that the effect of the spreading resistance varies as the square root of the geometric area of the electrode [166].

With the consideration of the above three elements, we can derive a simple model for the electrode electrolyte interface that fits well with the measured impedance graph from Fig 3.12. The model for a single electrode is shown in Fig 3.14. Where, C_i is the interfacial capacitance, R_t is the charge transfer resistance and R_s is the spreading resistance.

As can be seen from this model, the response of the system to low frequencies is dominated by the R_t term owing to the $1/f$ dependence of the capacitor. As the frequency is increased the effect of the R_t term decreases and the C_i term starts to dominate. This explains well the trends seen for the measured impedance from a single electrode.

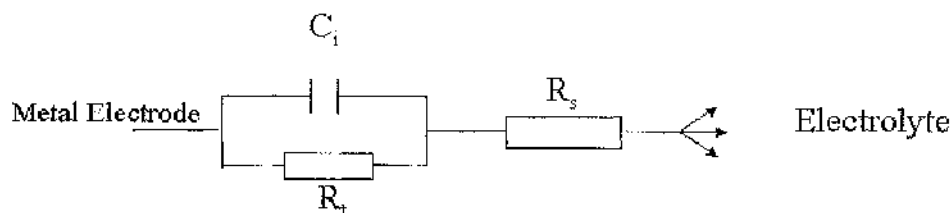


Figure 3.14: Electrical representation of the cell-electrode interface for a single working electrode.

The above model holds true for single electrodes though as I am presenting a multiple microelectrode design we must include the effect of having another electrode positioned close by in the solution. In this instance there is a parallel capacitive and resistive term linking the two electrodes. This can be seen in Fig 3.15.

The net effect of having the link between the 2 electrodes is the introduction of crosstalk between the electrodes. In order to reduce the effect of the crosstalk the designs of the arrays has minimised the impedance of the cell-electrode interface.

The final measurement from the arrays was to establish the interchannel resistance and capacitance with a view to evaluating the crosstalk between electrodes. This was measured by probing between 2 of the longest parallel

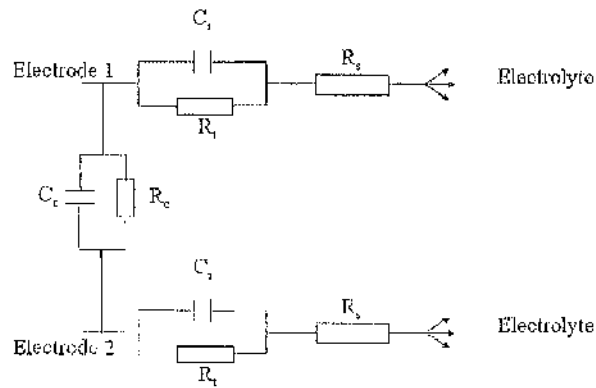


Figure 3.15: Electrical representation of the cell-electrode interface for a single working electrode.

metal tracks, which were physically next to each other for the 74 electrode array. This represented the worst case scenario for any of the channels both in the $50\mu\text{m}$ spaced 8-electrode arrays and the $5\mu\text{m}$ nearest spaced lines on the 74-electrode array. The value for the inter-channel resistance in this instance was $90\text{C}\Omega$ with an inter-channel capacitance of 0.3pF . This allows for discrete and independent cellular recording and stimulation from neighbouring electrodes.

Chapter 4

IPIX

For a visual prosthetic device to be viable, a means of collecting visible light and interpreting it in a manner similar to retinal neurons is paramount. For our purposes we have developed a silicon Active Pixel Sensor (APS) with neural network functionality. Although the fovea of the retina currently has a resolution ($1\mu\text{m}$) in excess of what can be achieved by silicon detectors ($3\mu\text{m}$ resolution), the processing of silicon has a continual drive towards ever increasing miniaturisation. As such, we chose to implement a silicon based detector which is likely, in time, to benefit from ever increasing scalability. The detector was designed at the Rutherford Appicton laboratories specifically to the requirements needed for a retinal implant chip. The work in this chapter demonstrates the characterisation of the detector to our specified requirements and it's applicability as a "substitute" retina.

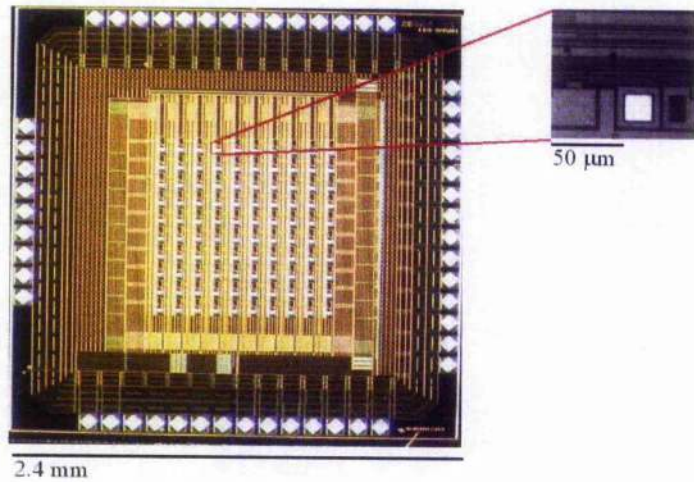


Figure 4.1: The 10x10 array of pixels is shown with the bond pads seen at the outer edges of the chip. A magnified image of a single pixel can be seen at the top right of the figure.

Our developed APS has a 10x10 array of $100 \times 100 \mu\text{m}$ pixels and is called the IPIX, an image of the chip can be seen in Fig 4.1 with a magnified image of a single pixel at the top right of the figure. The sampling rate of the pixels is 1kHz. Owing to the complex nature of the APS design, the neural networking is not employed on-chip in this first rendition of the chip. The neural network can be applied off chip via the control PC. For our initial proof of concept development, the 10x10 APS array is suitable [21] with each pixel producing 12kb/s of data. The next generation of the IPIX will be 25x25 array of pixels within 2mm x 2mm offering higher resolution.

This chapter introduces the various functional components of the IPIX design. We look at the characterisation of the Voltage Controlled Oscillator

(VCO) in terms of the frequency response to the applied voltage, the dynamic range of the photodiodes, the RMS output on the stimulation pulse and pixel crosstalk. We show the VCO can respond over a range of approximately 100Hz (+/- 5Hz) and that we can achieve stimulation pulses to a maximum of 3.3V with RMS noise less than 50mV.

Given the known response of retinal neurones under light stimulus, the electrical output of the detector system was designed to incorporate this response [56]. As a design requirement, the specified frequency of output pulse was 1ms relating directly to the temporal patterns of action potentials previously recorded from the retinal ganglion cells. Moreover the ability to modify the output pulse frequency and width [117], to address any variation in the optimal conditions was requested and implemented on chip at the design stage of the IPIX sensor. In addition to specifying a variable temporal nature to the pulse, an amplitude control factor was also required. As a result of having the ability to modify the output pulse characteristics in terms of frequency, pulse width and amplitude a desirable proof-of-concept system has been developed to probe and determine a successful functional retinal model.

In addition to the options we have to alter time and size of the output pulse we have the option to change the output waveform to either a monophasic pulse (square wave) or a balanced bi-phasic response (positive and negative square wave of equal amplitude and temporal duration) see Fig 4.2. The option to utilise a bi-phasic response mimics more closely the nat-

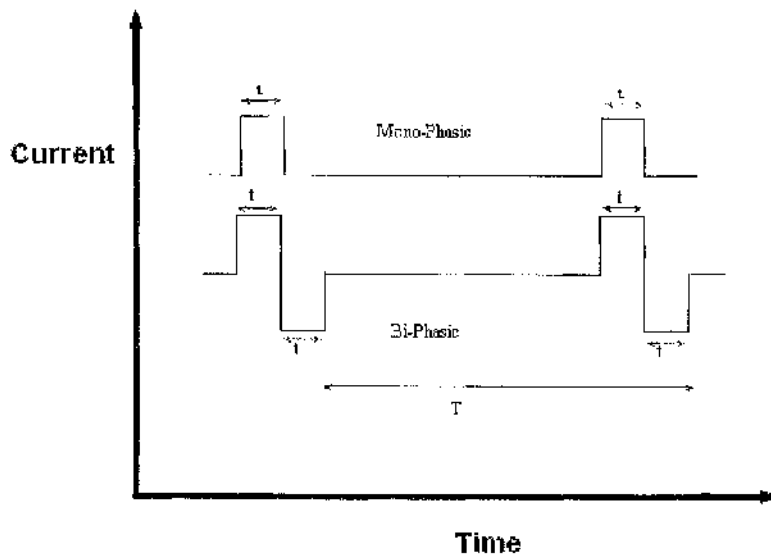


Figure 4.2: Schematic of a mono-phasic pulse (top) and a bi-phasic pulse (bottom). The time t corresponds to 1ms for a monophasic pulse or $500\mu\text{s}$ for the bi-phasic pulse. The bi-phasic pulse can be seen to represent a charge balanced system.

ural response of the positive and negative phase of an action potential (see section 2.1.7 and fig 2.7 previously) and should maintain a natural biological stimulation system where there is no residual charge in the tissue post stimulus.

Further to this, an ability to modify the optically detected signal to accommodate correlated neuronal stimulation is seen as a valuable tool for any prosthesis. Each of these components was specified at the design stage

and has been incorporated into the APS designed in collaboration with the Rutherford Appleton Laboratories.

4.1 The IPIX imaging device

The imaging sensor, the IPIX, has been developed through funding from an Engineering and Physical Science Research life sciences grant in conjunction with the Rutherford Appleton research laboratories.

All PCB readout electronics and acquisition software have been developed within the University of Glasgow by Dr. K. Mathieson. A summary of the input, output, bias and power pins are given in tables 4.1 through to 4.4 (see end of chapter).

4.1.1 IPIX Design

The IPIX chip consists of a 10x10 array of pixel sensing elements fabricated using a standard low power consumption complementary metal oxide semiconductor (CMOS) process. Each pixel is 100x100 μm and contains a single photodiode, a voltage buffer and a voltage controlled oscillator (VCO) which drive the bi-phasic output [123].

The outputs from the pixels are read along each row through a simple shift register and pointer, with each column being read fully within the row switching time. The pixel outputs from each row are fed into the VCO and

the output from the VCO utilised to generate a bi-phasic waveform used for retinal stimulation, a schematic overview is shown in figure 4.3.

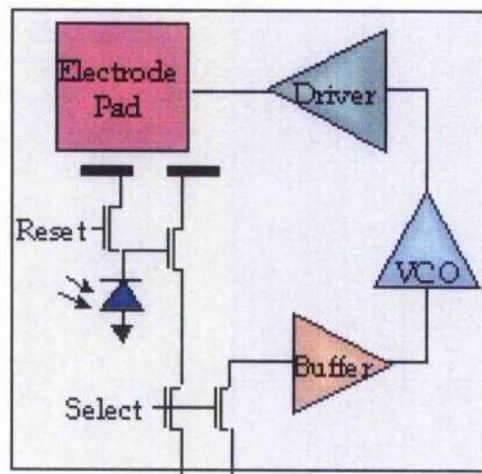


Figure 4.3: Schematic of a Pixel onboard the IPIX chip

The design of the IPIX chip allows for the characteristics of the stimulus pulses (frequency, pulse width and amplitude) to be controlled from a source external to the photodiode pixels. In this instance the output lines of the photodiodes are disconnected from the input lines, the voltage buffer, and instead fed out to the analogue input line of the National Instruments (NI) control card. This voltage level from the photodiodes can then be altered through the labview software and fed back into the voltage buffer on the pixel (or neighbouring pixels). In this way external control signals can be applied to the voltage controlled oscillator (VCO), allowing for signal processing off chip.

The readout of each column, in full, is employed to aid incorporation of on-chip neural network in the next version of the chip. With the current application of the neural network weighting functions, undertaken external to the chip, we have greater scope to change the architecture and weighting requirements of the network. The signals from the photosensor can be fed to a computer with a trained neural network, be modified accordingly and passed back to the input of the bi-phasic waveform generator that controls the stimulus pulse.

4.1.2 Design Parameters

The IPIX chip is designed as a 10x10 matrix of total size approximately $2380\mu\text{m} \times 2380\mu\text{m}$. The optimal response from the photodiodes are in the in the 490-570nm range which spans a significant proportion of the visible spectrum. The output frequency of the chip can be changed from 3Hz to 100Hz with the pulse shape switched between either mono-phasic or bi-phasic in nature. The operational voltage is 3.3V, -1.65V and 1.65V rails with the power consumption being typically below 0.3mW per pixel to minimise adverse effects of localised heating [119]. The pixel to pixel uniformity is 5% while operating in the linear range of the transistors. The processing of the chip is the $0.35\mu\text{m}$ AMS C35B4C3 process [118]. The use of smaller than $0.35\mu\text{m}$ technology is an option longer term, as this would reduce the heat dissipation by reducing the power requirements. It would also allow increased pixel density per unit area. The choice of $0.35\mu\text{m}$ technology is dictated by the cost and reliability for this the first chip iteration.

4.1.3 Photodiode

The photodiode is formed as an n-type well in a bulk p-type material. A typical 3 transistor readout scheme is employed with the photodiode to control the reset, integration and readout (See fig 4.4).

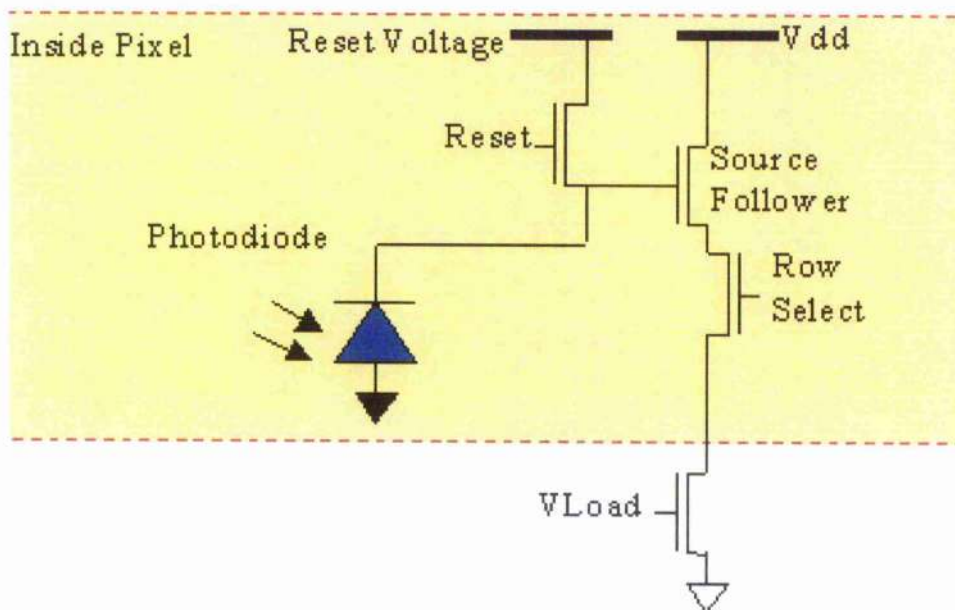


Figure 4.4: A schematic of a photodiode showing the 3 transistor readout scheme

When the reset voltage is applied, the capacitance of the photodiode is set to a value limited by the voltage reset transistor. Integration in the photo-

diode begins when the reset transistor is switched off and continues until the row is revisited, typically at a rate of 1kHz. Photons arriving in the bulk of the photodiode result in a photocurrent, the magnitude of the photocurrent is limited by the integration time (row revisit time), assuming saturation is avoided. The magnitude of the photocurrent is proportional to the incident light flux in the bulk of the silicon detector. During the integration, the photocurrent discharges the photodiode node until the readout through the voltage buffer (source follower) is initiated.

Even if the diode remained completely in the dark, a drop will always occur in the photocurrent due to dark currents. The magnitude of the dark current is minimal in effect, due to the relatively quick switching between the pixels and the low leakage of the transistors. It is more likely that stray light has a greater impact on the photocurrent levels. With careful control of the experimental arrangement however it is possible to minimise the affect of stray light to allow confidence in comparative results. A 3D surface profile of a single pixel is shown in figure 4.5, the large square is a bond pad with the photodiode situated at its bottom left corner.

4.1.4 Voltage Buffer

The voltage buffer stores the input voltage from the photodiode before passing to the VCO. This is necessary to maintain a true input drive voltage (eliminate loading) in between row re-visits. As is common in this type of application, it is a high input impedance unity amplifier.

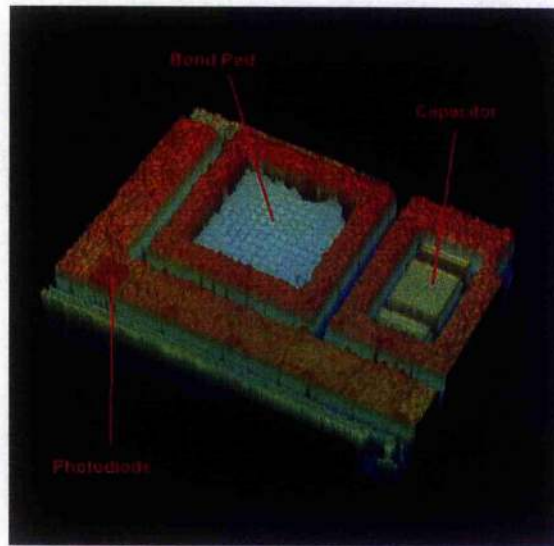


Figure 4.5: $100 \times 100 \mu\text{m}$ 3D scan of a single pixel, surface profiled at x100 Magnification

4.1.5 Voltage Controlled Oscillator

The Voltage Controlled Oscillator (VCO) is driven by the information contained in the source follower. The VCO converts the buffered input into a waveform suitable for triggering the bi-phasic control circuit which in turn outputs a stimulation pulse to the retinal ganglion cells. The frequency of the output waveform is controlled via the input voltage to a comparator within the VCO (typically between 0 and 2V). The voltage window set by the upper and lower thresholds of the comparator determine the rate, for a fixed voltage, at which the output of the amplifier will switch the state of the comparator. The output frequency range of the VCO over the 2V input

range is 3Hz to 100Hz.

Owing to the bulk effect transconductance 1/10th of the voltage is lost on each of the 2 transistors for the NMOS and PMOS processes. This implies that 0.9 on 2V and 0.9 on 1.8V would give 1.62V as the output of the transistor system. So the 2V operating range is reduced to 1.62V and therefore the frequency response of the VCO will be affected accordingly.

The VCO block diagram is shown in fig 4.6. The clocks driving the VCO ($\phi 1$ and $\phi 2$) are non-overlapping and generated on chip from a master clock. The master clock frequency, generated off chip, is 10kHz. The ratio of $\phi 1$ / $\phi 2$ are such that a single cycle will not be sufficiently large to change the state of the comparator. The ratio of C2 and C3 affect the voltage step observed from V_{amp} (the output from the amplifier). The window of the comparators thresholds determine the rate at which the polarity switching of the comparator is achieved in conjunction with the $\phi 1$ / $\phi 2$ rate.

The value of the capacitors is small (a few pF) and governed by space restrictions on chip. In effect this leads to a difference in the frequencies generated by neighbouring pixels through thermal (KTC) noise jitter. The value of the KTC noise effect at a frequency of 1.5Hz, the lowest operational frequency of the chip and hence the frequency of largest KTC effect is measured as less than 0.1Hz. This will not compromise the functionality of the device for retinal stimulation.

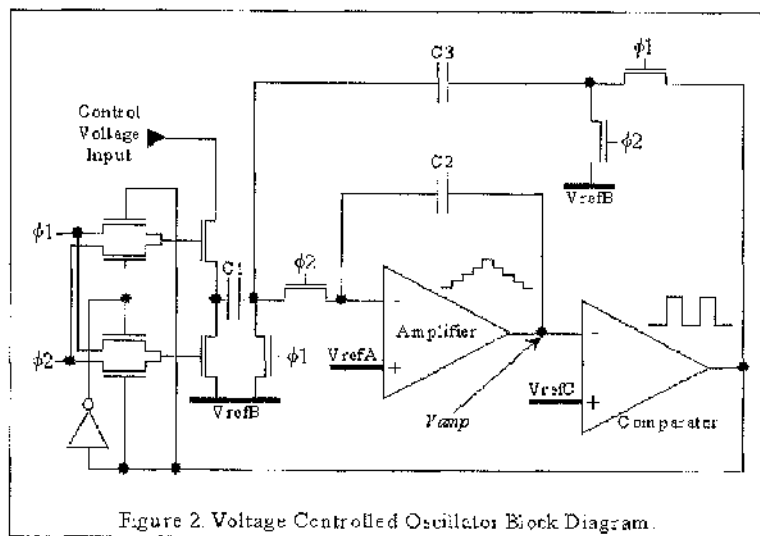


Figure 4.6: VCO controlled oscillator block diagram. The non-overlapping clock $\phi 1$ and $\phi 2$ which control the comparator switching rate are shown. The capacitors $C 1$ and $C 2$ which affect the voltage step from V_{amp} are also evident.

Output Driver - Bi-Phasic

It is important that each pixel can independently demonstrate a bi-phasic output signal. Initially the frequency of the output pulse will be synchronised via the initial reset, this however will be transient (1ms) as each pixel thereafter reacts to the differing light intensity presented.

The bi-phasic response from the central nine pixels is achieved using a tri-state inverter. The inverter is bi-phasically optimised to respond to an electrode of impedance of 30kOhms at 1kHz. Once the bi-phasic waveform has been generated, it is routed to bond pads on the edge of the chip which are wire bonded to the PCB. The PCB then routes to the micro-electrode arrays.

4.1.6 VCO Characterisation

Characterisation of the IPIX chip has included examination of the output frequency as a function of light intensity, varying output voltages, pixel uniformity, noise and cross talk levels.

Frequency output vs VCO driving voltage

As has previously been discussed, the output frequency from the IPIX chip is controlled through application of a voltage controlled oscillator. The input voltage to the VCO governs the rate at which the thresholds of the comparator are reached, and therefore the frequency of the output.

Comparator thresholds can be adjusted, though they have been fixed throughout the testing (with a range of 2V) to aid the repeatability of the analysis.

The control voltages to the VCO, for frequency analysis, are supplied external to the chip. By switching off the photodiode responses and externally applying a signal we benefit from the application of a calibrated, high precision and low noise voltage input to allow characterisation of the output frequency response.

The response from the VCO to a stepped input voltage can be seen in Fig 4.7. There appears to be a switch on voltage for the 3-stage transistors at 0.75V, this is higher than expected. We would expect a frequency varying output response, although not likely a linear one, to occur at voltage values only slightly in excess of 0.1V. A linear response after 0.75V is evident and is as expected. At 2.25V the voltage supply to the VCO is limited by the supply rail voltage with further stepping of the input voltage to the VCO having no effect on the frequency. All 9 centre pixels, those responsible for stimulating waveforms, can be seen to respond in a similar manner.

Figure 4.7 also shows the dynamic range that is achievable from the IPIX chip. The hashed box indicates the voltage that can be supplied from the photosensors and spans approximately 0.5V. This can be seen to correspond to a frequency variation of 30Hz in the linear response region. The dynamic range of the chip is fixed at 30Hz although the frequency span that this

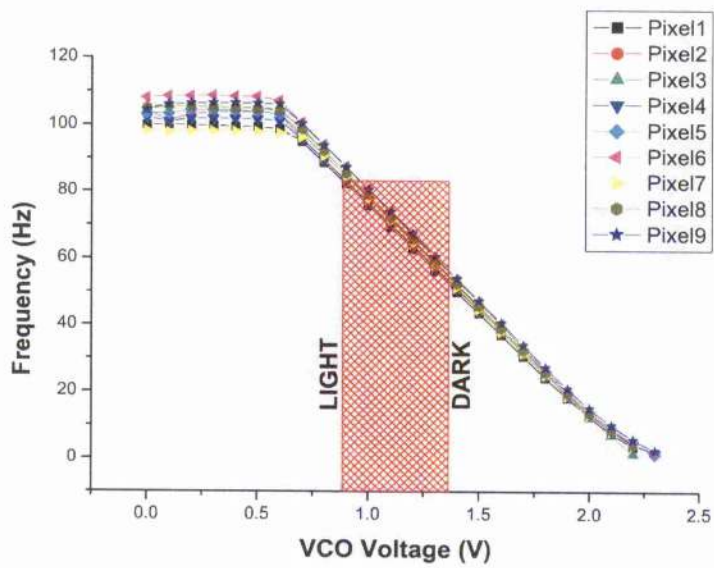


Figure 4.7: Frequency of the output stimulation pulses as a function of the voltage supplied to the voltage controlled oscillator

incorporates can be shifted by the altering of the thresholds of the comparator. An increased dynamic range can be achieved, if required, through software modulation within the neural network programming. For our proof of concept however, this is not seen as a limiting factor.

The variation in the pixel to pixel response can be seen in Fig 4.8. The frequency output of the VCO is measured via an Agilent Infiniium 54831D oscilloscope as is the deviation in the output frequency response for a fixed VCO voltage. In the linear range of operation (and below a voltage of 1.75V) of the VCO the pixel to pixel variation can be seen to be within $\pm 5\%$. After the 1.75V VCO supply voltage is exceeded, the variation becomes significantly larger. This is due to the higher supplied voltage initiating a lower frequency (a few Hz) response of the VCO. A deviation of 0.1 or 0.2 Hz in the low frequency signal results in a relatively higher ratio of signal to jitter than a similar deviation in a higher frequency signal.

Figure 4.9, shows the combined standard deviation in the pixel output frequency averaged across all the channels. As the voltage on the VCO is increased the standard error associated with the frequency output can be seen. This highlights more specifically the region at which the 3-transistor system initiates. The linear trend of the curve is in agreement with what would normally be expected for transistors operating above the switch on voltage. The reduction in the error with voltages above 0.75V is indicative of operating within the linear region of the transistor junctions.

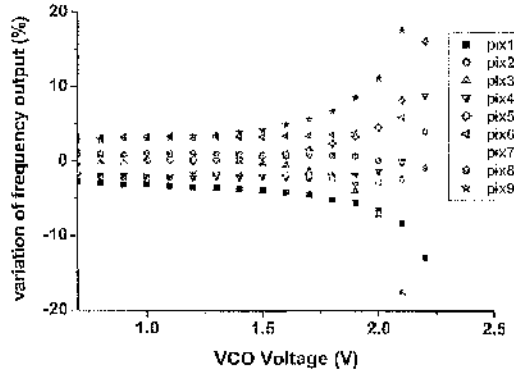


Figure 4.8: Variation in the frequency output of the stimulation pulses as a function of the voltage supplied to the voltage controlled oscillator.

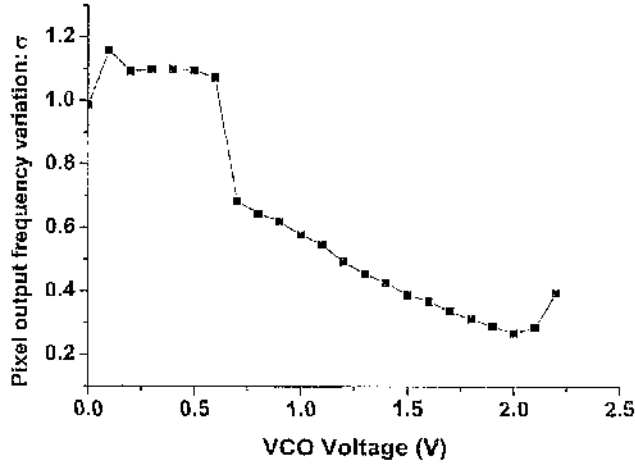


Figure 4.9: The standard deviation averaged across all pixels for the frequency output of the stimulation pulses as a function of the voltage supplied to the voltage controlled oscillator.

4.1.7 Light Response

The light response of the IPIX chip was determined under normal laboratory fluorescent lighting conditions. The chip was placed in a bright well-lit room and shielded from stray, non-normal light, via an optically blocking cylinder placed normal to the surface. The light was attenuated via neutral density filters placed on the surface of the cylindrical shield. The absolute intensity was not measured as the response to the relative intensity is seen as the significant measurement.

The measure of the light response was undertaken with 18 filtered intensities and can be seen in Fig 4.10. From Fig 4.10 the light response of the detector can be seen to be linear (plotted on a log-linear scale) in nature within the optimal conditions of the VCO and span a frequency range of approximately 30Hz. It is possible to affect the 30 Hz range in this instance by controlling the row revisit time.

The light response also indicates that the first 5 neutral density filters had little effect on changing the frequency. In terms of the transmitted light intensity this correlates to a required attenuation of 75 %. Hence under normal lighting and under our standard operating conditions the voltage level on the transistors are not reaching the 0.75V switch on requirements as shown in fig 4.7 previously. Thereafter, the behaviour follows a linear frequency output in accordance with a linearly increasing attenuation. If the master clock frequency is altered on the chip and this re-visits the pixels at a different time interval (slower) then the pixel integration time will be longer

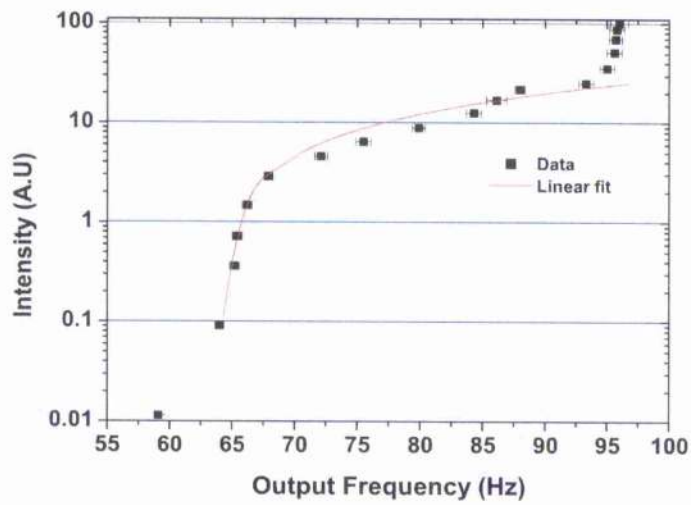


Figure 4.10: Neutral Density filter Light variation vs. frequency output Hz. The red line is a least square fit to the experimentally realised values.

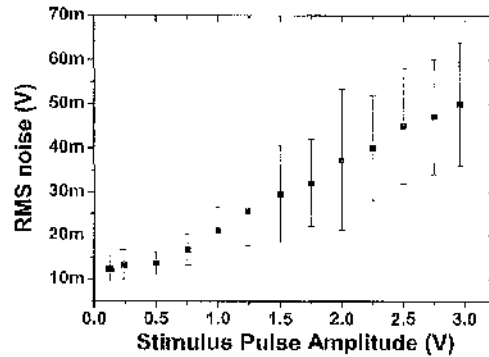


Figure 4.11: Stimulation pulse amplitude with associated RMS Noise output from a single channel

and it is likely that there will be a more useful readout range of the pixels response.

4.1.8 Stimulation Pulse Amplitude

In addition to the ability to vary the frequency output of the detector, the amplitude of this response can also be altered. This is varied on the PCB (via a potentiometer) and allows the readout electronics to be varied to a maximum of 3.3V.

This is seen to be one of the key variables for our stimulation studies. One of the principal aims of our research is to experimentally determine the threshold limits for repeatable stimulation of retinal ganglion cells. The ability to easily change the output voltage of the IPIX stimulation pulse is of significant benefit.

The results for the RMS noise against the stimulation pulse amplitude are shown in figure 4.11. The RMS noise level and the deviation on the RMS noise level can be seen to increase linearly above the 0.75V switch-on voltage for the transistors.

4.1.9 Pixel Cross Talk

The final measurement of the pixel response is to determine the associated cross talk on neighbouring pixels with respect to the stimulation pulse amplitude. The output voltage from Pixel 1 was increased from 0.5V to 3V and the effect on neighbouring pixels measured. Fig 4.12 shows the 9 stimulating pixels and the exploded view the numbering used for experimentation.

The results for the cross talk studies can be seen in Fig 4.13 and Fig 4.14. Fig 4.13 shows the peak voltage cross talk on the neighbouring pixels as a function of pulse amplitude. At low pulse heights, below 1V, the effects of cross talk are limited to only the nearest pixels. The effects of cross talk are not ever significant on pixels 7,8 or 9 even at 3V pulse heights.

In fig. 4.14, the cross talk investigations are shown as a percentage of the stimulus pulse amplitude (as applied to pixel 1) on the neighbouring pixels. It can be seen that each of the pixels offers a constant percentage value of cross talk with increasing voltage application to pixel 1. Additionally there can be seen to be an exponential decay in the crosstalk value with the pixel number. Notice also that no significant cross talk could be measured on

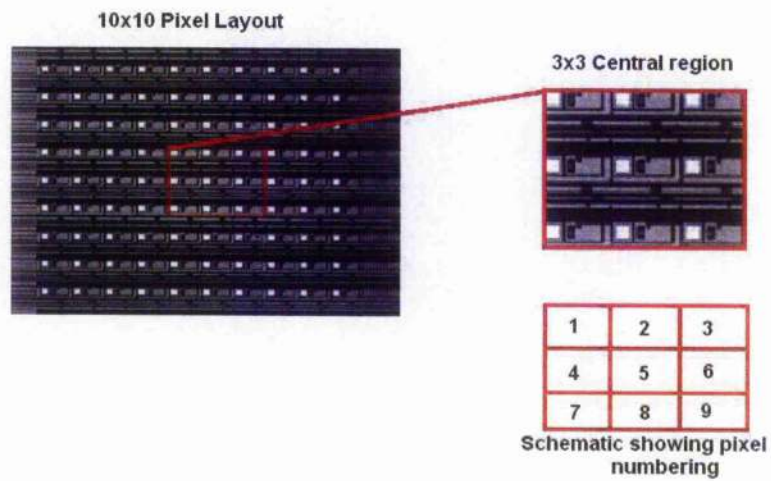


Figure 4.12: Pixel layout showing the 10x10 array and then zoomed into the central region. Bottom right is a schematic showing the numbering of the pixels as referenced in this work.

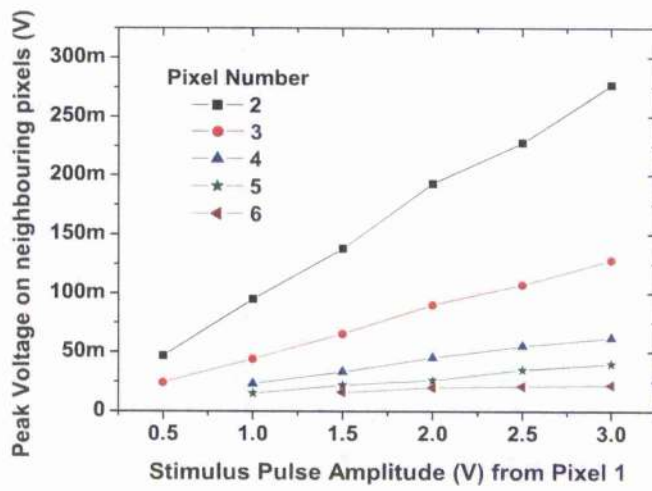


Figure 4.13: Pixel cross talk measured on neighbouring pixels as the voltage increased on pixel 1

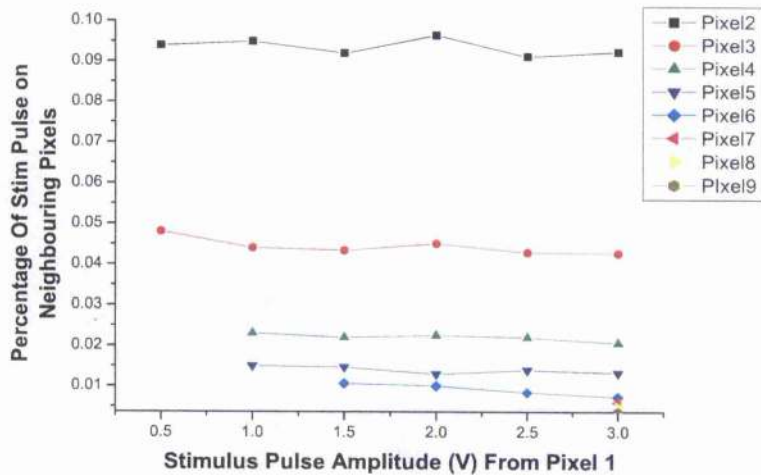


Figure 4.14: Percentage of an increasing stimulation pulse, as applied to pixel 1, detected on neighbouring pixels.

pixels 7, 8 or 9.

In view of the pixel layout (see Fig 4.12), it is likely that the main component of the crosstalk measurements arise not from the chip but from the layout of wires routing the pixel outputs on the PCB. See Figure 4.15 for the PCB layout with the IPIX chip located.

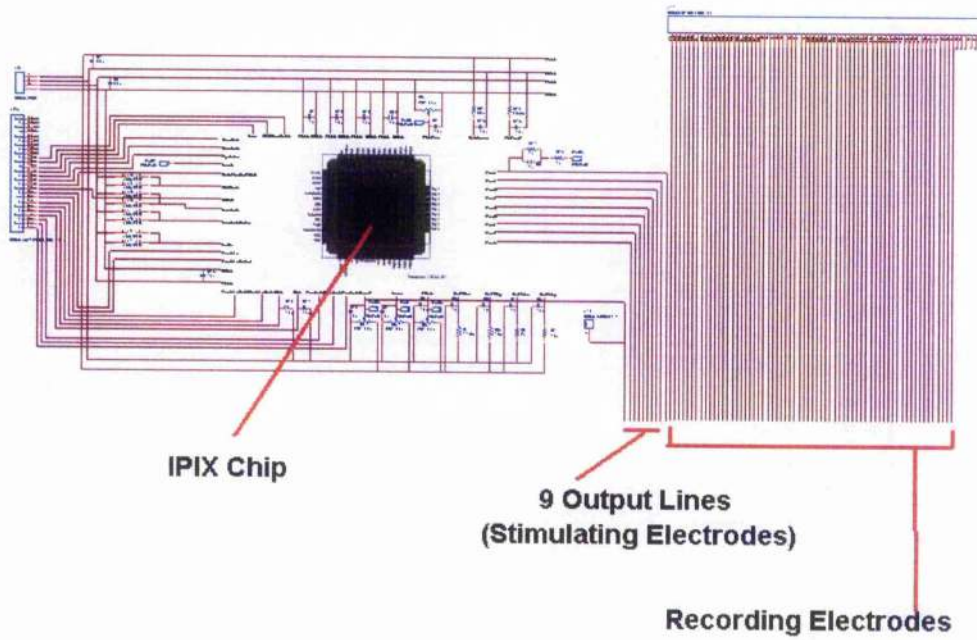


Figure 4.15: PCB layout showing the 9 stimulating tracks close to each other and the IPIX chip in the central region of the figure. The crosstalk measurements are likely to be a result of having the output channels running parallel.

Table 4.1: The IPIX input pin abbreviated terms and full description.

| Input Pins | Type | Description |
|-------------------------------|----------|---|
| RstB | CMOS | Reset Signal to the VCO and logic |
| ClkRow | CMOS | Clock to control the row select shift register |
| Sin | CMOS | Input to the row select shift register |
| RowRst | CMOS | Reset signal to the pixels in a selected row. |
| RowSel | CMOS | Controls the selection timing for the row. |
| Update | CMOS | Stores the control voltage to the VCO in a row. |
| ExtPhiRefClk | CMOS | Alternative external clock for driving the Phi Generator |
| ClkSel | CMOS | Selects between MClk and ExtPhiRefClk. |
| MClk | CMOS | Master clock to control the Bi-phasic timer and Phi-Generator. |
| SrcSel | CMOS | Selects internal / external source for all pixels except the centre 9. |
| SrcSelCntr | CMOS | Selects internal or external source for centre 9 pixels. |
| BiEn | CMOS | Enables / Disables the Bi-Phasic operation. |
| TestIn | Variable | External input to all except the centre 9 pixels Range 0.5V to 2.5V. |
| TestInCntrl[0:2] ₆ | Variable | External inputs to centre 9 pixels Range 0.5V to 2.5V. |

Table 4.2: The IPIX output pin abbreviated terms and full description.

| Output Pins | Type | Description |
|--------------------------------------|------|--|
| Sout | CMOS | Output from the row select shift register. |
| PixOut _j 0:2 _j | CMOS | Outputs from the three central columns. |
| Pix 1 to 9 | CMOS | Outputs from the 9 central pixels. |

Table 4.3: The IPIX bias pin abbreviated terms and full description.

| Bias Pins | Type | Description |
|-----------|-------------|--|
| Lth | -1.15V | Lower threshold. |
| Hth | 0.85 | Higher threshold. |
| ARef | 0V | VCO amplifier centre voltage. |
| Acas | 0V | VCO amplifier cascade device bias. |
| RefCbn | 150 μ A | NMOS bias to the window comparators in the VCO. |
| RefCbp | 150 μ A | PMOS bias to the window comparators in the VCO. |
| RefAbn | 180 μ A | NMOS bias to the amplifier in the VCO. |
| RefABp | 150 μ A | PMOS bias to the amplifier in the VCO. |
| PSFref | 100 μ A | Bias to the PMOS source follower in the pixels. |
| ColBias | 50 μ A | Bias to the readout columns / NMOS source followers. |

Table 4.4: A Table 2

| Power Pins | Type | Description |
|------------|-------------|--|
| VDDD | 1.65V | Digital power supply. |
| GNDD | -1.65V | Digital ground. |
| VDDA | 1.65V | Analogue power supply. |
| GNDA | -1.65V | Analogue ground. |
| VRst | Variable | Reset voltage to photodiodes in the pixels. |
| RefCbp | 150 μ A | Power supply to the Bi-Phasic output driver. |

Chapter 5

Biological results from in-vivo testing

5.1 Introduction

This chapter demonstrates the results that have been achieved in-vivo with the frog retina. We have successfully demonstrated the feasibility of our combined technologies to record activity from retinal neurones. Data indicating the successful stimulation of spatially discrete neurones in a controlled manner is also presented.

The performance of our combined technologies is evaluated as a prototype design with a view towards a retinal prosthesis. There have been various approaches globally examining the response of retinal cellular activity to engineered devices [22, 28] however, the applied combination of an active

pixel sensor as an optical sensor with a flexible microelectrode array is specific to the work undertaken within this thesis. Our engineered representation of the retina is shown in figure 5.1.

Evaluation of the device in-vivo has been subject to the quality of the recordings made from the retina. The detection of retinal activity indicates the successful preparation of retinal tissue. The recording of signals from the multi-electrode array allows for an insight into the correlated signal processing of the retina. Through multiple site recording, we can also determine with confidence threshold activation levels of retinal ganglion cells [57].

We have performed in-vivo experiments to evaluate the threshold limits for successful stimulation of the retinal ganglion cells. Using one of the electrodes as a stimulation site, we have passed an electrical signal directly onto the retinal ganglion cells and used neighbouring electrodes to record the resulting cellular activity [46]. The results from these initial studies are presented.

There is no information presented on the qualification of the device as an implantable retinal prosthesis. As such there has been no formal testing to evaluate the biocompatibility of our system in-vivo. The materials that have been used are known to be biocompatible through cross reference with other work in the field as covered in section 4.7 and 4.8 and in references [7, 8, 9]. Indeed, the only true means of determining the viability of a long-term implant is through field studies. Once the device has been successfully

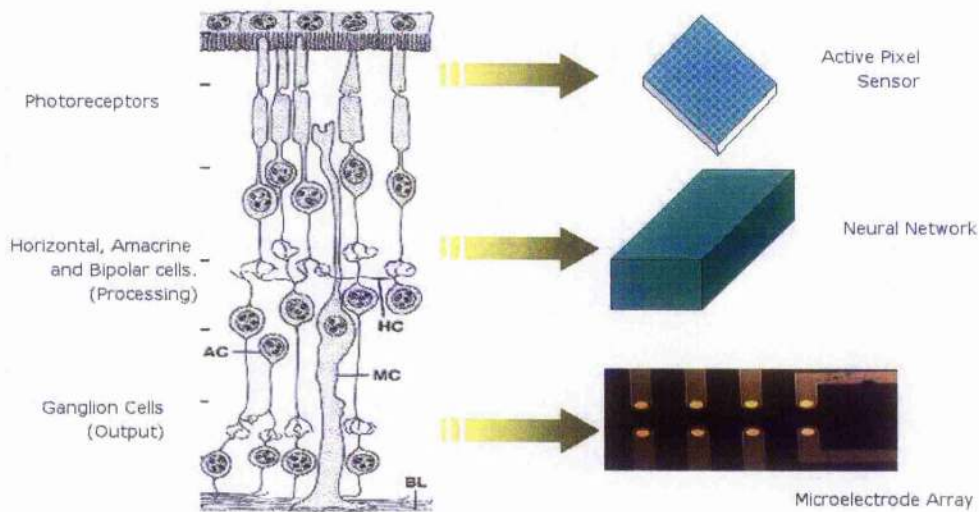


Figure 5.1: Overview of engineering representation of biological system

and extensively proven to be a viable means of communicating information to and from the retina we can evaluate the viability as a long term prosthesis in further work as done in the work by the following groups [48, 52, 58, 60, 65, 70].

5.2 Sample Preparation

In order to achieve optimal electrochemical signal detection, good coupling between the array and the cellular tissue must be achieved. Excess fluid on the surface of the retina must be adsorbed to maximise the cell / electrode interface. Once this has been satisfied excellent results can be obtained.

5.2.1 Biological Tissue preparation

All tissue preparation is conducted in accordance with home office regulations. Animals are only used that have been in storage for a short time due to the altered feeding patterns degrading the quality of the retinal tissue.

With the brain and spinal cord of the frog, *rana temporaria*, destroyed the heart can be observed to still beat. This administers a flow of oxygen to the eye cup and helps preserve the integrity of the tissue for extended testing periods. The frog does not need to be maintained for the duration of the testing as it functions well at room temperature whereas mammalian animals need careful anaesthesia and control.

All preparation of the tissue is conducted under red light illumination owing to the insensitivity of the frog retina for this wavelength. The upper and lower eyelids are removed at the first surgical step.

The reference platinum electrode is then inserted through the centre of the frog body to ensure a suitable electrical ground for the experimental setup.

The cornea and lens are then removed and the aqueous humour is absorbed from the eye. Failing to remove the fluid layers at this stage results in a flow of liquid into the eyecup and would result in shorting between the

electrodes on the surface of the retina. The vitreous humour is then removed and this, being of a gelatinous consistency, does not pose the same requirement for fluid absorption. Generally, the vitreous humour will detach with the lens upon removal, providing the proper preparation of the sample. In general, the fluid layers of the retina are removed four times using suitable absorbing paper to ensure the likelihood of successful testing.

For our arrangement, the right retina is most often used as it is more easily accessible with our apparatus. There is no difference offered by either retina and the left retina is utilised only if the right retina, under optical inspection appears to be functionally compromised.

The array and the reference platinum electrode are then positioned onto the retinal surface. Green LED illumination then provides light stimulus to the retina and determines the success of the preparation. At this stage, the array can be repositioned to ensure that there is maximum signal strength in the recorded ERG. Finally, the retina is allowed to sit for 30 minutes to allow the re-absorption of any small amounts of remaining fluid and to allow the pigment to redistribute post surgery. Thereafter, the experimentation is viable and optimised.

5.2.2 Initial preparation studies.

With the retina tissue prepared, the array is adjusted via a micro-manipulator to be in contact with the retinal surface. Initial measurements of the retinal

response are undertaken with a platinum wire placed on the retinal surface. Light intensity steps 0.1, 1, and 10 log units are measured and the response logged. The array is then used to measure the response and a comparison undertaken to determine the quality of the retina / electrode contact. If under visible light conditions any variation is recorded via the array then the array position is adjusted to minimise this effect and ensure consistency in the future recordings. See Fig 5.2 for representation of the microelectrode array inserted in the frog eyecup and in contact with the ganglion cells of the retina.

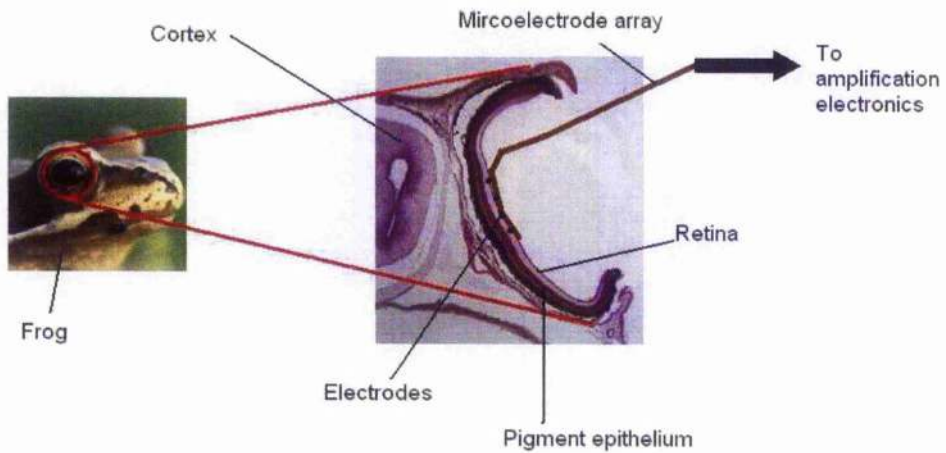


Figure 5.2: Overview of preparation of the frog retina and the array implanted into the eyecup. The electrode array is inserted with the electrodes face down and in contact with the ganglion cells of the retina.

In addition to adjusting the position of the array, adjusting the pressure applied to the electrode region of the array on the retinal surface may be required. In most cases this needs to be adjusted in parallel with recordings from the neuronal cells. The array is designed such that excessive force is unlikely to be applied to the retina and cause any long term damage through compression. There does exist the possibility however that significant pressure when applied to the retina can degrade the quality of the signals recorded in-vivo. If there is a lack of pressure applied to the electrode region of the array the electrical coupling to the cells will be limited and high noise levels recorded.

5.2.3 Signal Amplification

The 8-electrode arrays terminate with a 16 pin low noise LIMO connector, see Fig. 5.3. The wire connections from the array to the LIMO are tinned in a 350°C solder bath to reduce the impedance loss and signal noise. The 74-electrode arrays are coupled to the readout PCB by a low resistivity gold wire z-axis connector. Both these arrangements benefit from the ability to remove and replace electrode arrays in a short timescale compared to the viable recording time (approximately 4 hours due to the cold blooded nature of the frog and the absorption of oxygen from the atmosphere) of the frog retina. This allows multiple experimental investigations on a single biological preparation.

The recorded biological signals from the retina undergo a x1200 fixed am-



Figure 5.3: 8-electrode array connected to low noise 16 channel LIMO connector

plification through a custom built module (each channel being AC coupled to remove any DC offset, see appendix 1 for module layout) ensuring optimal signal definition and reduced loss. Each stage in the design of the readout employs low noise electronics and terminations. Our currently available electronics allow 16 channel amplification and will be extended in future work to accommodate the 64 readout channels of the 74 electrode arrays (64 readout + 9 stimulating + 1 earth = 74 electrodes).

Recordings from the electronics in-vivo measure the noise level to be typically below $8\mu\text{V}$ over a frequency range of 3Hz to 8kHz. The output from the amplifier modules are connected to a National Instruments data acquisition card (E-Series, PCI) on a dedicated PC.

In order to assess the quality of the recorded signals from the array, an array independent recording is made of the retinal response. This recording is achieved from a single strand of platinum wire placed on the surface of the retina and routed out through an independent amplification module. This separate single channel employs a x1000 AC coupled amplifier, 50Hz notch filter and a variable DC offset. The output is read into the DAC card via a monitoring oscilloscope. This allows for the quality and viability of the retinal preparation to be established prior to advancing the array onto the retina.

5.2.4 Data Acquisition Software

The successful recording of retinal activity has been verified utilising two separate software programs. The first, WinWCP, was written by the University of Strathclyde [19]. The second is custom designed software written by A. Moodie (PhD student at the University of Glasgow).

Initial retinal recordings were undertaken via the WinWCP software which allows for a maximum of 8 channels of recorded data. For the 8-electrode arrays this software was adequate. The principal drawback was the inability to record large volumes of high resolution data over long time periods. This was due to limitations in the fixed size data buffer for each readout channel. Data could be recorded for time periods of a few seconds if the resolution was typically 10ms but at a resolution of 0.1ms (our desired readout rate) the available recording time was a few 100ms. For application to the 64 electrode

readout system, the 8-channel maximum readout capabilities is not suitable.

The software developed in house by A. Moodie has several key advantages over the WinWCP software and addresses all of the foreseen shortcomings of the WinWCP software. The first major advantage is the scalability of the recording package to monitor any number of channels. This is a key advantage in the drive towards increasing electrode numbers for correlated signal processing. The user interface is also tailored more specifically to log the components of the study, through a header file, and export the data in a manner that is consistent with our analysis packages. The recording of the data files is such that the data can be acquired at 10kHz for a time period only limited by the available disk storage. This is of enormous advantage and allows for long experimental data acquisition periods.

5.3 Recorded Signals

The signals recorded from the retina are of small amplitude owing to the detection of changes in cellular potential through the movement of ions across the cellular membrane. Typically the signals will be of the order of a few $100\mu\text{V}$. Given the low noise of the system (typically below 8μ across all channels for a good preparation) we can detect multiple cellular responses.

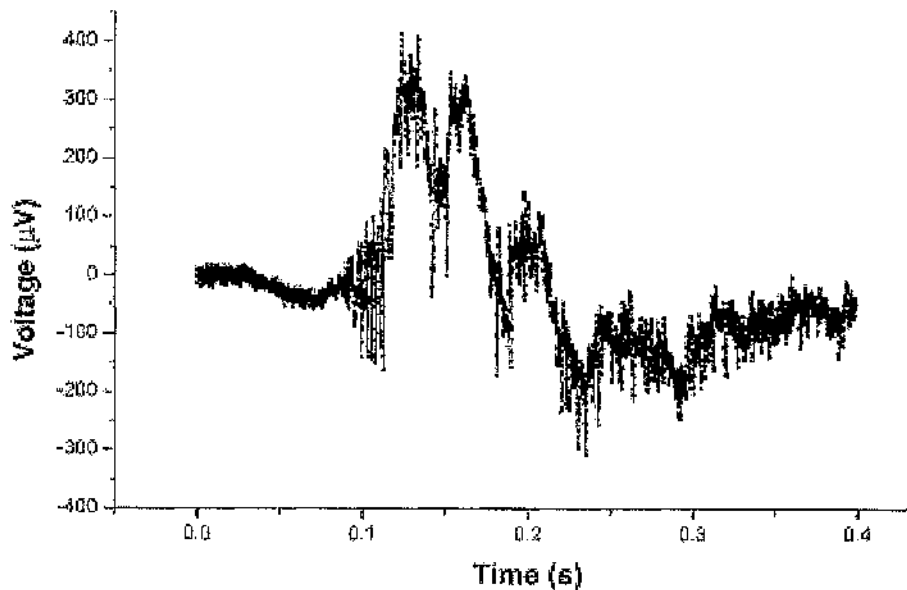


Figure 5.4: Electrorretinogram with superimposed spiking activity

An example of a typical response from the retina under a bright light stimulus can be seen in Fig 5.4. The recording started at the onset of light, time 0. After approximately 9 ms, the photoreceptive cells have detected the light stimuli and pass this information to the output cells (the ganglion cells) and this response can be seen in Fig 5.4. There are 2 key components in the recorded waveform, a slow response termed the Electrorretinogram (ERG) seen to modulate the signal and several shorter responses superimposed on this slow waveform, the action potential (AP).

The two signals are significant for retinal studies. The signal strength of

the ERG indicates the health of the retina and the viability of the preparation. The ERG is a measure of the mass response of all cells in the retina under light stimulation.

The ERG is composed of 3 main components [135] classified as the a, b, and c- waves. A overview of typical relative magnitudes and temporal responses of each of these components are shown in figure 5.5. The origin of these components are from varying layers of the eye. The a-wave originates in the photoreceptor layer. The b-wave was discovered (Dowling) to have its origins within the Muller Glial cells. Finally, the c-wave originates in the pigment epithelium layer which is verified by in-vitro studies. Each of these components sums to have the form of ERG as shown in figure 5.4.

The recording of the superimposed fast acting AP response on top of the ERG shown in fig 5.4 is the key subject of study for our experiments as the AP contains information corresponding the response from a single cell, in an encoded manner, required by the brain. The time at which the AP signals are evident and the number of the APs contain all the relevant information on the visual scene passed to the visual cortex from the retina [26, 76, 103, 124].

Once the signal strength of the ERG is determined it can be filtered to leave the AP response. This is typically achieved by Fast Fourier transforming (FFT) the signal to remove all the frequency components below 80Hz.

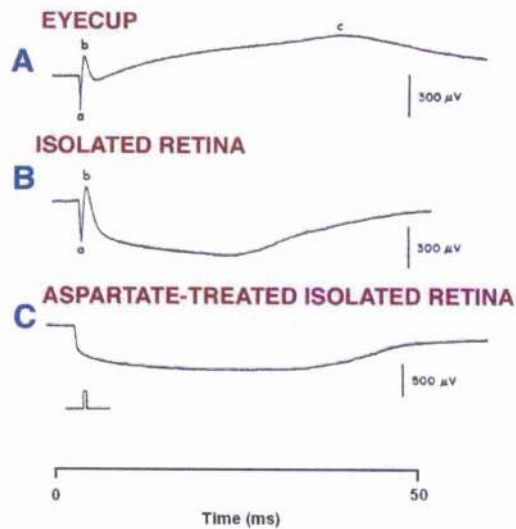


Figure 5.5: The breakdown of a typical measured ERG response into its 3 main components, the a,b and c-waves.

As the AP response is of the 1kHz range, there is no signal loss resulting from this analysis technique. Alternatively, a fitting algorithm can be employed to the ERG and this subtracted from the dataset. This is the preferred method for removing artefacts that are evident after electrical stimulation of the cells and will be discussed in greater detail in subsequent sections.

By way of comparison, the reduction in the electrode size from $50\mu\text{m}$ to $5\mu\text{m}$ allows for individual cell coupling. Shown in fig 5.7 is a single action potential recorded from a planar array fabricated on Indium Tin Oxide (courtesy of K. Mathieson). The inclusion of the $5\mu\text{m}$ result is to show the capabilities of electrodes of this diameter in absence of data from the 74 electrode array.

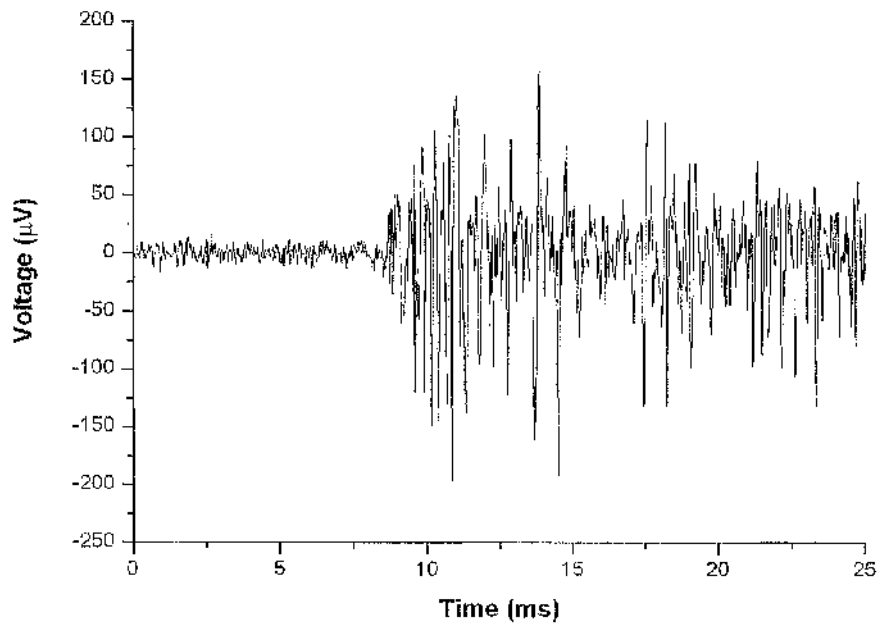


Figure 5.6: Recorded retinal activity upon light activation with the electroretinogram removed using a 80Hz high pass FFT filter.

Once the ERG signal has been removed the AP information is more evident, Fig 5.6. There are multiple APs shown in Fig 5.6. In effect, we are recording multiple cellular responses on a single electrode. Owing to the $7\mu\text{m}$ diameter cells that output the information from the retina, the ganglion cells, and the $50\mu\text{m}$ diameter recording electrodes this is not an unexpected result. If a ganglion cell is positioned directly on top of the electrode then large cell responses can be seen. Fig 5.6. If recorded activity indicates a high density of APs of visibly varying amplitude or pulse shape we can often correlate

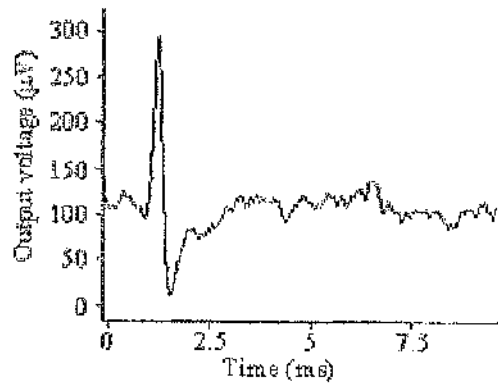


Figure 5.7: Recordings from a electrode of $5\mu\text{m}$ diameter. The recording was made on an ITO array of electrode size $5\mu\text{m}$.

this to the detection of proximal (often multiple) cellular activity. As this signal is superimposed upon the leading signal we get the effects of latent pulse shaping, amplitude modulation or an excess of AP spike trains over a single unit response. This indicates the high quality of the system that has been developed and also the need to move from the $50\mu\text{m}$ electrodes, used here, to smaller electrodes. Although electrodes of $5\mu\text{m}$ were fabricated, they were not used in conjunction with *in-vivo* experimentation before the conclusion of this thesis. Parallel experimentation with electrodes of similar size fabricated at Glasgow University on ITO array [5] have shown the viability of such studies.

5.3.1 Light Evoked Response

The retina responds to light in the manner of an all or nothing response. Specifically, this means that a given intensity of light must be incident on the retina before the retina will respond with an action potential. It follows therefore that the intensity of light has a direct impact on the firing rate of the cells and the output train of action potentials that will result. Higher intensities of light can be seen to result in quicker response times from retinal tissue when light is incident as a pulse. If the light is continuous in duration the retina will light adapt.

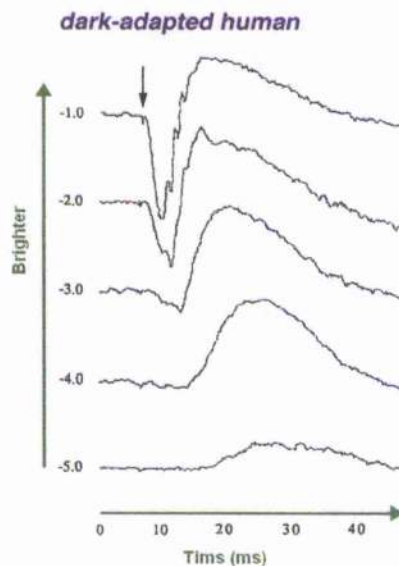


Figure 5.8: Electroretinogram showing faster response from the retina to increasing intensity for the human. (From Webvision.med.utah.ed)

The rate at which the retina responds to a given intensity of light is evident from the rate at which the ERG develops and this can be seen in Fig 5.8. For 4 log units as shown, the form of the ERG can be seen to differ both in terms of the amplitude and the time at which the maximum amplitude is reached. The form of the ERG can also be seen to vary as the light reaches high intensities. The generally positive nature of the ERG at low intensities is preceded by a negative waveform at high intensities. This is a physiological result and is indicative of the various components that make up the ERG. Specifically under high illumination the a-wave proceeds the onset of the b-wave. Oscillatory potentials also become apparent on the ERG at higher intensities (above a threshold) and correspond to the previously discussed APs.

It is conceivable therefore that if we can detect individual action potential we can measure this response time, or the difference in responses resulting from varying intensities as shown in Fig 5.8.

Evident for lower intensity light stimuli is that the number of evoked responses is significantly less than for stimulus at higher intensities. At very high intensities, the number of APs is also subject to reduction due to the inhibitory nature of the retina.

5.3.2 Cellular Classification

Given that there exist many cell types in the frog retina, and that they respond to different components of the visual scene, we have looked at determining the cell type in contact with the array electrodes. The cellular response under the onset of light has been demonstrated highlighting the ON cell response, fig 5.9. There exist cells, which inversely respond to the termination of light (OFF cells). We have also been successful in the recording of their response and this can be seen in Fig 5.10. These individual cell types were not directly targeted through experimentation, however, owing to the spread of these cell types throughout the retina we were able to repeatably record ON and OFF cell responses across multiple experiments.

The AP response of the off cells can be seen to be of similar magnitude to the that detected from the ON response. This is as expected given the cellular mechanism for the generation of the AP is the same. Figure 5.11 shows multiple ERG recordings made from 4 $50\mu\text{m}$ electrodes at the same time across 4 locations on the retina.

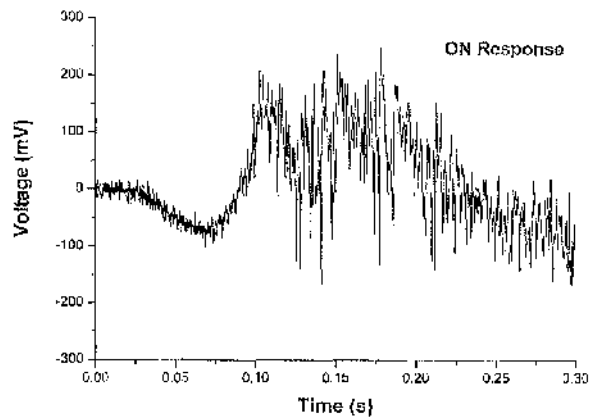


Figure 5.9: Recordings from an 8-electrode array of the ON cell response in relation to the initiation of light at the retinal surface. Recordings were made at 10kHz sampling rate and the recording starts at the onset of light at the retinal surface. $t=0$.

5.4 Stimulation Studies

For any form of retinal prosthesis to be viable, a means of eliciting a response in the neuronal pathway must be established. The approach we have developed to record neuronal information has proved that good contact with the retina has been achieved. This is a prerequisite to the following retinal stimulation studies.

It is important to evoke the signal in a way that is comparable to the natural response. As we have demonstrated, we can record APs temporal and amplitude characteristics (figs 5.6-5.11). A stimulus pulse should incorporate

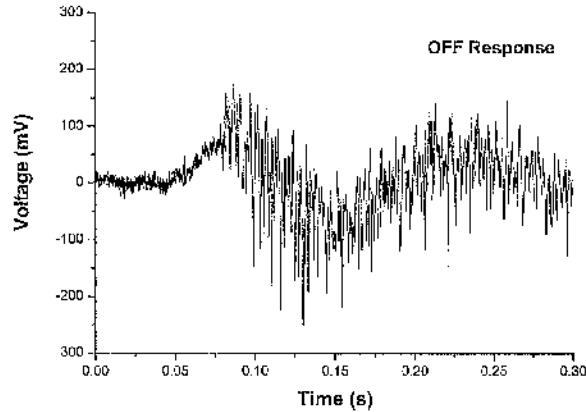


Figure 5.10: Recordings from an 8-electrode array of the off cell response in relation to the termination of light at the retinal surface. Recordings were made at 10kHz sampling rate and the recording starts at the termination of light on the retinal surface, time = 0.

this information and locally influence ganglion cells on the retinal surface. By this means we can selectively influence the locality of visual stimulus on the retina with this information being conveyed to the visual cortex.

5.4.1 Single electrode stimulation studies

Our initial investigations for stimulation of the retina were undertaken via a single electrode on the 8-electrode array. A variable amplitude square wave voltage pulse was applied to the electrode, and the response of the retina could be detected on the neighbouring recording electrodes.

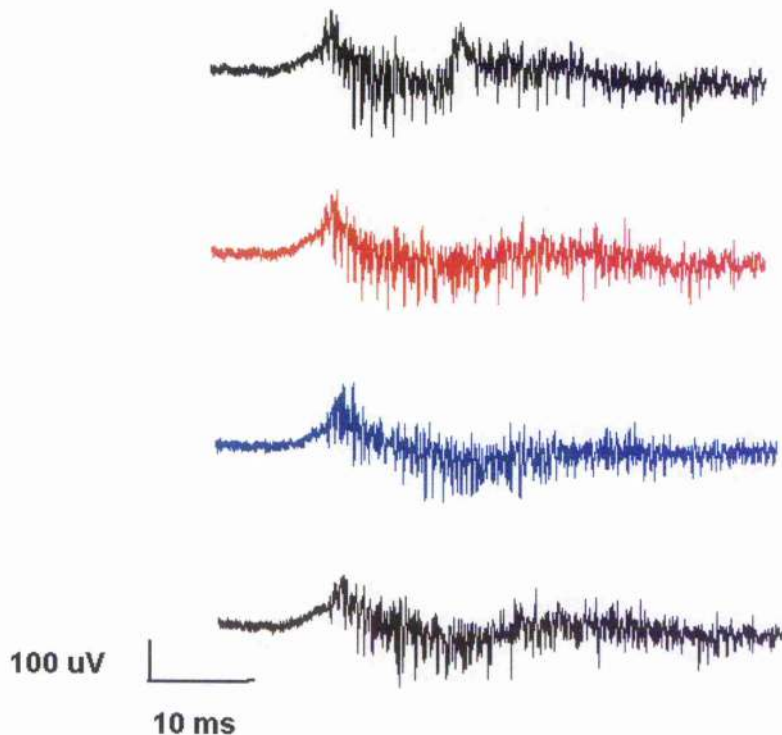


Figure 5.11: Recordings from 4 electrodes of $50\mu\text{m}$ diameter. The 4 electrodes are showing the OFF response at independent points on the retinal surface. The light termination started at time 0 and recording continues for 100 ms. The amplitudes of the responses are all of the order $-200\ \mu\text{V}$ to $100\ \mu\text{V}$.

5.4.2 Stimulation Artefact

When an electrical stimulus pulse is applied to the retina, the comparatively large voltage pulse forces the (recording channel) amplifiers of the system to

saturate. The net effect is that there is a recovery time for the amplifiers which is of the order of several 10's of μs for low voltage pulses. It can be seen that action potentials are superimposed on this artefact at voltages above the stimulation threshold of approx 400mV, See Fig 5.11 showing the associated artefact with applied voltage stimulation. It follows therefore that the applied voltage pulses to the biological system should be as low as required for electrical activation of the tissue.

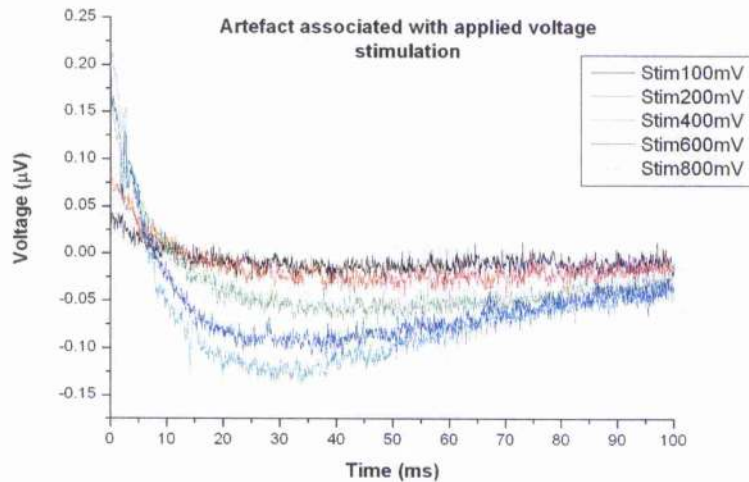


Figure 5.12: The stimulation artefact as recorded on a $50\mu\text{m}$ electrode $50\mu\text{m}$ away from the stimulation site. The amplitude of the artefact was measured for 5 voltage increments for a 1ms pulse applied to, and measured from the same electrodes.

In order to analyse the data, the stimulation artefact must be removed.

We have investigated two separate methods for achieving this. The first is the simple fitting of an exponential decay which mimics the RC decay component of electronics. Although this method can be fitted in good agreement with the falling curve, the combined overshoot of the electronics and recovery, especially at voltage levels above 400mV stimulus, is not described well by this model.

The second method involves fitting a non-linear curve to the recorded data. In order to achieve this successfully without adversely affecting the recorded action potentials the fitting curve must be sampled at a period in excess of the pulse width of the APs. Failure to achieve this will fit the curve to the APs and upon subtraction of the artefact, data corresponding to the APs will be removed. A fitting period of 3ms between data points, some 3 times larger than the frequency response of an AP. Using this method we can achieve excellent correlation in our fitted curve and a high confidence in retaining the AP as shown in Fig 5.13, a measured waveform of an action potential.

Once a suitable curve has been fitted to our data, we FFT our data with a low frequency cut off limited at 80Hz. This removes additional noise in relation to mains noise and the ERG response. Once this is achieved the data is in an analytical form suitable for neurobiological signal analysis.

5.4.3 Voltage threshold for cellular stimulation

Given that we can successfully record and manipulate the data into a comparative form we can look more specifically at determining the effects of applying a voltage stimuli. The first key investigation is to determine at what voltage we can elicit a response from the retinal cells in a manner similar to that recorded under light activation or so called threshold conditions.

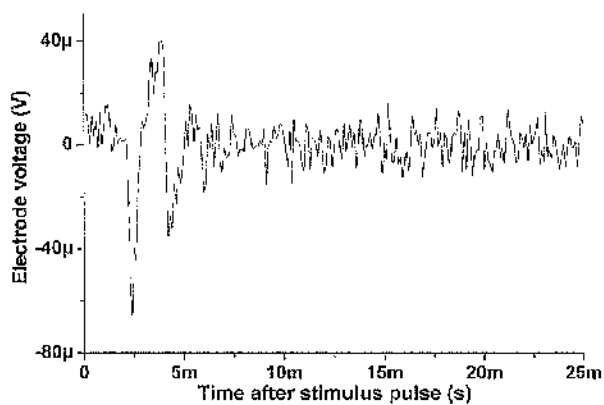


Figure 5.13: Measured waveform of a single action potential recorded from a 400mV applied electrical pulse.

In order to minimise effects of spontaneous firing from the retinal tissue affecting our analysis, experiments were repeated to ensure consistency. The stimulation circuitry allowed voltage pulses to a maximum of 2.5V to be applied. At this voltage the potential to damage the cells exists so studies

were limited to 1.4V.

For our studies it was discovered that a voltage of 400mV was the minimum voltage level required to repeatably elicit a retinal action potential. Typically, a single action potential would result. For voltages in excess of this threshold level, the resulting response of the retina included multiple APs. Interestingly, the increased voltage levels did not influence significantly the rate at which the initial AP was recorded. The amplitude of the recorded APs was, as expected, not influenced by the amplitude of the stimulus voltage.

5.4.4 Action Potential recording from an applied voltage stimulus

Given that the environment for the stimulation studies was not altered throughout the period of viable retinal recordings, investigations were undertaken to determine if temporal patterns of APs could be observed.

In order to determine the temporal AP information from the response to an applied electrical input we filtered the raw recorded data as described in section 5.4.2. Using multiple stimulation experiments, approximately 18 for each voltage level used, we could detect true AP responses from any noise in the system. AP responses filtered in this way resulted in variances in recorded timescales of less than 0.1ms.

A point to be constantly aware of is the need to ensure that the system of applying the electrical pulses is optimised such that the minimum voltage required for stimulation is used. It has been shown in chapter 4, section 4.1.9, that there is associated crosstalk with stimulation pulses and that although it has not been seen to be significant in affecting the quality of the recordings made it is still however a possible source of noise.

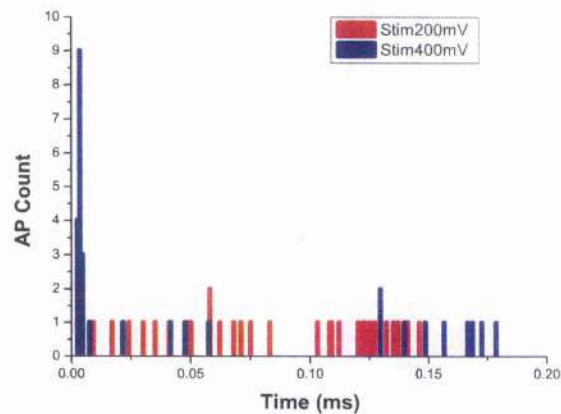


Figure 5.14: Temporal occurrence of APs over 18 trials in response to an applied voltage pulse of 1ms.

The relationship to the response of the retina at the stimulation threshold voltage level of 400mV and at a voltage of 200mV (half the experimentally realised required voltage level) can be seen in Fig 5.14. The key components shown in Fig 5.14 are the confinement of the initial APs to within 10ms for the 400mV stimulus and the lack of any other significant recorded AP

activity thereafter. There is no such peak for the 200mV stimulus pulse and this is indicative that locally the threshold stimulation voltage value has been reached.

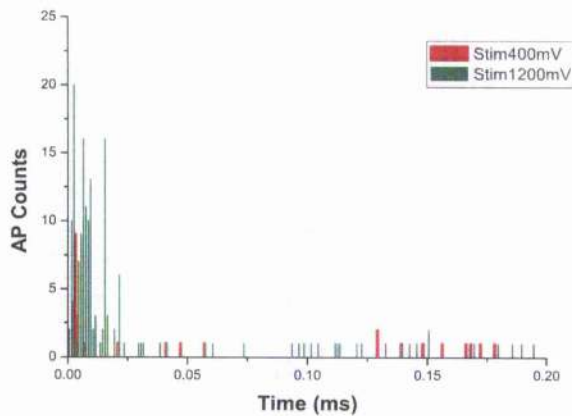


Figure 5.15: Temporal spike occurrence in response to applied voltages of 400mV and 1200mV

The correlation of the 400mV threshold voltage to a voltage significantly in excess of this value, 1200mV can be seen in Fig 5.15. There exists an obvious difference in the retinal response in this instance. At 1200mV the number of responses and the spread in the timing at which APs are evident is broadened to across a range of 25ms post stimulus pulse and it is difficult to discern a single peak. The broadening in the detected signal may result from stimulation of cellular tissue deeper in the retina and hence, it takes longer for the signals to pass to the output cells being monitored. Alternatively, it is possible that cells much further away on the retinal surface are being

activated and a response is being detected from a longer range.

In order to show the quality of the fabrication , Fig 5.16 shows an image of an electrode array post experimentation. As can be seen, there is no delamination of the polyimide multiple layers and the electrodes are still visibly in good condition, with the exception of electrode 6 which was non-functional from the outset.



Figure 5.16: Image of a microelectrode array post test. As can be seen the electrodes are still well coated with platinum black (except for electrode 6 which was not working pre test) and there is no delamination of the polyimide layers.

5.4.5 Stimulus Range

The final investigation, using a single stimulus electrode, looked at the range of influence of an applied stimulus pulse. Through applying the stimulus at

one edge of the 8-electrode array it was possible to record activity along the length of the $50\mu\text{m}$ pitched electrodes of the array, see figure 5.17 and 5.18.

For a pulse of 400mV , data from the nearest neighbour to the stimulating electrode ($50\mu\text{m}$) indicates that 34 action potentials are detected within 45ms with more than half (18) occurring within 25ms of the stimulation pulse. For a recording site $160\mu\text{m}$ from the stimulating electrode, 16 APs are detected with 4 occurring in under 25ms . This indicates that the 400mV threshold voltage can influence the membrane potential significantly at a range of $160\mu\text{m}$. Alternatively, a 400mV pulse applied as a local stimulus can affect an output ganglion cell approximately 15 cells away.

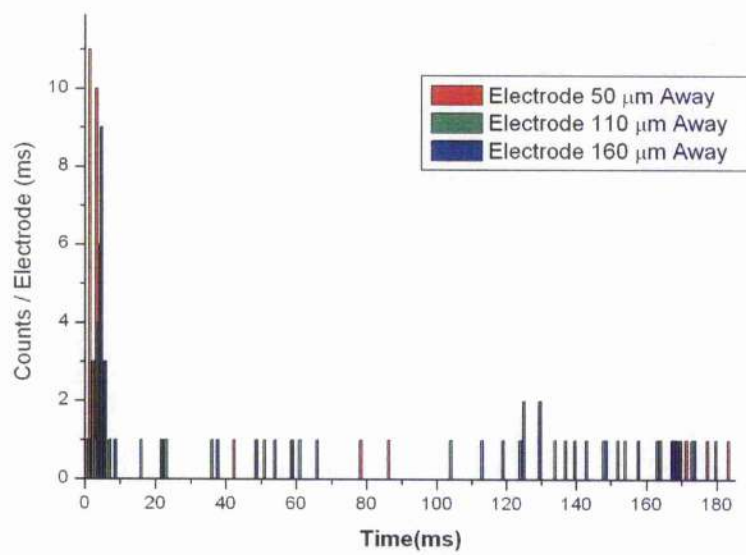


Figure 5.17: Graph showing the time of detection of AP's on electrodes with varying distance from the stimulation electrode.

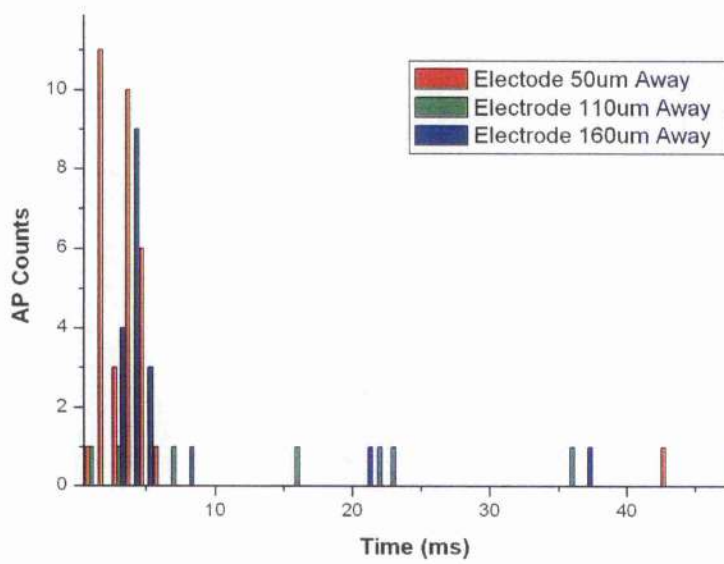


Figure 5.18: Graph showing an increased time resolution of fig 5.15 indicating more specifically the detection of AP's on electrodes with varying distance from the stimulation electrode.

Chapter 6

Conclusions

A system has been described that combines the technologies of engineering, physics and neurobiology to excellent effect and does so via the prototyping of a retinal prosthesis. Described in this thesis is the culmination of research pioneering the use of flexible substrate technologies as a platform on which to deliver the capability to record and stimulate, in a non-invasive manner, retinal neuronal tissue. The application of our systems for monitoring and inducing a voltage response from neurones of the visual system has been presented and therein the possibility of rehabilitation of sensory perception in the retina has realistically been developed.

We look forward, with anticipation, to the development of microelectrode array systems as an approach to address many of the limitations posed by single unit response measurements currently available via neurophysiological patch clamping or micro-pipette techniques. Through the work undertaken

in this thesis to record from large numbers of neuronal cells and through the studies by Humayun, Zrenner, Litke, and Rizzo [35, 84, 82, 13], an understanding of neural coding in the retina is being established. It is my belief that through the multiple simultaneous recordings of stimulated activity, by the means developed and described in this thesis and more broadly in this field, we can successfully employ our understanding of the neural systems to interact and communicate information to and from retinal ganglion cells and allow for rehabilitation of visual sensation.

The fabrication of flexible substrate arrays posed many difficulties especially as the ability to scale the dimensions of the arrays while maintaining a standard process was paramount. What was achieved, was a scalable, flexible, reliable and biocompatible fabrication process complimented with electrodeposited platinum electrodes providing a stable platform for electrical coupling to retinal ganglion cells. Other than polyimide [173] based micro-electrode arrays, the use of PDMS [114] is also becoming established as a useful and attractive alternative material for electrode fabrication. PDMS however, currently lacks the scalability and yield requirements to be useful in high density array development [177] and lacks the ease of control over flexibility the fabrication techniques for polyimide offers. My fabricated polyimide arrays were typically no more than $18\mu\text{m}$ thick as this was the ideal rigidity for testing purposes and upon electrical characterisation exhibited more than $90\text{G}\ \Omega$ inter-channel resistance with the inter-channel capacitance of the order 0.3pF . This allows for discrete, independent cellular recording and stimulation.

For platinum electrodes of $50\mu\text{m}$ diameter an electrode-electrolyte interfacial impedance of $20\text{k}\Omega$ at 1kHz was typical. For electrodes of $5\mu\text{m}$ an impedance of $80\text{k}\Omega$ was measured at 1kHz . From human studies by Humayun [35] and work undertaken by Rizzo, [57] the characteristics of my fabricated $5\mu\text{m}$ and $50\mu\text{m}$ electrodes are similar to those used for their $400\mu\text{m}$ and $100\mu\text{m}$, $55\text{k}\Omega$ electrodes which were successful for retinal studies [190]. What has been achieved in this thesis is the realisation of electrode diameters that permit increased densities over previous studies. The use of my $5\mu\text{m}$ fabricated electrodes has been estimated to allow for normal visual resolution or a resolution of $20/20$ [96] as opposed to $20/200$ at a resolution $50\mu\text{m}$ and a $20/400$ resolution with electrodes of $100\mu\text{m}$, which are still significantly smaller than those used by Humayun for in-vivo studies. Of the current successful trials only Greenberg and Strett [178, 130, 180] have reported fabricating electrodes of $50\mu\text{m}$ or less.

The development of a hexagonal close packed array system on flexible substrates with 74-electrodes is also in excess of what has been realised as functional arrays both within the research environment and commercially [35, 104, 177, 126]. The scalability in the fabrication process also ensures that should the layout or size of electrodes require to change then this can be accommodated to some extent in any future trials.

A key benefit of our system was the ability to record, at high densities, independent responses from spatially discrete neurones. The combination of our low noise (of typically $8\mu\text{m}$ RMS in-vivo) recording electronics (compara-

ble to what is currently commercially available [104, 126]) are complimented by the techniques for preparing the retina and commonly achieved a signal to noise ratio of 25:1. This allowed for a high degree of confidence in determining actual retinal response upon stimulus and the determination of accurate measures for both optical and electrical stimulation thresholds. For the *Rana temporaria* frog an electrical stimulation threshold for healthy retinal action potential activation was 400mV (for a typical 50 μ m electrode), this is significant as the size of the cell stimulated by this voltage is comparable to that found in the foveal region of the primate visual system.

The detection of the visual scene was undertaken using a specifically designed optical sensing active pixel sensor, the IPIX. The 10 x 10 CMOS pixellated device was fabricated via a standard 0.35 μ m process with total dimension 2mm x 2mm. Each pixel was seen to respond to incident light through the on-pixel photodiode. This is an advantage over other systems in that there is no need for external optically sensing systems and that there are 100 independent sensing pixels [179, 35, 181]. As its output, the IPIX chip responded with a series of frequencies similar to the action potential response of the retina and of a period dictated by the intensity of the incident light. The output frequency response of the IPIX was bi-phasic, and charge balanced, with the peak voltage variable to a maximum of 3.3V. Importantly to the effectiveness of the IPIX chip as a "substitute" retina, the frequency, amplitude and period of the response to light stimulus can be easily varied. This, in conjunction with the neural networking capabilities of the chip allows the possibility to incorporate efficiently the neural coding outcomes from

retinal studies.

6.0.6 Future Work

This thesis has initiated research into flexible substrate polyimide based devices that can be seen to offer the possibility, in the longer term, to restore vision. Clearly however there exists a substantial gap between the devices that have been described in this thesis and devices which will ever be considered as potential implantable devices. It is my belief that for the successful culmination of this research, a global collaboration is required. There are several areas that would be of benefit to this project and are areas I would like to have researched. They will remain as further work for this project and will hopefully one day be realised.

In order to gain the maximum benefit from the pixel sensor and deliver this information to the retina, the neural network architecture of the retina must be understood. What is not known is the form of the network that the architecture should be based upon [106]. The reasons for this are that we are limited by our incomplete knowledge of the cellular responses of the retina and the diversity of their functions. Without knowing how the retina processes the visual scene we cannot conclude what is the best architecture for neural networks. Although there has been a body of work undertaken to achieve this, the results of in-vivo experimentation are not trivial to determine without direct feedback from the subject [29, 84, 102]. There exists the possibility of performing experiments on the stoat which will give an indication of the feasibility of computationally generated neural networks. The

binocular vision of the stoat is represented as two independent images on the visual cortex. By this means we can stimulate one retina with a known image and record the response from the visual cortex. The other retina is stimulated by the IPIX chip and recordings of activity in the visual cortex made (hopefully with reasonable spatial resolution). By correlation of the optically recorded image response, in relation to the response under electrical stimulation conditions from the IPIX, we can 'tune' the neural network to optimise the evoked response. Under stimulation both optically and via the IPIX, with the same image represented, a summation of response in the visual cortex should be observed. This is an approach that may well be adopted in future trials.

What is also not understood is if the retina has become damaged through degenerative diseases, how does this affect the processing in the remaining tissue and is the stimulation thresholds for activation of the tissues affected. We have shown with a high degree of success the ability to stimulate healthy retinal tissue. We have not evaluated, nor had any means to evaluate, the requirements for stimulating tissue which has become degenerate. It is conceivable that the stimulation thresholds will be similar as the tissue nearest the array electrodes, the ganglion cells, have been shown through physiological studies to be affected last by AMD or RP [185, 186, 187]. Future work to identify this as a measured result from the electrode arrays would be of significant benefit to the scientific community.

As with any fabrication process, several materials were utilised with the

development of the polyimide based microelectrode arrays allowing for the best use of our fabrication facilities and forming the basis of the arrays presented in this thesis. As previously suggested, a material which showed significant promise and may well be a possible substitute for polyimide as a platform for the development of flexible arrays is Polydimethylsiloxane (PDMS) [10]. The main fabrication challenge for this material is its low surface energy. This is evident through the poor adhesion of deposited metals onto its surface. Various approaches were undertaken throughout this thesis in attempts to utilise PDMS, including oxygen plasma surface treatment. Although it was possible to fabricate low electrode count arrays on PDMS, the possibility to establish a scalable process was never realised. This was further limited by the expansion of PDMS while under vacuum. High purity, low resistivity metal deposition requires a high vacuum level and PDMS would expand, even if under tensile stress, to offer a "herringbone" structure upon relaxation [107]. For our high density fabrication techniques we required a linear surface profile. Where this was not possible, electrical continuity across the entire surface layer was difficult to achieve.

The project has offered a excellent platform on which to build future microelectrode arrays and I believe it can form the basis on which to build single cell stimulating devices. We have shown the ability to electrically elicit a response from tissue though have not managed to confidently and reliably place the device in-vivo to stimulate and record from single cells. The analysis of the recorded waveforms using principal component analysis or cross correlational analysis [182, 183, 184] may herald this spatial information.

With the development of higher density arrays, the dependency on "off-line" techniques such as principal component analysis will decrease through the physical realisation of single cell recording.

As technology advances, and the confidence in engineered neuronal devices becomes established, I believe that the retinal prosthesis described in this work will be a viable approach to reconstruct vision. It is also possible that through our understanding of the retina, a direct outgrowth of the brain, we will begin to uncover the mechanisms behind many more neuronal dystrophies. Through continual support of neuroscientists, engineers and physicists I believe that what is described in this thesis may one day become a platform for the regeneration of higher sensory, cortical functionality.

Bibliography

- [1] Christopher Adams *et al.*, "Development of flexible arrays for in vivo neuronal recording and stimulation", *Nuclear Instruments and Methods in Physics Research A* **546**, pp154-159, 2005.

- [2] Eyal Margalit, "Retinal Prosthesis for the blind", *et al.*, *Survey of Ophthalmology*, Vol 47, No.4, 2002.

- [3] Wentai Liu *et al.*, "A Neuro-Stimulus chip with telemetry unit for retinal prosthetic device", IEEE, *Journal Of Solid State Circuits*, Vol 35, No. **10**, 2000.

- [4] A. Litke, "The retinal readout array", *Nuclear Instruments and Methods in Physics Research A* **310**, pp389-394, 1991.

- [5] K.Mathieson *et al.*, "Detection of retinal signals using position sensitive microelectrode arrays", *Nuclear Instruments and Methods in Physics research A* **513**, pp 51-56, 2003.

- [6] Eyal Margalit and Srinivas R. Sadda, "Retinal Optic Nerve Diseases", *Artificial Organs*, **27**, Blackwell Publishing, pp963-974,2003

- [7] Carl T. Hanks *et al.*, In vitro models of biocompatibility : A review, *Dent. Materials* **12**, pp186-193, 1996.
- [8] C. de Haro *et al.*, Electrochemical platinum coatings for improving performance of implantable microelectrode arrays. *Biomaterials* **23**, pp 4515-4512, 2002.
- [9] Jong-Mo Seo *et al.*, "Biocompatibility of polyimide microelectrode array for retinal stimulation", *Materials Science and Engineering*, **C24**, pp185-189, 2004.
- [10] J.Garra *et al.*, "Dry Etching of polydimethylsiloxane for microfluidic systems", *J. Vac.Sci.Tech. A*,**20**, pp975-982, 2002.
- [11] RN Fariss, ZY Li and AH Milan, "Abnormalities in rod photoreceptors, amacrine cells, and horizontal cells in human retinas with retinitis pigmentosa." *American J. of Ophthalmology*, **129**, pp 215-223.
- [12] E Strettoi *et al.*, "Morphological and functional abnormalities in the inner retina of the rd/rd mouse. *J. Neuroscience*. **22**, pp 5492-5501.
- [13] J. F. Rizzo *et al.*, Methods and perceptual thresholds for short-term electrical stimulation of the human retina with microelectrode arrays, *Investigative Ophthalmology and Visual Science*, Vol **44**, No 12, pp5355-5361, 2003.
- [14] J. F. Rizzo *et al.*, "Perceptual Efficacy of Electrical Stimulation of Human Retina with a microelectrode array during short term surgical trials." *Investigative Ophthalmology and Visual Science*, Vol **44**, No 12, pp5362-5369, 2003.

- [15] Andrew E. Grummet *et al.*, "Multi-Electrode stimulation and recording in the isolated retina", *Journal of Neuroscience Methods*, **101**, pp 31-42, 2000.
- [16] W.H. Dohelle and W.G. Mladejovsky, "Phosphenes produced by electrical stimulation of human occipital cortex and their applications to the development of a prosthesis for the blind", *J. Physiology*, **243** pp 553-575, 1974.
- [17] Q. Wai, K.D. Wise, J.D. Anderson "A high-yield microassembly structure for three-dimensional micro-electrode arrays" *IEEE Trans. Biomed. Eng.* **47** No. **2**, pp 281-289, 2000.
- [18] Vadim S. Polikov *et al.* "Response of brain tissue to chronically implanted neural electrodes", *J. Of Neuroscience Methods* **148:1**, pp1-18. 2005.
- [19] Deupster, <http://innovol.sibs.strath.ac.uk/physpharm/software/winwep.shtml>. Strathclyde Electrophysiology Software, 2003.
- [20] K.Mathieson *et al.*, "Large-area Microelectrode arrays for recording of neural signals, *IEEE Transactions on Nuclear Science*, Vol **51**. No 5. 2004."
- [21] A.Litke, N.Bezayiff, E.J. Chichilnisky *et al.*, "What does the eye tell the brain?: Development of a System for the Large Scale Recording of Retinal Output Activity.", *IEEE*, 2003.
- [22] C. Sokirnjak, Pawel Hottowy *et al.*, "Electrical stimulation of mammalian retinal ganglion cells using dense arrays of small-diameter

- electrodes", *Artificial sight*, Springer Series Biological and Medical Physics/Biomedical engineering.
- [23] C. Sekirnjak, Pawel Hottowy *et al.*, "Electrical stimulation of mammalian ganglion cells with multi-electrode arrays", *J. of Neurophysiol.*, Feb 2006.
- [24] David. A. Berkholder, "Cell Based Biosensors using Microelectrodes", *Thesis submitted to Electrical Engineering University of Stanford.* 1998.
- [25] "Brain Facts : A Primer on the Brain and Nervous System", *Society For Neuroscience* , 1121 14th Street NW, suite 1010, Washington DC.
- [26] E. J. Chichilnisky and F. Rieke, "Detection Sensitivity and Temporal Resolution of Visual Signals near Absolute Threshold in the Salamander Retina", *The Journal of Neuroscience*, **25(2)**, (2005) pp318-330.
- [27] V. J. Uzzell and E. J. Chichilnisky, "Precision of Spike Trains in Primate Retinal Ganglion Cells", *J. Of Neurophysiol* **92**, (2004), pp 780-789.
- [28] W.Dabrowsi, P.Grybos, A.M. Litke, "A low noise multichannel integrated circuit for recording neuronal signals using microelectrode arrays", *Biosensors and Bioelectronics* **19**, (2004) 749-761.
- [29] D.A. Cole, M.V. Viola, L. Yow, M.S. Humaym, J.D. Weiland. R. Greenberg and E. Greenbaum, "The U.S. Department of Energy's Artificial Sight Program, *10th Annual conference of the International FES Society* (July 2005).

- [30] Junyan Yang and David Martin, "Microporous conducting polymers on neural microelectrode arrays II. Physical Characterisation", *Sensors and Actuators A113*(2004) pp. 204-211.
- [31] J. Delbeke, M.F. Brelen, I. Obeid, F. Duret and C. Veraart, *10th Annual Conference of the International FES Society* (July 2005).
- [32] E. Quenneville, M.D. Buschmann et al., *IEEE Transactions on Biomedical Engineering*, **51**(12), 2004 pp.2164-2173.
- [33] S.Baba, "Low-cost Flip Chip Technology for Organic Substrates", *FUJITSU Sci. Tech. J.* **34**(1), Sept 1998, pp78-86.
- [34] S.I. Fried, H.A. Hsueh and F.S. Werblin, "A method for generating precise temporal patterns of retinal spiking using prosthetic devices", *10th Annual Conference of the International FES Society* (July 2005).
- [35] Mark S. Humayun, James. E. Weiland et al., "Visual preception in a blind subject with a chronic microelectronic retinal prosthesis", *Vision Research* **43** 2003, pp.2573-2581.
- [36] Yasuhiko Jimbo, Nahoko Kasai et al., "A system fro MEA-Based Multisite Stimulation", *IEEE Transactions on Biomedical Engineering*, **50**(2), Feb 2003.
- [37] Jaideep Mavoori, Andrew Jackson et at., "An autonomous implantable computer for neural recording and stimulation in unrestrained primates", *Journal of Neuroscience Methods*, **148** 2005, pp 71-77.

- [38] Jong-Mo Seo, Sung June Kim et al., "Biocompatibility of polyimide microelectrode array for retinal stimulation", *Materials Science and Engineering*, **24**, 2004, pp 185-189.
- [39] K.D. Wise, D.J. Anderson et al., "Wireless Implantable Microsystems: High-Density Electronic Interfaces to the Nervous System", IEEE Invited Paper, *Proceedings of the IEEE* **92(1)** 2004. pp 76-97.
- [40] Helga Kolb. "How the Retina Works", *American Scientist*, **91**, 2003.
- [41] Michael Lewicki, "A review of methods for spike sorting: the detection and classification of neural action potentials", *Network : Comput. Neural Sys.* **9** (1998).
- [42] John I.Loewenstein, Sandra R.Montezuma and Joseph F.Rizzo III,"Outer Retinal Degeneration: An Electronic Retinal Prosthesis as a Treatment Strategy", *Arch. Ophthalmol.* **122** (2004), pp587-596.
- [43] Marcus. Eger,"Information Theoretical Methods for the Functional Adjustment of Retina Implant Parameters", *PhD thesis submitted to University of Paderborn*, Nov 2001.
- [44] Mark S. Humayun,"Intraocular retinal prosthesis". *Tr. Am. Opth. Soc* **99** (2001), pp 271-300.
- [45] Thomas Stieglitz et al."Micromachined, Polyimide-based devices for Flexible Neural Interfaces", *Biomedical Microdevices* **2(4)** (2000). pp 283-294.

- [46] Ofer R. Ziv, Joseph F. Rizzo III, Ralf J. Jensen, "In vitro activation of retinal cells : estimating location of stimulated cell by using a mathematical model", *Journal of Neural Engineering* **2** (2005), pp s5-s15.
- [47] Nigel H. Lovell, Luke E. Hallum et al., "Advances in Retinal Neuroprosthetics", *Submitted as a book chapter to the IEEE/Wiley edited book on Neuroengineering/Neuro-Nanotechnology volume.*
- [48] Alan Y. Chow, Vincent Y. Chow et al., "The Artificial Silicon Retina Microchip for the Treatment of Vision Loss From Retinitis Pigmentosa". *Arch. Ophthalmol.* **122** (2004), pp 460-469.
- [49] Robert W. Thompson Jr, G. David Barnett et al., "Facial Recognition Using Simulated Prosthetic Pixelized Vision", *Investigative Ophthalmology and Visual Science* **44(11)** (2003), pp 5035-5042.
- [50] Jorg Sommerhalder, Evolyne Oueghalani et al., "Simulation of Artificial Vision: I. Eccentric reading of isolated words, and perceptual learning." *Vision Research* **43**, (2003), pp 269-283.
- [51] M. Sandison, A.S.G Curtis and C.D.W Wilkinson, "Effective extracellular recording from vertebrate neurons in culture using a new type of microelectrode array", *Journal Of Neuroscience Methods* **114**, (2002), pp 63-71.
- [52] Matthias Gross, Dominique Altpeter et al., "Micromachining of flexible neural implants with low-ohmic wire traces using electroplating", *Sensors and Actuators A* **96** (2002), pp 105-110.

- [53] Jorg-Uwe Meyer, Thomas Stieglitz et al., "High Density Interconnects and Flexible High Density Assemblies for Active Biomedical Implants.", *IEEE Transactions on Advanced Packaging* **24(3)** (2001), pp 366-374.
- [54] Tracy Cameron, Gerald E. Loeb et al., "Micromodular implants to provide electrical stimulation of paralysed muscles and limbs". *IEEE Transactions on Biomedical Engineering* **44(9)**, (1997), pp 781-790.
- [55] J. D. Weiland, J. R. Greenberg et al., "Clinical trial of a prototype retinal prosthesis." . *10th Annual Conference of the International FES Society* (July 2005).
- [56] Mohanasankar Sivaprakasam, Wentai Liu et al., " A Variable Range Bi-Phasic Current stimulus Driver Circuitry for an Implantable Retinal Prosthetic Device." . *IEEE Journal of Solid-State circuits* **40(3)**, (2005), pp 763-771.
- [57] Andrew E. Grummet, John L. Wyatt Jr. and Joseph Rizzo III, "Multi-electrode stimulation and recording in the isolated retina." *Journal of Neuroscience Methods* **101**, (2000), pp 31-42.
- [58] Eberhart Zrenner, "Will Retinal Implants Restore Vision?". *Science* **295**, (2002), pp 1022-1025.
- [59] John I. Lowenstein, Sandra Montezuma and Joseph Rizzo III, " Outer Retinal Degeneration : An Electronic Retinal Prosthesis as a treatment Strategy". *Arch. Opthamol* **122**, (2004), pp 587-596.

- [60] P. Heiduschka and S. Thanos, "Implantable Bioelectronic Interfaces for Lost Nerve Functions", *Progress in Neurobiology* **55**, (1998), pp 433-461.
- [61] John Raiti and Benjamin Kimia, "Cortical Vision Prosthesis". www.lens.brain.edu/igr/cortical-prosthesis-proposal.htm.
- [62] Richard A. Normann, Edwin M. Maynard et al., "A neural interface for a cortical vision prosthesis", *Vision Research* **39**, (1999), pp 2577-2587.
- [63] Hiroaki Oka, Ken Shimono et al., "A new planar multielectrode array for extracellular recording: application to hippocampal acute slices.", *Journal of Neuroscience Methods* **93**, (1999), pp 61-67.
- [64] J. Rodrigues, Dolores Ceballos et al., "Polyimide cuff electrodes for peripheral nerve stimulation", *Journal of Neuroscience Methods* **98**, (2000), pp 105-118.
- [65] Carlos Gonzalez and Manuel Rodriguez, "A flexible perforated micro-electrode array probe for action potential recording in nerve and muscle tissue", *Journal of Neuroscience Methods* **72**, (1997), pp 189-195.
- [66] Thomas Stieglitz, "Flexible biomedical microdevices with double-sided electrode arrangements for neural applications.", *Sensors and Actuators A* **90**, (2001), pp 203-211.
- [67] M. S. Humayan, "Intraocular Retinal Prosthesis", *Tr. Am. Ophthalm. Soc.* **99**, (2001), pp 271-300.
- [68] A. M. Litke, "An advanced pixel detector", *Nuclear Instruments and Methods A* **386**, pp 167-171.

- [69] A. M. Litke, "The Retinal Readout System: An Application of Microstrip Detector Technology to neurobiology", *Elsevier*
- [70] A. Blau, Ch. Zeigler et al., " Characterization and optimization of microelectrode arrays for in vivo nerve signal recording and stimulation". *Biosensors and Bioelectronics*. **12(9-10)**, (1997), pp 883-892.
- [71] Stephen C. DeMarco, Gianluca Lazzi et al., " Computed SAR and Thermal Elevation in a 0.25mm 2D Model of the Human Eye and Head in response to an Implanted Retinal Stimulator : Part I: Models and Methods.", *Transactions on Antennas and Propagation* (May 30th 2002).
- [72] S. C. Mailley, M. Hyland et al.. " Electrochemical and structural characterization of electrodeposited iridium oxide thin-film electrodes applied to neurostimulating electrical signal", *Materials Science and Engineering* **21**, (2002), pp 167-175.
- [73] Pierre Thiebaud, Cynthia Beuret et al., " An array of Pt-tip microelectrodes for extracellular monitoring of activity of brain slices.", *Biosensors and Bioelectronics* **14**, (1999), pp 61-65.
- [74] R. E. Marc et al., "", *Progress in Retinal and Eye Research* **22**, (2003), pp 607-655.
- [75] David Keating, Stuart Parkes et al.. " The multifocal ERG: Unmasked by selective cross-correlation.". *Vision Research* **42**, (2002), pp 2959-2968.

- [76] Nijole Gutmaniene, Natasa Svirskiene and Gytis Svirskis, " Firing properties of frog tectan neurons in vitro". *Brain Research* **981**, (2003), pp 213-216.
- [77] H.Nakagawa and N. Matsumoto, "Current source density of ON / OFF channels in the frog optic tectum", *Progress in Neurobiology* **61**, (2000), pp 1-44.
- [78] Daniel A. Butts and Daniel S. Rokhsar, " The Information Content of Spontaneous Retinal Waves", *The Journal of Neuroscience*. **21(3)**, (2001), pp 961-973.
- [79] Eizaburo Doi, Toshio Inui et al., " Spatiochromatic Receptive Field Properties Derived from Information-Theoretic Analyses of Cone Mosaic Responses to Natural Scenes.", *Neural Computation* **15**, (2003), pp 3979-417.
- [80] Lutz Hesse, Thomas Schanze et al., " implantation of retinal stimulation relectrodes and recording of electrical stimulation responses in the visual cortex of the cat.", *Graefe's Arch. Clin. Exp. Ophthalmol.* **238**, (2000), pp 840-845.
- [81] Kristian Donner, Simo Hemila and Ari Koskelainen, " Light Adaptation of Cone Photoresponses Studied at the Photoreceptor and Ganglion Cell Levels in the Frog Retina.", *Vision Res.* **38(1)**, (1988). pp 19-36.

- [82] A. M. Litke, E. J. Chichilnisky et al., "Large-scale imaging of retinal output activity", *Nuclear Instruments and Methods in Physics Research A* **501**, (2003), pp 298-307.
- [83] Richard Normann, "Sight Restoration for individuals with profound blindness", *University of Utah John Moran Eye Center*.
- [84] Joseph F. Rizzo III, John Wyatt et al., "Methods and Perceptual Thresholds for Short-Term Electrical Stimulation of Human Retina with Microelectrode Arrays.", *Investigative Ophthalmology and Visual Science* **44(12)**, (2003), pp 5355-5361.
- [85] Stanislav Reinis "Some principals for Decoding Local Neuronal Systems in the Mammalian Central Nervous System.", *Department of Psychology, University of Waterloo, ON. N2L 9G1, Canada*.
- [86] Justin Keat, Pamela Reinagel et al., "Predicting Every Spike : A Model for the Responses of Visual Neurons.", *Neuron* **30**, (June 2001), pp 803-817.
- [87] Hyuneui Lim, Yeouhee Lee et al., "Reduction in Surface resistivity of polymers by plasma source ion implantation." *Surface and Coatings Technology* **160**, (2002) pp 158-164.
- [88] Xinyan Cui and David C. Martin, "Fuzzy gold electrodes for lowering impedance and improving adhesion with electrodeposited conducting polymer films." *Sensors and Actuators* **103**, (2003), pp 384-394.
- [89] Petra Margarete Klinge, Morad ali Vafa et al., "Immunohistochemical characterization of axonal sprouting and reactive tissue change after

- long-term implantation of a polyimide sieve electrode to the transected adult rat sciatic nerve.”, *Biomaterials* **22**, (2001), pp 2333-2343.
- [90] In-Seop Lee, Chung-Nam Whang et al., ” Biocompatibility and charge injection property of iridium film formed by ion beam assisted deposition.” *Biomaterials* **24**, (2003), pp 2225-2231.
- [91] Elke Guenther, Bianca Troger et al., ” Long-Term survival of retinal cell cultures in retinal implant materials.”, *Vision Research* **39** (1999), pp 3988-3994.
- [92] P. O. Renault, P. Villain et al., ” Damage mode tensile testing of thin gold films on polyimide substrates by X-ray diffraction and atomic force microscopy” , *Thin Solid Films* **424**, (2003), pp 267-273.
- [93] J. M. Pastor and M. A. Rubio, ” Instabilities in the growth of compact electrodeposits.”, *Physica D* **96**, (1996), pp 384-395.
- [94] Vasile V. Cosofret, Miklos Erdosy et al., ” Electroanalytical and surface characterization of encapsulated implantable membrane planar microensors.”, *Analytica Chimica Acta* **314**, (1995), pp 1-11.
- [95] Jiu-Ha Hwang, K. S. Kilpatrick, T. O. mason and E. J. Garboczi, ” Experimental limitations in impedance spectroscopy: Part IV. Electrode contact effects.”. *Solid State Ionics* **98**, (1997), pp 93-104.
- [96] Daniel Palanker, Alexander Vankov, Phil Huie and Stephen Baccus, ” Design of a high-resolution optoelectronic retinal prosthesis.” *Neural Eng.* **2**, (2005), pp 105-120.

- [97] James D. Weiland, David J. Anderson et al., " In Vitro Electrical Properties for Iridium Oxide Versus Titanium Nitride Stimulating Electrodes." *IEEE Transactions on Biomedical Engineering* **40**, (2002), pp 1574-1579.
- [98] Seung-Joon Paik, Yonghwa park and Dong-Il 'Dan' Cho, " Roughened polysilicon for low impedance microelectrodes in neural probes.", *J. Micromesh. Microeng* **13** (2003), pp 373-379.
- [99] Y. Nakamura, Y. Suzuki and Y. Watanabe, " Effect of oxygen plasma etching on adhesion between polyimide films and metal.", *Thin Solid Films* **290-291** (1996), pp 367-369.
- [100] Edward Cotlier and Robert Weireb, "Retinitis Pigmentosa: Defined from a Molecular Point of View.". *Survey of Ophthalmology* **43(4)** (1999), pp 321-334.
- [101] Christophe Beauquin and Frederic Gaillard, "Responses of Class R3 Retinal Ganglion Cells of the Frog to Moving Configurational Bars: Effect of the Stimulus Velocity.", *Comp. Biochem. Physiol.* **199A(1)**, (1998), pp 387-393.
- [102] Ralf Hornig, Thomas Laube et al., "A method and technical equipment for an acute human trial to evaluate retinal implant technology.", *J. Neural Eng.* **2**, (2005), pp 129-134.
- [103] luke c. Hallum, gregg J. Suaning, David S. Tauberman and Nigel H. Lovell, " Simulated prosthetic visual fixation, saccade, and smooth pursuit.", *Vision Research* **45**, (2005), pp 755-788.

- [104] www.multichannelsystems.com
- [105] <http://www.krasnow.gmu.edu/CENlab/lectures/CS1734-2006-Nernst.ppt>
- [106] Elio Raviola, "A molecular approach to retinal neural networks.", *Funct. Neurol.*, **17 No. 3**, (2002), pp 115-119.
- [107] X. Chen. J.W. Hutchinson, "Herringbone buckling patterns of compressed thin films on compliant substrates.", *Journal of Applied Mechanics*. **71**, pp 597-603.
- [108] N. E. Medeiros and C. A. Curcio, "Preservation of Ganglion Cell Neurons in Age-Related Macular Degeneration", *Inv. Opth. and Vis. Science* **42**, (2001), pp 795-803.
- [109] M. Humayun, M. Prince et. al, "Morphometric analysis of the extramacular retina from postmortem eyes with retinitis pigmentosa", *Inv. Opth. and Vis. Science* **40**, (1999), pp 143-148.
- [110] D. H. Bourla and T.A. Young, "Age-Related macular Degeneration: A Practical Approach to a Challenging Disease.", *Progress in Geriatrics* **54**, (2006), pp 1130-1135.
- [111] C. Sekirnjak et.al, "Electrical stimulation of Mammalian Ganglion Cells with Multielectrode Arrays", *Translational Physiology* **95**, (2006), pp 3311-3327.
- [112] www.iso.org.

- [113] R. Eckhorn et. al, "Visula resolution with retinal implants estimated from recordings in cat visual cortex.", *Vision Research* **46**, (2006), pp 2675-2690.
- [114] Courtney Davidson, "Retinal Prosthesis Provides Hope for Restoring Sight.", *Lawrence Livermore National Laboratory*, S and TR, (2003).
- [115] J. Garra, T.Long et al., " Dry etching of polydimethylsiloxane for microfluidic systems", *J. Vac. Sci. Technol. A* **20(3)**, (2002), pp 975-981.
- [116] R. W. Rodieck, "The First Steps in Seeing", Sinauer Associates Inc. U.S. (1998) p92, ISBN-10: 0878937579, ISBN-13: 978-0878937578.
- [117] Tetsuo Furumiya, David C. Ng et al., "Functional verification of pulse frequency modulation-based image sensor for retinal prosthesis by in vivo electrophysiological experiments using frog retina", *Biosensor and Bioelectronics* **21** (2006), pp 1059-1068.
- [118] Keiichiro Kagawa, Koutaro Yasuoka et al., "Pulse-Domain Digital Image Processing for Vision Chips Employing Low-Voltage Operation in Deep-Sub Micrometer Technologies", *IEEE Journal of Selected Topics in Quantum Electronics* **10(4)**, 2004, pp 816-828.
- [119] M. Sawan, J. Coulombe and Y. Hu. "Design and implementation of High Power Efficiency Modules for a Cortical Visual Stimulator", *10th Annual Conference of the International FES Society* (July 2005).
- [120] Phillip R. Troyk, David E. A. Dettlefsen, Glenn A. DeMichele, "A 16-channel stimulator ASIC for use in an intracortical visual prosthesis", *10th Annual Conference of the International FES Society* (July 2005).

- [121] Phillip R. Troyk, Stuart Cogan and Glenn A. DeMichele, "Compliance supply-limited driving of Iridium Oxide (AIROF) electrodes for maintenance in a safe operating region.", *10th Annual Conference of the International FES Society* (July 2005).
- [122] Spencer L. Smith, Jack W. Judy and Thomas S. Otis, "An ultra small array of electrodes for stimulating multiple inputs into a single neuron.", *Journal of Neuroscience Methods* **133**, (2004), pp 109-114.
- [123] D. Ziegler, P. Linderholm et al., "An active microphotodiode array of oscillating pixels for retinal stimulation", *Sensors and Actuators A* **110(1-3)**, pp 11-17.
- [124] Matthias H. Henning and Klaus Funke. "A biophysically realistic simulation of the vertebrate retina". *Neurocomputing* **38-40**, (2001), pp 659-665.
- [125] Helmut Spieler, "Front-End Electronics and Signal Processing". Conference Talk, ICFA 2004.
- [126] Panasonic Medical probes, <http://med64.com/>
- [127] Data from British Eye Research Foundation. http://www.berf.org.uk/html/media/facts_and_figures.html *HDMicroSystems Product Datasheet*
- [128] Data from British Eye Research Foundation http://www.berf.org.uk/html/research/eye_diseases.html Alan R. Harvey, Ying Hu, Simon G. Leaver "The visual system", *Progress in Retinal and Eye Research*. **25**, (2006), pp 449 - 499.

- [129] Alan Y. Chow et al, "The Artificial Silicon Retina Microchip for the treatment of visio loss from Retinitis Pigmentosa", *Arch. Ophthalmol* **122**, (2004), pp 460-469.
- [130] A. Stett, W.Barth et al., "Electrical multisite stimulation of the isolated chicken retina", *Vision Research*, **40**, (2000), pp 1785-1795.
- [131] Eduardo Fernandez et al, "Population coding in spike trains of simultaneously recorded retinal ganglion cells", *Brain Research* **887**, (2000), pp 222-229.
- [132] Marcus Meister and Michael J. Berry, "The neural code of the retina". *Neuron* **22:1**, (1999), pp 435-450.
- [133] Markus Meister et al, "Multi-neuronal signals from the retina: aquisition and analysis" *Journal of Neuroscience* **51:1**, (1994), pp 95-106.
- [134] Daniel Palanker, Alexander Vankov et al., "Design of a high-resolution optoelectronic retinal prosthesis", *J. Neural Eng* **2**, (2005), pp 105-120.
- [135] W. Einthoven and W. Jolly, "The form and magnitude of the electrical response of the eye to stimulation by light at various intensities", *Quarterly Journal of Experimental Physiology* **1**, (1908), pp 373-416.
- [136] L. J. W Breckenridge et. al "Advantages of using microfabricated extracellular electrodes for in-vitro neuronal recording", *Journal of Neuroscience Research* **42**, (1995), pp 266-276.
- [137] M. A. J Bongard H. Urbschat and P. Rujan "Massive parallel multielectrode recording from retinal ganglion cells experimental design and analysis", *European journal of neuroscience* **10**, pp 356-356.

- [138] D. A. Borkholder, J. Maluf et al. "Microelectrode arrays for stimulation of neural slice preparations", *Journal of Neuroscience Methods*, **77** (1997), pp 61-66.
- [139] M.G. Bove et al. "Interfacing cultured neurones to planar substrate microelectrodes - characterisation of the neuron-to-microelectrode junction." *Bioelectrochemistry and Bioenergetics* **38**, (1995), pp 255-265.
- [140] Brivanlou I.H, D.K Warland and M.Meister, "Mechanisms of concerted firing among retinal ganglion cells." *Neuron*, **20** (1998), pp 527-539.
- [141] P. Connolly et. al "An extracellular microelectrode array for monitoring electrogenic cells in culture", *Biosensors and Bioelectronics* **5**, (1990),pp 223-234.
- [142] P. Connolly et al. "Bioelectronic interfacing: Micro- and nanofabrication techniques for generating predetermined molecular arrays". *Tibtech*, **12**, (1994), pp 123-127.
- [143] T. Dalbasti, A. Erdem and M. Ozsoz. "Multielectrode array for simultaneous recording of glucose, oxygen and electrocorticography from cerebral cortex in experimental focal epilepsy" *biosensors and bioelectronics*, **13**, (1998), pp 881-888.
- [144] S. H. A. DeVries "Mosaic arrangement of ganglion cell receptive fields in the rabbit retina". *Journal of Neurophysiology*, **78**, (1997), pp 2048-2060.
- [145] J. A. C. Dow P. Connolly et al, "Novel methods for the guidance and monitoring of single cells and simple networks in culture", *Cell Sci Suppl*, **8**, (1987), pp 55-79.

- [146] M. H. Droge et al., "Multielectrode analysis of coordinated, multisite, rhythmic bursting in cultured CNS monolayer networks", *Neurosci* **6**, (1986), pp 1583-92.
- [147] M. K. Fejtl et al., "Multi-site recording as a new tool to study epileptogenesis in organotypic hippocampal slices", *European Journal of Neuroscience*, **10**, (1998), pp 44-44.
- [148] W. G. Gross, E. Kreutzberg, A. Mayer, "A new fixed array multi-microelectrode system designed for long term monitoring of extracellular single unit neuronal activity in-vitro", *Neuroscience Letters*, **6**, (1997), pp 101-105.
- [149] W. G. Gross and W. Y. Lin, "Transparent indium tin oxide electrode patterns for extracellular, multisite recording in neuronal cultures", *Journal of neuroscience methods*, **15**, (1985), pp 243-52.
- [150] A. E. R. Grumet, J. L. Wyatt, "Ten micron diameter electrodes directly stimulate retinal ganglion cells and axons", *Investigative Ophthalmology - Visual Science* **40**, (1999).
- [151] D. Heck, "Investigating dynamic aspects of brain function in slice preparations - spatiotemporal stimulus patterns generated with an easy to build multielectrode array." *Journal of Neuroscience Methods*, **58**, (1995), pp 81-87.
- [152] S. S. Honma, T. Nakamura and W. Honma, "Synaptic communication of cellular oscillations in the rat suprachiasmatic neurones", *Neuroscience letters*, **294(2)**, (2000), pp 113-116.

- [153] Y. Y. Ito, T. Kanda, et al. "A culture of neurones of a microelectrode array in a hybrid retinal implant", *Investagative Ophthalmology Visual Science*, **40**, (1999), pp s734-s734.
- [154] Y. K. Jimbo, "Electrical stimulation and recording from cultured neurones using a planar electrode array", *Bioelectrochemistry and Bioenergetics* **29**, (1992), pp 193 - 204.
- [155] Y. K. Jimbo, "Recording neural activity by electrode - array substrates". *Electrochemistry*, **67(3)**, (1999), pp 276-279.
- [156] J. M. A. Kowalski et al. "Neuronal networks with spontaneous correlated bursting activity - Theory and simulating", *Neural Networks*, **5**, (1992), pp 805-822.
- [157] C. A. McDowell, J. Guillory and R. Normann, "Simultaneous multielectrode, multiunit recordings of ganglion cell responses to full field chromatic stimuli", *Investagative Ophthalmology Visual Science*, **36**, (1995), S931.
- [158] M. Meister, J. Baylor and D. A. Shatz, "Synchronous bursts of action potentials in ganglion cells of the developing mammalian retina", *Science*, **252**, (1991), pp 939-43.
- [159] M. Meister, J. Baylor, " Multi-neuronal signals from the retina - acquisition and analysis", *Journal of neuroscience*, **51**, pp 95-106.
- [160] S. I. K. Morefield et al, "Drug evaluations using neuronal networks cultured on microelectrode arrays", *Biosensors and Bioactuators*, **15**, (2000), pp 383-396.

- [161] R. E. Normann, "A silicon based multielectrode array: the foundation for a cortically based visual prosthetic", *Vision research*, **36**, (1996), pp 1146-1156.
- [162] R. E. Normann et al., "High-resolution spatio-temporal mapping of visual pathways using multi-electrode arrays", *Vision Research*, **41**, (2001), pp 1261-1275.
- [163] J. Rizzo, A. Edell, D. Wyatt and J. Jensen, "Single unit recordings following extracellular stimulation of retinal ganglion cell axons in rabbits", *Investigative Ophthalmology*, **38**, (1997), pp 182-192.
- [164] R. S. Segev et al. "Observations and modelling of synchronised bursting in two-dimensional neural networks", *Physical Review E*, **640**, (2001), pp11921 - 11929.
- [165] R. S. Segev, M. Shapira and Y. Ben-Jacob. "Formation of electrically active clustered neural networks", *Physical Review Letters*, **90(16)**, (2003).
- [166] Kovacs G.T.A, "Microelectrode models for neural interfaces", *In enabling technologies for cultured neural networks* (1994), pp 121-165.
- [167] "Design and fabrication of a microelectrode array for iodate quantification in small sample volumes", *Sensors and Actuators B: Chemical*, **113(1)**, (2006), pp 80-87.
- [168] Brian. A. Hollenberg, Cecilia D. Richards et al., "A MEMS fabricated flexible electrode array for recording surface field potentials", *Journal of neuroscience methods*, **153(1)**, 2006, pp147-153.

- [169] Seung-Joon Paik, Yonghwa Park and Dong-il 'Dan' Cho, "Roughened polysilicon for low impedance microelectrodes in neural probes", *Journal of Micromechanics and Microengineering*, **13**, (2003), pp 373-379
- [170] Zhiyun Hu, Dao Min Zhou, Robert Greenberg and Thomas Thundat, "Nonpowder molding methods for creating implantable high-aspect-ratio electrodes on thin flexible substrates", *Biomaterials* **27**(9), (2006), pp 2009-1017
- [171] L. Giovannardi, Kristin H. Gilchrist et al., "Low-cost microelectrode array with integrated heater for extracellular recording of cardiomyocyte cultures using commercial flexible printed circuit technology", *Sensors and Actuators B: chemical* **113**(1), (2006), pp 545-554.
- [172] H. Takahashi et al., "Microelectrode array on folding polyimide ribbon for epidural mapping of functional evoked potentials" *IEEE Transactions on biomedical Engineering* **50**(4), (2003), pp510-516.
- [173] Jong Mo Seo Atung June Kim et al., "Biocompatibility of polyimide microelectrode arrays for retinal stimulation", *Materials science and engineering* **24**(1-2), (2004), pp 185-189.
- [174] Bard A. J. and Faulkner L. R, "Electrochemical Methods" John Wiley and Sons, New York (1980)
- [175] Bockris, J. and Reddy A. K. N. "Modern Electrochemistry", Plenum Press, New York, (1970).

- [176] McAdams E. T. and Jossinet J., "Electrode-Electrolyte interface impedance: The limit current of linearity", *Annual International Conference of the IEEE Engineering in Medicine and Biology Society* **13(4)**, (1991), pp18.5-6.
- [177] E Claverol-Tinture, M Ghirardi et al., "Multielectrode arrays with elastomeric microstructured overlays for extracellular recordings from patterned neurones", *Journal of neural Engineering* **2**, (2005), pL1-L7.
- [178] Greenberg R.J., Humayun N.S and E. de Juan, "Electrical stimulation pulse-width determines the target cell in the frog and the human retina". *Investigative Ophthalmology and Visual Science* **38**, (1997), pp 183-.
- [179] Akihiro Uehara. Yi-Li Pan et al., "Micro-sized photo-detecting stimulator array for retinal prosthesis by distributed sensor network approach", *Sensors and actuators*, **120**, (2005), pp 78-87.
- [180] Reinhard Eckhorn, Marcus Wilms et.al, "Visual resolution with retinal implants estimated from recordings in the cat visual cortex", *Vision Research* **46(17)**, (2006), pp2675-2690.
- [181] M. Schwarz, L. Ewe et al., "Single chip CMOS imagers and flexible micro-electronic stimulators for a retina implant system", *Sensors and Actuators A* **83 (1-3)** , (2000), pp 40-46.
- [182] A. M. Gerstein and A. M. Aertsen, "Representation of cooperative firing activity among simultaneous recorded neurones", *Journal of neurophysiology* **54**. (1985), pp 1513-1528.

- [183] M. Meister, J. Pine and D. A. Baylor, "Multineuronal signals from the retina : aquisition and analysis". *Journal of neuroscience methods*, **51**, (1994), pp 95-106.
- [184] Eduardo Fernandez et al., " Population coding in spike trains of simultaneously recorded retinal ganglion cells", *Brain Research*. **22**, (2000), pp 222-229.
- [185] Andreas Wenzel, Christian Grimm et al, "Molecular mechanisms of light-induced photoreceptor apoptosis and neuroprotectino for retinal degeneration.", *Progress in retinal and eye research* **24(2)**, (2005), pp 275-306.
- [186] Andrea Bringmann, Thomas Pannicke et al.," Muller cells in the healthy and diseased retina.", *Progress in Retinal and Eye Research* **25(4)**, (2006), pp 397-424.
- [187] Robert E. Marc, Bryan W. Jones et al.," Neural Remodeling in retinal degeneration", *Progress in Retinal and Eye Research*, **22(5)**, (2003), pp 607-655.
- [188] K. C. Wilker and P. Rakic., "Distribution of photoreceptor subtypes in the retina of diurnanl and nocturnal primates", *Journal of Neuroscience* **10(10)**, (1990), pp 3390-4401.
- [189] W. Nerust "Die elektromotorische Wirksamkeit der Ionen," *Phys. Chem* **4**, 1889, pp 129-181
- [190] M. S. Humayun, J. D. Weiland et al., "Visual perception in a blind subject with chronic microelectronic retinal prosthesis", *Vision Research*, **43(24)**, (2003), pp2573-2581.
- [191] D. R. Merrill, Marom Bikson and J.G.R. Jefferys, "Electrical stimulation of excitable tissue: design of effacious and safe protocols". *Journal of Neu-*

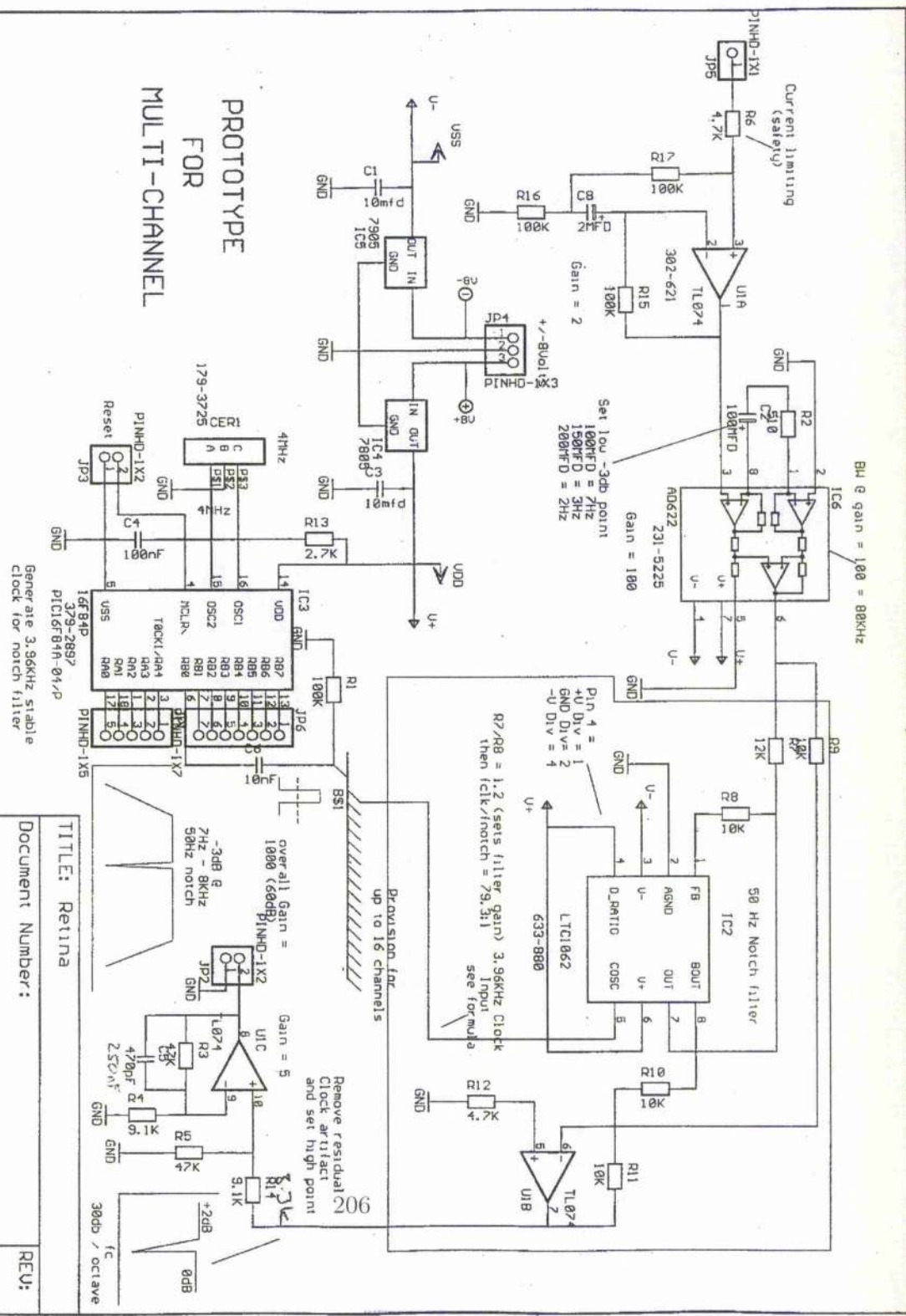
roscience, **141**, (2005), pp 171-198. [?] Murray. D.J. (1988), A History of Western Psychology, 2nd ed., Prentice Hall, Englewood Cliffs, N. J.

Appendix A

appendix1

A signal initially undergoes a x2 gain from a buffer amplifier. A second amplification stage AC couples the signal to remove any DC offset and provides a x100 amplification. This amplified signal is then filtered by a 50Hz notch filter to remove any mains interference. A final stage provides a x5 amplification factor providing a total gain of 1000 for the system. The bandpass for this circuit is 7kHz to 8kHz (-3dB point). The layout for a single channel can be seen in figure for appendix 1. This is replicated 16 times for the 16 channel amplification module.

PROTOTYPE FOR MULTI-CHANNEL



TITLE: Retina

Document Number:

REV:

Date: 21/11/2003 09:25:42a

Sheet: 1/1